INVESTIGATION OF THE PROPAGATION OF LIGHT IN SPHEROIDAL CORE-SHELL NANOPARTICLES WITH PASSIVE AND ACTIVE DIELECTRIC CORES

By

Tolasa Tamasgen Hirpha

A DISSERTATION SUBMITTED TO THE GRADUATE PROGRAM IN PARTIAL FULFILLMENT OF THE REQUIREMENT FOR THE DEGREE OF DOCTOR OF PHILOSOPHY IN PHYSICS (CONDENSED MATTER PHYSICS)

AT

ADDIS ABABA UNIVERSITY

ADDIS ABABA, ETHIOPIA

MAY 2024

ADDIS ABABA UNIVERSITY
DEPARTMENT OF PHYSICS

The undersigned hereby certify that they have read and recommend to the Graduate Program for acceptance a dissertation entitled "**Investigation of the propagation of light in spheroidal core-shell nanoparticles with passive and active dielectric cores**" by **Tolasa Tamasgen Hirpha** as a requirement for the degree of **Doctor of Philosophy in Physics (Condensed Matter Physics)**.

Dated: May 2024

Approved by the Examination Committee

External Examiner:	Dr. Mulualem Abebe (Associate Professor) Jimma Institute of Technology
Internal Examiner:	Prof. Teshome Senbeta Addis Ababa University
Research Supervisors:	Dr. Belayneh Mesfin (Associate Professor) Addis Ababa University
	Dr. Sisay Shewamare (Associate Professor) Wolkite University
Chairman:	Dr. Desalegn Ayehu (Associate Professor) Addis Ababa University

ADDIS ABABA UNIVERSITY

Date: **May 2024**

Author: **Tolasa Tamasgen Hirpha**

Title: **Investigation of the propagation of light in spheroidal core-shell nanoparticles with passive and active dielectric cores**

Department: **Physics**

Degree: **Ph.D.** Convocation: Year: **2024**

Permission is herewith granted to Addis Ababa University to circulate and to have copied for non-commercial purposes, at its discretion, the above title upon the request of individuals or institutions.

Signature of Author

Table of Contents

List of Tables

List of Figures

DEDICATION

First of all, I give this work to Almighty God. Next, I dedicate this work to your memories: my mother, Dadhitu Urgessa, and father, Tamasgen Hirpha, out of heartfelt thanks and devotion for their unwavering love and support, which has enabled me to admire them both for all of my life. Dad, Mom, and all of you, I love you all forever. Stay safe in your everlasting home.

DECLARATION

I hereby declare that this dissertation is my original work and has not been presented for a degree in any other University. All sources that supplied details to support the dissertation has been appropriately acknowledged.

Tolasa Tamasgen: ——————————————————

Email: tolasatamasgen2014@gmail.com

This dissertation has been submitted for examination with our approval as University advisors.

Dr. Belayneh Mesfin:——————————————————

Email: belaynehmes@yahoo.com

Dr. Sisay Shewamare:——————————————————

Email: sisayshewa20@yahoo.com

Abbreviations

NCs	Nanocomposites
CSNCs	Core-Shell Nanocomposites
Φ	Electric Potentials
D	Electric Displacement
L	Depolarization Factor
LFEF	Local Field of Enhancement Factor
$\|A\|^2$	Magnitude of the LFEF for Spheroidal CSNCs
IOB	Induced Optical Bistability
BD	Bistability Domain
LO	Linear Optics
NLO	Nonlinear Optics
SPR	Surface Plasmon Resonance
LSPR	Local Surface Plasmon Resonance
ε_h	Dielectric constant (permitivity) of host matrix
ε_d	Dielectric constant (permitivity) of in the cores
ε_m	Metallic dielectric constant (permitivity) of the shells
$\varepsilon_m^{'}$	Real parts of metallic dielectric function
$\varepsilon_m^{''}$	Imaginary parts of metallic dielectric function
ω	Frequency of incident radiation
ω_p	Plasma frequency of bulk
γ	Damping constant
χ	Nonlinear kerr coefficient (nonlinear susceptibility)
v	Electron damping constant.

Acknowledgments

First of all, I want to start by expressing my gratitude to the Alfa-Omega Almighty God for his favors and miracles, which have consistently enabled me to complete this dissertation.

Afterwards, I would want to sincerely thank, appreciate, and show my admiration to Dr. Belayneh Mesfin, my advisor, for his supervision, sound advice, and kindness during this study research. In addition, I thank and show my gratitude to my co-advisor, Dr. Sisay Shewamare, for his support during this research study.

In addition, I am pleased to Dr. Garoma Dhaba for his unreserved sharing of his knowledge and cooperation with the technical parts of writing and manuscript preparation. I also appreciate Dr. Teshome Hambisa's guidance, which gives me strength. I express my gratitude to Drs. Gammachis Sakata, Genene Shiferaw, Wondimagegn Besha, Abebe Tadese, and Mesfin Diro for providing me with advice and support during my time using Yambo and DFT software.

I also dedicate this work to all my families and brothers, Hirkissa, Sileshi, Fanta, Fayisa, and Tuli Temesgen. I thank Hirkissa and Sileshi Temesgen, who supported me psychologically and even financially when I stayed in academic study at Addis Ababa University.

Next, I dedicated to my beloved wife, Meaza Girma, for your unwavering endurance, bravery, and selflessness throughout the times I was fully focused on this endeavor. I genuinely feel honored by your constant encouragement, and I love you. Additionally, I dedicated this work to my daughters Debi, Haragalfi, and son Dandi Tolasa. May God continue to bless you all.

Finally, I am grateful to Bonga University for sponsoring and financing me during my studies. I forward my thanks to all my friends, instructors, and colleagues who support me in every aspect, directly or indirectly, for their constructive advice and appreciation for the success of this dissertation. And I am also reverently thankful to Addis Ababa University, Department of Physics, Physics Department secretary (Mom Tsilat Adinew, and Yeshi), all my instructors, and staff.

Abstract

Nonlinear optics (NLO) is the study of the interaction of intense laser light with matter. In the last few years, a great deal of progress has been made in our comprehension of nonlinear polarization mechanisms and how they relate to the structural properties of materials. In our work, we studied the effects of depolarization factor (L), metal fraction (p), permittivity of the host matrix (ε_h) and interfacial layer on the local field enhancement factor (LFEF), induced optical bistability (IOB), and bistability domain (BD) of spheroidal core-shell nanocomposites (NCs) embedded in passive or active dielectric cores. Solving Laplace's equation in the quasistatic limit, we obtained expressions of the electric potentials in the various regions of the NCs. Then, by introducing L and the Drude-Sommerfeld model into these expressions, we derived the equation of LFEF in the core of the NCs and studied their IOB as well as BD, theoretically and numerically. The results show that (i) firstly, whether L, p, and/or ε_h vary or kept constant, the LFEF of the spheroidal core-shell NCs possesses two sets of peaks with passive dielectric core, whereas there is one set of peaks with active dielectric core. In NCs with passive dielectric core, an increase in any of these parameters resulted in a more pronounced LFEF peaks in the first set of resonances. With both passive and active dielectric cores, increasing L increases the peaks of LFEF, whereas increasing p decreases the peaks of LFEF of the same material with active dielectric core. Moreover, the highest peak of LFEF is obtained by increasing L than p or ε_h indicating that changing the geometry of NCs has the highest effect on the LFEF. Equally increasing ε_h, intensities of LFEF of the NCs decrease, when the dielectric core is passive and increase when the dielectric core is active. (ii) Secondly, the study reveals that when L decreases, the bistable region of IOB of the NCs increases. However, when p increases at constant L and ε_h, the

bistable region gets wider. When ε_h increases, the IOB region is achieved at larger values of the incident field. Also, the IOB produced was narrower in the passive dielectric core than in the active one, showing that the type of core material also influences the IOB of the NCs. Moreover, when L changes, the region of BD also changes in both types of cores, while changing p or ε_h in both types of cores causes the BD to vanish or emerge. (iii) Thirdly, a system consisting of metal/dielectric spheroidal NCs with interfacial layer (I), the LFEF increased successively in the given frequency range with a single peak with an increase in thickness. Consequently, the LFEF in the passive medium is red-shifted with no appreciable change in peak magnitude as the radius (r) increases, whereas the LFEF in the active host medium increases. We also studied the possibility of LFEF increasing in passive and active dielectric host matrices as p grows. In brief, the LFEF, IOB, and BD in each core are sensitive to changes in the values of L, p, and ε_h. Hence, varying these parameters leads to the possibility of tuning the domains of the LFEF, IOB, and BD, which can be employed in potential applications such as optical sensing, nonlinear optics, and quantum optics.

Chapter 1

Background of the Study

1.1 Introduction

The recent development of reliable, extremely sensitive, and selective detection methods has been made possible by developments in nanotechnology and nanoscience, and these methods are expected to overcome several shortcomings of traditional detection technologies[1–3]. Nanoscience and nanotechnology refer to the control and manipulation of matter at nanometer scale dimensions [4]. However, as the field continues to evolve, nanoscience holds great potential for addressing societal challenges and driving technological advancements by managing material dimensions [5, 6]. It also encompasses the development, processing, characterization, and use of materials and devices [7]. The nanotechnologies are technologies emerging from new nanostructured materials from the electronic properties of quantum dots, or from fundamentally new types of architectures based on nanodevices for use in computation and information storage and transmission. Hence, it is the understanding and control of matter at dimensions between approximately $1-100$ nanometres, where unique phenomena enable novel applications like drug delivery, energy storage, sensing and detections and others [8, 9].

In spite of this, nanomaterials and nanostructured materials are created through modification using size, composition, molecular, and supramolecular techniques [10]. So, the optical properties of metal nanoparticles are most likely influenced by shape, size, and other dielectric materials [11]. Studying the unique characteristics seen when the size of the nanoparticles is altered, especially via reduction, is another area of interest for nanotechnology [12]. Then, one nanometer is the hundredth of a virus's size. Today, electronics that are 1000 times smaller than human cells are being created at the nanoscale [13].

Furthermore, the shape of nanoparticles also has an effect on the optical properties of nanomaterials with noble metal nanostructures, which may all be adjusted to enhance their performance in a range of applications [14]. A metal nanoparticle's plasmon resonance frequencies depend more sensitively on the particle's shape and others, particularly at nanometer-length scales. Generating highly controllable plasmon resonances in nanoparticles throughout a wide spectrum range is crucial as it can lead to a multitude of novel applications in photonic, optoelectronic, spectroscopic, and medicinal fields [15, 16]. As a result, a wide range of metal nanoparticle shapes, including nanorods, nanoprisms, nanoshells, nanostars, and nanocages, have attracted a great deal of attention [17].

Consequently, the distribution of electric fields inside the nanocomposite can be determined by the material characteristics and structure when an electromagnetic wave interacts with it. The increase in the electromagnetic field strength within the core-shell nanocomposites (CSNCs) in comparison to the incident field is detected by the local field enhancement factor [18, 19]. This enhancement can arise due to various mechanisms, including plasmonic resonances, surface plasmon polaritons, or other localized electromagnetic modes supported by the composite structure [20, 21]. The local field enhancement factor is an important parameter in applications such as sensing [22], catalysis [23], and optical devices

[24]. As a result of the mediums and electromagnetic field interacting more, it can increase the sensitivity of sensors. By focusing the field at the active regions of catalysis, it can increase chemical reactions. It has the potential to affect the nanocomposite's emission, absorption, and scattering characteristics in optics, resulting in tunable optical responses [25, 26].

The effect of field enhancement at nanoscale metallic structures is critical to optical phenomena [27]. Nowadays, it is widely accepted to enhance the electromagnetic (EM) field at the interface of core-shell nanomaterials [28]. Thus far, several spectroscopic analyses and experimental confirmations of the enhancement effect have been reported, along with the creation of EM enhancement models and their computations [29]. In the beginning, metal spheres or spheroids in homogeneous media were the subject of electrostatic (or quasistatic) models [30, 31]. Later on, pure electrodynamic solutions of highly particular geometries were provided, as well as electrodynamic corrections of these computations [32]. Recently, the local electric field with various shapes like circular, ellipsoidal, triangular, or tetrahedral nanowires and sizes at the nanoscale has been extensively studied by many scholars [33].

Then again, we investigated the nonlinear response of CSNCs as optical bistability (OB). OB provides controlling light with light in mediums, and it just refers to an optical effect where a system exhibits two different values of the local field for a single value of the input field [34, 35]. As a result, the shell can strengthen this output, producing a significant local field enhancement at the plasmon resonance frequencies as OB [36]. However, the constituent properties of the material from which the composite is formed have an impact on the optical properties of nanoscale composite materials from which OB is produced [37]. Because the electromagnetic fields of incident and scattered waves

must cross boundary borders in two locations, the optical properties of the core and shell materials have a consequence on the electromagnetic response of a coated material [38]. In recent years, OB has generated a great deal of interest as a subject of research, as it may have important applications in optical data processing, all-optical logic and computing systems [39], optical memory elements, optical transistors, and logical devices for high-speed all-optical information processing [40]. In addition, the OB regions are correspond between switching on and off inset curves. From this context, we investigated bistability domain (BD) which is generated between the offset and onset curves of OB fields. Hence, in CSNCs, BD is the range of output states that show bistable curve regions within the mediums. Typically, a core material which is encapsulated within a shell material form a switching "on"and "off"OB states using different types of nanocomposite materials.

As a result of their interesting optical characteristics and potential uses without causing a significant changes to the bulk host medium, materials containing nanoscale inclusions have drawn a lot of attention in recent years. Nonlinear optical phenomena like local enhancement fields and optical bistability can arise when the applied electric field is greater than the atomic electric field strength. Optical nonlinearity might not always be achieved by applying an ordinary, a high-in electromagnetic pulse, such a laser. Therefore, it is necessary to improve the nanoinclusion mediums to enhance the applied field. So, by adding these small nanoinclusions, in variously shaped nanoinclusions, to the bulk medium, one can modify its properties and increase the applied electromagnetic field. Sisay and Mal'nev investigated the local field enhancement at the core of spherical nanoinclusions in a linear dielectric host matrix [41], while O.A. Buryl and associates investigated the local field enhancement at the core of elliptical nanoinclusions in a dielectric host matrix [42]. The findings of these investigations shows the results of unusual local field enhancement

when the frequency of the incident electromagnetic wave approaches the surface plasmon frequency of the metal part of the inclusions. According to Bohren et al. (2008), the redshift of plasmon resonance is usually influenced by the local dielectric environment in spherical metal nanoparticles, with a weak resonance magnitude tuning [43]. Additionally, Naseri, T., and Pourkhavari, F. analyzed the field enhancement and OB behavior of the core-shell ellipsoidal nanoparticle using simply numerical methods, taking into account the impacts of the host medium, metal fraction, and geometrical factor at their interface [44]. Considering all these inquiries, we found a large number of investigations that were carried out to get the enhanced field and OB using spherical and cylindrical core-shell nanoinclussion shapes. Thus, it is evident from this that not enough consideration is being given, specially spheroidal core-shell NCs in composing core into two items and further investigation regarding core-shell NCs is still needed on this nonlinear optical topic.

From this point of view, we are motivated to study the core-shell nanoparticles to succeed in developing nanomaterials and nanostructures with the desired properties. Because of the variety of materials and configurations it covers as well as the capabilities and applications it is giving, nanoparticle, linear, and nonlinear optics (NLO) is a broad research area. Due to the multidisciplinary nature of the subject, numerous academics and researchers from various backgrounds are able to learn unique information from various perspectives and therefore develop the field in various ways. Here, we were inspired as researchers to pursue this work from an optical standpoint based on the investigation of nanoparticles, i.e., silver/gold nanoparticles (spheroidal), in order to further develop the potential of the NLO, which provides significant benefits to particles in industrial lasers, telecommunications, sensors, and medical applications.

Additional studies investigated the plasmonic properties (extinction, absorption, scattering cross sections, and field enhancement factor) of spheroidal core-shell nanoparticles [45]. The impact of the surrounding dielectric constant and the depolarization factor as a geometric factor on the OB and absorption spectra of coated spheroidal NCs has been investigated [46, 47]. To the best of our knowledge, the effect of passive and active dielectric cores on local field enhancement factor (LFEF), induced optical bistability (IOB), and bistability domain (BD) has not been extensively investigated for spheroidal CSNCs. In addition, the effects of the interfacial layer of spheroidal CSNCs in passive and active host matrices are not studied as well. Thus, in the present study, we theoretically and numerically investigated the effects of passive and active dielectric cores, metal fractions, thickness, radius, interfacial layer, and host matrices on the LFEF, IOB, and BD in spheroidal core-shell NCs. Therefore, we are interested in investigating the effects of geometric factor, L, metal factor, p, thickness, t, radius, r, interfacial layer, I, and permitivity of host mediums ε_h on the spheroidal core-shell NCs in passive and active dielectric cores and host matrix.

1.2 Literature Review

1.2.1 The Maxwell equations

The classical theory of electromagnetic radiation, developed by Scottish physicist James Clerk Maxwell (1831-1879), was the first to characterize electricity, magnetism, and light as distinct manifestations of the same phenomenon [48, 49]. Maxwell established that electric and magnetic fields move through space as waves moving at the speed of light with the publication of "A Dynamical Theory of the Electromagnetic Field"in 1865. According to his theory, light is a wave that undulates in the same medium that generates electric and magnetic phenomena [50].

Typical nonlinear optics (NLO) materials have a distinctive crystal structure that is anisotropic to electromagnetic radiation. Understanding induced polarization's nonlinear behavior and being able to evaluate and manage how it affects light propagation through materials are key goals of nonlinear optics. The Maxwell equations are able to describe the NLO phenomenon. The starting point of the electromagnetic theory of propagation of electromagnetic radiation in material media is the Maxwell's equations for the macroscopic electromagnetic field [51, 52]:

$$\nabla \times \vec{H} = \vec{J} + \frac{\partial \vec{D}}{\partial t}, \tag{1.2.1}$$

$$\nabla \times \vec{E} = -\frac{\partial \vec{B}}{\partial t}, \tag{1.2.2}$$

$$\nabla \cdot \vec{D} = \rho_F, \tag{1.2.3}$$

$$\nabla \cdot \vec{B} = 0. \tag{1.2.4}$$

where $\vec{E}$ is the electric field, $\vec{B}$ is the magnetic induction, $\vec{H}$ is the magnetic field intensity, $\vec{J}$ is current density, and ρ_F is the free charge density, $\vec{D}$ is the electric displacement, $\varepsilon_0 = 8.85 \times 10^{-12} F/m$ is the free space permittivity, and $\mu_0 = 4\pi \times 10^{-7} H/m$ is the free space permeability.

Polarization is the dipole moment per unit volume of a material system which depends on the strength $\tilde{E}(t)$ of an applied optical field. In the case of conventional (i.e., linear) optics, the induced polarization depends linearly on the electric field strength in a manner that can often be described by the relationship as:

$$\widetilde{P}(t) = \varepsilon_0 \chi^{(1)} \widetilde{E}(t) \tag{1.2.5}$$

where $\widetilde{P}(t)$ is linear polarization, $\chi^{(1)}$ is a linear susceptibility and ε_o is the permittivity of the free space.

The advancement of NLO materials is closely related to the development of nonlinear optics [53, 54], and its application of a strong electric field induces a nonlinear polarization. This electric field is the product of an externally applied, powerful laser source. The following polarization equation can be used to mathematically characterize the NLO effect on the molecular level as [55]:

$$\widetilde{P}(t) = \varepsilon_0 \chi^{(1)} \widetilde{E}^1(t) + \varepsilon_0 \chi^{(2)} \widetilde{E}^2(t) + \varepsilon_0 \chi^{(3)} \widetilde{E}^3(t) + ... \tag{1.2.6}$$

$$\widetilde{P}(t) = \widetilde{P}^{(1)} + \widetilde{P}^{(2)} + \widetilde{P}^{(3)} + ...$$

where $\widetilde{P}(t)$ is polarization, $\widetilde{E}(t)$ is field strength, $\chi^{(2)}$ and $\chi^{(3)}$ are second order and third order nonlinear optical susceptibilities.

In general, nonlinear optics is a field of optics that describes the changes of the optical properties of materials in the presence of light. This behavior is contrary to everyday experience, but is firmly rooted in the interaction of light with matter at atomic scales. An effect resulting from nonlinear optics arises from light at large intensities within materials.

The electric displacement $\vec{D}$, magnetic field $\vec{H}$, and the current density $\vec{J}$ are defined by constitutive equations

$$\vec{D} = \varepsilon_0 \vec{E} + \vec{P} = \varepsilon_0 \varepsilon \vec{E} \tag{1.2.7}$$

$$\vec{H} = \frac{1}{\mu_0} \vec{B} - \vec{M}. \tag{1.2.8}$$

$$\vec{J} = \sigma \vec{E}. \tag{1.2.9}$$

where $\vec{P}$ and $\vec{M}$ are the electric and magnetic polarizations, σ is the conductivity of the medium, ρ_F is the density of external charges; and ε_0 and μ_0 are the electric and magnetic permittivity in vacuum, respectively; ε is the relative dielectric permittivity of the medium. For the sake of simplicity, we shall limit ourselves to the non-magnetic media ($\mu = 0$). Thus,

after substitution of Eqn. (1.2.5)−(1.2.7) in Eqn. (1.2.1−1.2.4) the electromagnetic wave equation can be derived as follows:

$$\nabla \times (\nabla \times \vec{E}) + \mu_0 \sigma \frac{\partial \vec{E}}{\partial t} + \varepsilon_0 \mu_0 \frac{\partial^2 \vec{E}}{\partial t^2} + \mu_0 \frac{\partial^2 \vec{P}}{\partial t^2} = 0. \tag{1.2.10}$$

Moreover, the optical polarization $\vec{P}$ in Eqn. (1.2.7) induced in the medium by propagating electromagnetic wave can be expressed by a Taylor series:

$$\vec{P} = \varepsilon_0 \chi^{(1)} \vec{E} + \varepsilon_0 \chi^{(2)} \vec{E}\vec{E} + \varepsilon_0 \chi^{(3)} \vec{E}\vec{E}\vec{E} + ... \tag{1.2.11}$$

where $\chi^{(1)}$, $\chi^{(2)}$, ... are the susceptibility tensor and $\vec{E}$ is the propagating electric field. The first term in Eqn .(1.2.8) describes linear polarization component while higher terms are responsible for nonlinear contribution. Thus, the wave Eqn. (1.2.8) can be modified:

$$\nabla \times (\nabla \times \vec{E}) + \mu_0 \sigma \frac{\partial \vec{E}}{\partial t} + \varepsilon_0 \mu_0 (1 + \chi^{(1)}) \frac{\partial^2 \vec{E}}{\partial t^2} + \mu_0 \frac{\partial^2 \vec{P}_{NL}}{\partial t^2} = 0, \tag{1.2.12}$$

where $\vec{P}_{NL} = \varepsilon_0 \chi^{(2)} \vec{E}\vec{E} + \varepsilon_0 \chi^{(3)} \vec{E}\vec{E}\vec{E} + ...$

The typical values of $\chi^{(2)}$ and $\chi^{(3)}$ for the usual kind of crystals are $\chi^{(2)}$ is 10^{-9} esu and $\chi^{(3)}$ is 10^{-14} esu. Therefore, for the weak incident optical field the nonlinear contribution in polarization can be neglected ($\vec{P}_{NL} \to 0$) and Eqn. (1.2.12) becomes the well known ordinary wave equation:

$$\nabla \times (\nabla \times \vec{E}) + \mu_0 \sigma \frac{\partial \vec{E}}{\partial t} + \varepsilon_0 \mu_0 (1 + \chi^{(1)}) \frac{\partial^2 \vec{E}}{\partial t^2} = 0. \tag{1.2.13}$$

In this case, the polarization response of a medium to a given monochromatic component $\vec{E}(\omega, \vec{r})$ of applied field is limited only by the electric permittivity ε; the other frequency components of the field do not affect on $\vec{P}_L(\omega, \vec{r})$ or $\vec{E}(\omega, \vec{r})$. If the applied field is an intense laser field, the second- and/or third-order polarization components expressed by Eqn. (1.2.12) may no longer be neglected.

Then, the nonlinear term containing $\vec{P}_{NL}$ in Eqn. (1.2.12) can be recognized as a source that can emit coherent radiation at a new frequency. Thus, nonlinear polarization induced in the media by propagating monochromatic electromagnetic wave is responsible for optical harmonic generation.

1.2.2 Nonlinear optics

Nonlinear optics (NLO) is the study of phenomena that occur as a consequence of the modification of the optical properties of a material system by the presence of light [56–58]. Typically, only laser light is sufficiently intense to modify the optical properties of a material system. The beginning of the field of nonlinear optics is often taken to be the discovery of second-harmonic generation by Franken, et al. (1961), shortly after the demonstration of the first working laser by Maiman in 1960 and sending the red light of a ruby laser ($\lambda = 6943\mathring{A}$) onto a crystal of quartz, they were able to observed a tiny production of ultraviolet light [59]. NLO phenomena are "nonlinear"in the sense that they occur when the response of a material system to an applied optical field depends in a nonlinear manner on the strength of the optical field. For example, second-harmonic generation occurs as a result of the part of the atomic response that scales quadratically with the strength of the applied optical field. Consequently, the intensity of the light generated at the second-harmonic frequency tends to increase as the square of the intensity of the applied laser light.

In nonlinear optics, the NLO materials play a significant role, particularly in information technology and industry, and in the last ten years, however, have seen the success of this work in its applications [60]. This can mostly be attributed to an increase in NLO material performance. A great deal of progress has been made in our comprehension of

nonlinear polarization mechanisms and how they relate to the structural properties of materials. This evolution has been significantly influenced by the recent developments in fabrication and growth methods for synthetic materials. The goal is to formulate materials that exhibit significant nonlinearities while complying with all application-specific technological requirements, such as a broad transparency range, quick response, and high damage threshold [61].

However, advancements in nonlinear effects in devices, in addition to their process ability, flexibility, and interface with other materials, paved the way for the investigation of new nonlinear effects of materials and the introduction of new concepts. It is anticipated that the realization of key optical devices in optical fiber communication [62, 63], and optical computing [52] that make the most of light characteristics, such as parallel and spatial processing capabilities and high speed, will come about as a result of optical solitons, optical switching, quantum information processing chips, optical communication networks, and optical computing systems, and memory, which depend on light intensity [58, 64, 65].

Therefore, let us investigate how the dipole moment per unit volume or polarization $\widetilde{P}(t)$ of a material system relies on the strength $\widetilde{E}(t)$ of an applied optical field in order to more properly characterize what we mean by optical nonlinearity. In particular, the linear polarization provides an extensive description of the light-matter interaction when the intensity of the incident radiation is sufficiently small; whereas the nonlinear optical response of a medium depends on the strength of the applied optical field, $\widetilde{E}(t)$. This interaction of light to matter by EM and the formation of nonlinear response process. Due to the numerous fundamental issues and great promise for a wide range of applications, local electromagnetic field fluctuations and related enhancement of nonlinear optical phenomena in metal-dielectric composites near penetration threshold have recently drawn significant

attention [57, 66].

1.2.3 Optical bistability in nonlinear composite materials

We know that the optical bistability (OB) is a phenomenon in which the output intensity of light can exhibit two stable states for a given input intensity. It has played a significant role in the development of nonlinear optics and has applications in areas such as optical switching and computing. The history of OB dates back to the 1960s when researchers began exploring the nonlinear optical response of materials [67]. In 1964, Arthur L. Schawlow and Charles H. Townes proposed the concept of OB in a paper titled "Infrared and Optical Masers"where they discussed the possibility of bistable behavior in lasers. In 1966, Robert W. Hellwarth proposed the idea of OB based on the intensity-dependent refractive index of a medium. He suggested that a nonlinear medium could exhibit two stable states of light transmission depending on the input intensity.

In the 1970s and 1980s, significant progress was made in developing theoretical models to explain OB [68]. Theoretical frameworks such as the Maxwell-Bloch equations and the semi-classical approach were used to describe the behavior of nonlinear systems and to understand the mechanisms of OB. Researchers explored various physical mechanisms for achieving OB, including saturable absorption, Kerr nonlinearity, and resonant absorption or dispersion effects [57]. The development of more advanced experimental techniques and the availability of new nonlinear materials allowed for further exploration and characterization of OB in different systems.

Optical bistability has been explored for its potential applications in areas such as optical switching, optical memories, and all-optical computing [64, 69, 70]. The OB offers the possibility of controlling light signals using other light signals, enabling the development of optical devices with enhanced functionality. Ongoing research focuses on improving

the performance of optical bistable devices, exploring new materials and systems, and developing novel approaches to achieve all-optical signal processing and computing [71, 72]. In summary, the history of OB traces back to the mid-1960s with theoretical proposals followed by experimental demonstrations in the early 1970s. Since then, significant progress has been made in understanding the underlying physics, developing theoretical models, and exploring potential applications of OB in the field of nonlinear optics.

Nonlinear OB refers to a phenomenon in which the optical response of a material or system exhibits two stable states for a given input power [57, 73]. These two states correspond two different output intensities. Nonlinear OB output is an important concept in the field of nonlinear optics and has an applications in areas of optical computing, optical switching, and information processing. In this case we attempt to study some types of nonlinear OB as follows:

Kerr bistability

Kerr bistability is the name given to a phenomena that is seen in nonlinear optics when light interacts with a material medium [74, 75]. The physicist Roy Kerr, who originally characterized it in the 1960s, is honored by the name. When a material exhibits Kerr bistability, the intensity of the incident light affects the substance's refractive index. The way light travels through a material is determined by its refractive index. The refractive index in a Kerr media varies nonlinearly with light intensity. The occurrence of two stable states for the light's intensity, or bistability, can result from the nonlinearity of the refractive index under specific circumstances. This indicates that there are two possible output intensities for a given input intensity.

Using kerr effect we obtained OB in core-shell NCs. Then, consider a material whose intensity-dependent polarization is given by the third-order nonlinear susceptibility, $\chi^{(3)}$,

in order to comprehend how optical bistability is generated utilizing the Kerr effect with susceptibility [76].

The material's induced polarization P is determined as we see in Eqn. (1.2.6):

$$P = \varepsilon_0 \chi^{(1)} E^1 + \varepsilon_0 \chi^{(3)} E^{(3)} \tag{1.2.14}$$

where E is the incoming light's electric field, $\chi^{(1)}$ is the linear susceptibility, and ε_0 is the vacuum permittivity. The material's linear response is represented by the first term on the right side of the equation, and the nonlinear response resulting from the Kerr effect is represented by the second term.

The polarization and the material's refractive index, n, are connected by the following equation:

$$n^2 = 1 + \chi^{(1)} E + \chi^{(3)} |E|^2. \tag{1.2.15}$$

where the electric field's strength is denoted by E.

A basic configuration consisting of an optical cavity filled with a Kerr medium is examined. This cavity is formed by enclosing the Kerr medium between two mirrors. Once within the hollow, the incident light repeatedly moves back and forth. Assume for the moment that the Kerr medium is low-transmission. Since the input light is low intensity in this condition, the linear susceptibility $\chi^{(1)}$ largely determines the medium's refractive index. The Kerr effect grows with incident light intensity, and the third-order nonlinear susceptibility component $\chi^{(3)}|E|^{(2)}$ becomes significant.

The refractive index rises with increased intensity due to the nonlinear part in the equation. An increase in the refractive index causes more constructive interference to occur within the cavity, which raises the intensity of the intracavity. The refractive index rises more because of the greater intracavity intensity's amplified Kerr effect via the $\chi^{(3)}|E|^2$

term. The refractive index and light intensity positive feedback loop causes a sharp spike in transmitted intensity, which induces a high-transmission state transition.

The light-matter interaction's two stable states are equivalent to its two distinct equilibrium solutions. The self-action of light in the Kerr medium gives birth to the bistable behavior [77]. The refractive index stays largely constant and the output intensity closely tracks the input when the input intensity is below a predetermined threshold. On the other hand, the output intensity increases to a greater value and the refractive index changes dramatically when the input intensity exceeds the threshold. The system demonstrates hysteresis, which means that the output intensity is dependent on both the input's past and present values. Numerous systems, including gases, liquids, and solid-state materials, have been examined for Kerr bistability. Information storage, signal processing, and optical switching are some of its possible uses. Kerr bistability is an interesting topic in nonlinear optics because it allows one to manipulate and regulate light pulse transmission by taking use of Kerr media's nonlinear response.

Therefore, the Kerr bistability is based on the nonlinear optical response known as the Kerr effect, which occurs in materials with an intensity-dependent refractive index. In Kerr bistable systems, the refractive index of the material changes with the intensity of the incident light. This leads to two stable states of the system, typically referred to as the "on"and "off"states. This is an optical mechanism that changes its refractive index inversely dependent on the intensity of the source light. The first bistable state resides at a given intensity where no optical mechanism is used. The second state resides at the point where a certain light intensity causes the light to resonate to the corresponding refractive index.

Absorptive bistability

Absorptive bistability occurs in materials that exhibit an intensity-dependent absorption coefficient. When the input power exceeds a certain threshold, the material undergoes a transition from a low-absorption state to a high-absorption state. This results in the bistable behavior of the optical system. This utilizes an absorber to block light inversely dependent on the intensity of the source light. The first bistable state resides at a given intensity where no absorber is used. The second state resides at the point where the light intensity overcomes the absorber's ability to block light.

The process of the optical bistability in composite materials

The physical requirements for OB are an intensity-dependence refractive index and an optical feedback mechanism. A system is said to be optically bistable if it can exhibit two steady output states for the same input intensity over some range of input values. The switching up and down operations typical in a hysteresis cycle originates from the rise of instability. A physical state is said to be unstable when, after displaying the system a little from this steady point, the system does not return to it and goes further from it. In other words, for an unstable state, even the slightest perturbation removes the system from it. The searches for instabilities turn out to be crucial in the study of OB phenomena not only from the theoretical viewpoint but also for the possibilities for practical and technological applications. Since its first discovery in late 1970's, OB has been found existing in many different optical systems. One of the simplest examples of bistable systems is a Fabry-Perot resonator with the cavity filled with a medium that presents saturable absorption or nonlinear dispersion [78–80].

These optical properties of silver nanoparticles have been recently studied extensively

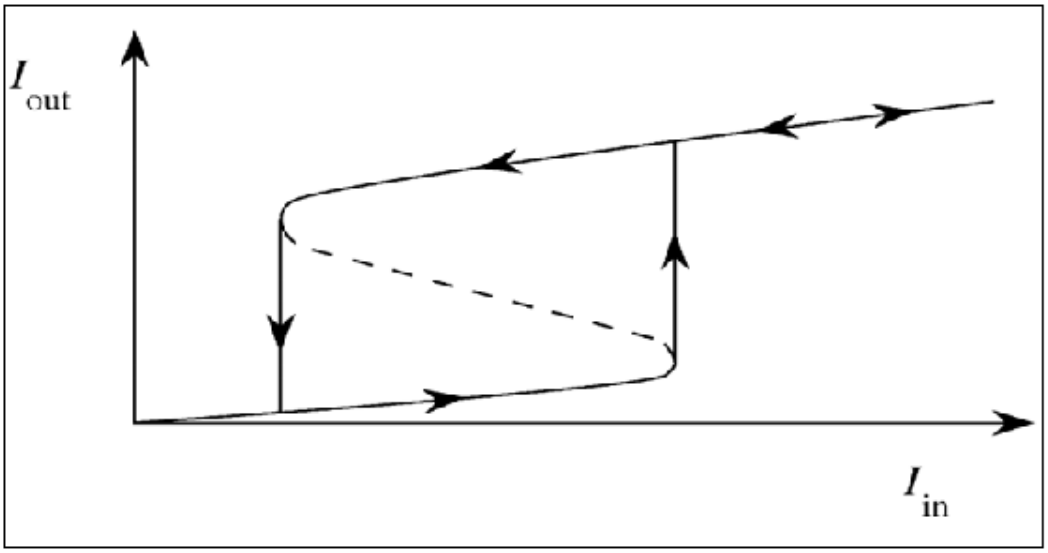

Figure 1.1: Typical input-versus-output characteristics of a bistable optical device [**?**].

and metal/dielectric composite have found various applications in different fields of science and technology site. The original study of the effective optical properties of composite materials were to the analysis of linear media and by considering the contribution of the local field of the particle it is extended to study of the materials with nonlinear part. This is strongly dependent on the nanoparticles size, shape, volume fraction, spatial distribution and the properties of the surrounding matrix. Control over these parameters enables such metal/dielectric nanocomposite to become promising media for development of precious/novel nonlinear materials in nanodevices and optical elements.

Optical bistability switching on and off

Optical bistability switching refers to the transition between the two stable states of an optical system: the "on"and "off"- state. The optical bistability can be described as the process of transitioning from one state to the other are stated as follows [73, 77, 81]:

Switching on

When the system is in the "off"state, it exhibits low output intensity or refractive index. To switch on the optical bistability, an input power or intensity is increased beyond a certain threshold level. This increase in input power causes a nonlinear response in the system, leading to a transition from the "off"- state to the "on"- state.

The exact mechanism for switching on in optical bistability depends on the specific type of bistable system. For example, in Kerr bistability, the increase in input power induces a change in the refractive index of the material [76, 82], resulting in a transition to the "on"state. Similarly, in absorptive bistability, the input power surpasses the threshold, causing a transition from the low-absorption state to the high-absorption state, resulting in the "on"state as shown in Fig. 1.1.

Switching off

Conversely, switching off in optical bistability involves transitioning from the "on"state to the "off "state. This can be achieved by reducing the input power or intensity below a certain threshold level. The process of switching off depends on the specific characteristics of the bistable system. In Kerr bistability, decreasing the input power causes the refractive index to return to its original value, leading to the transition to the "off"state. In absorptive bistability, reducing the input power below the threshold causes the material to transition back to the low-absorption state, resulting in the "off"state.

The switching on and switching off processes in optical bistability are dynamic and reversible, allowing for control and manipulation of the system's output characteristics. By carefully adjusting the input power or intensity, one can toggle between the "on"and "off"states, enabling applications such as optical switching, information processing, and

optical computing.

1.2.4 Bistability domain in nanocomposite materials

Bistability refers to a system or process that can exist in two stable states. In the context of domains, a bistability domain (BD) refers to a region or range of conditions in which a system or process exhibits bistability. At the onset of optical bistability (OB), there is a critical point where the output versus input characteristics have an infinite slope and merge between two points [83]. Then, as the intensity is applied, the OB in the mediums vicinity of this critical point is characterized by critical rising up and slowing down after second stability [84]. Thus, when intensity is applied to the system, the output BD comprises the regions between the bistability states. Hence, the BD is directly proportional to the applied field. Thus, in the locality of the critical point, all bistability regions are included between the inset regions.

If a system can alternate between two different stable steady states but cannot stop in between states, it is said to be bistable. A bistable system will always exhibit hysteresis, which means that in order for the stimulus to move the system to a different steady state where it might stay as the stimulus diminishes it must cross a threshold [85, 86]. We understand bistability domains better, by considering that a chemical reaction in a mediums can be exist between two different states, A and B. The reaction can be influenced by factors such as temperature, pressure, or concentration. In certain conditions, the system may favor state A, while in other conditions, it may favor state B. The range of conditions in which both states are stable is known as the bistability domain. Therefore, the domain has onset fields that are lower than those of the first bistability domain and a relatively small frequency range. Throughout the domain, the lowest bistability onset fields are observed.

By considering this, the steady-state curve develops in a region with a negative slope

and takes on an S-shaped form if we increase the intensity, I_I further (Fig. 1.2) [87]. Therefore, as seen in Fig. 1.2, we investigated at the multivalued function of intensity in in this particular instance. In this case as shown from Fig. 1.2, the system has three output states in the given intensities ranging for values $I_{\downarrow} < I_I < I_{\uparrow}$. The system is bistable because the one that is located in the area with a negative slope is unstable. In the event that we raise the incident field intensity rapidly to I, the system will have to abruptly switch to the higher transmission branch. The system stays in the upper branch until we reach value I if we now gradually reduce the incidence intensity. After that, the system returns discontinuously to the lower transmission branch. We so have a cycle of hysteresis.

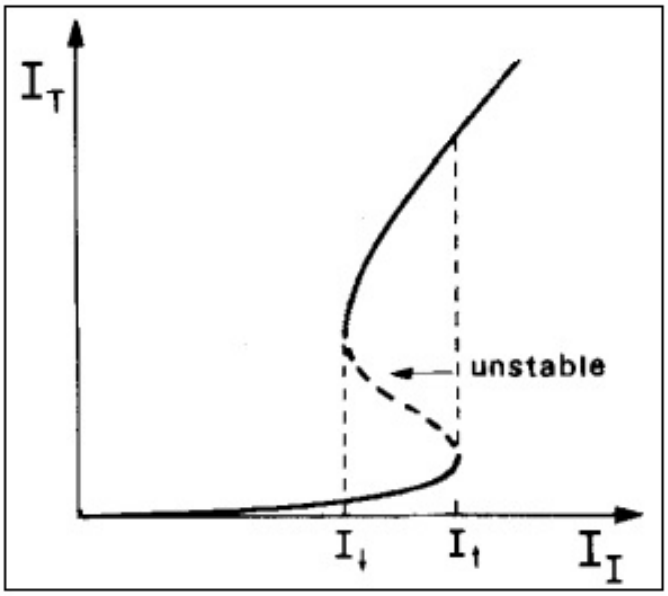

Figure 1.2: Scheme of bistability domain.

Conclusively, the bistability domain can be visualized as a region in a parameter space, where the axes represent the influencing factors, and the region represents the range of values where bistability occurs. Within this domain, small changes in the influencing factors may not cause an immediate transition from one state to another. Instead, the

system remains in its current state until a specific threshold is reached, at which point a rapid transition to the other state occurs. Bistability domains are observed in various scientific fields, including physics, chemistry, biology, and engineering. They have practical applications, such as in the design of electronic circuits, where bistable elements (such as flip flops) are used to store and manipulate binary information [88, 89].

1.2.5 Plasmonics of nanostructures

The history of plasmonics of nanostructures can be traced back to the early 20th century when scientists began studying the interaction of light with metallic materials [90]. However, it wasn't until the late 20th century that the field of plasmonics started to gain significant attention and progress rapidly. Strong optical fields that couple to plasmonic nanostructures interact with the system's free electrons to produce an intrinsically nonlinear optical response that includes Kerr effect, sum frequency generation, and higher-harmonic production [91, 92].

In the 1960s, the concept of surface plasmons was introduced by Ritchie, who described the oscillations of free electrons at the surface of a metal. This led to early studies on surface plasmon resonance (SPR), which is the phenomenon of enhanced light-matter interactions occurring at the interface between a metal and a dielectric medium. SPR became an important technique for biosensing and thin-film characterization.

During the late 1990s and early 2000s, researchers began investigating plasmonic properties of individual metallic nanoparticles. They found that the localized surface plasmon resonance (LSPR) of nanoparticles [93], which arises from the collective oscillations of free electrons in the nanoparticle, could be tuned by controlling the size, shape, and composition of the nanoparticles. This discovery opened up new possibilities for tailoring plasmonic properties and exploiting them for various applications. Therefore, plasmonics is a field of

research that focuses on the interaction between light and free electrons in a metal structure, called plasmons. When light interacts with a metal nanostructure, it can excite collective oscillations of the free electrons, leading to the formation of plasmons. These plasmons can have unique properties that are different from those of individual photons or electrons, making them useful for various applications in nanophotonics and nanoelectronics.

In this case nanostructures play a crucial role in plasmonics as they can confine and manipulate plasmons at the nanoscale. By designing and engineering the size, shape, and composition of nanostructures, researchers can control the behavior of plasmons and tailor their properties for specific applications [20, 94]. Some common types of nanostructures used in plasmonics include nanoparticles, nanowires, nanorods, nanocubes, and nanoshells. These structures can be made from different metals, such as gold, silver, or aluminum, which have favorable plasmonic properties in the visible and near-infrared regions of the electromagnetic spectrum. The field of plasmonics of nanostructures is rapidly evolving, with ongoing research focused on developing new fabrication techniques, understanding fundamental plasmonic phenomena, and exploring novel applications. These advancements have the potential to revolutionize various fields, including telecommunications, biosensing, energy harvesting, and information processing [95].

Surface plasmon resonance

The physical phenomenon of surface plasmon resonance (SPR) was initially observed by Wood in 1802 and has since found practical uses in sensitive detectors that can identify protein sub-monomolecular coverage [96, 97]. SPR, has developed over the past three decades from a rather esoteric physical phenomenon to an optical tool that is frequently employed in chemical, biological, and physical studies where it is important to characterize (bio)molecular interactions. The existence of free electrons at the interface between two

materials is necessary for the creation of surface plasmons (SPs, also known as plasmon polaritons); in reality, this nearly invariably means that one of the materials is a metal (often gold) with a high concentration of free conduction electrons. This requirement simply arises from using Maxwell's equations to analyze a metal/dielectric contact.

Hence, there are many reasons why nanoparticles are interest to the scientific community. A nanoparticle matrix is used to either dissolve, trap, encapsulate, or adhere to the medication [98, 99]. One of the important properties of nanoparticles is that they exhibit SPR. When electric fields of light are directed at nanoparticles, the surface plasmons become excited and begin to resonate. This electric field also creates a separation of charge, which can be seen in Fig. 1.3, that then forms a dipole oscillation in the same direction as the electric field of light. Therefore, the frequencies being the same i.e., when the frequency of incident light matches the natural frequency of surface plasmons on a metal surface, surface plasmon resonance (SPR) enables both strong absorption and scattering of incident light, and these effects can be measured using UV-VIS spectrometers. Hence, the resonance peaks are generated at the interface media when the electron oscillation frequency and the incident light wave frequency are equal [100].

The characteristics of the particle, such as its size, form, kind of metal, and dielectric material surrounding the medium (which may include air), determine the SPR band intensity and wavelength. Although other metals like Cu have been utilized in earlier times, the band intensity is highest for Ag and Au. Ag has the strongest bands and sharpest peaks, although Au is the most often utilized material to investigate this effect since it is inert and compatible with nature.

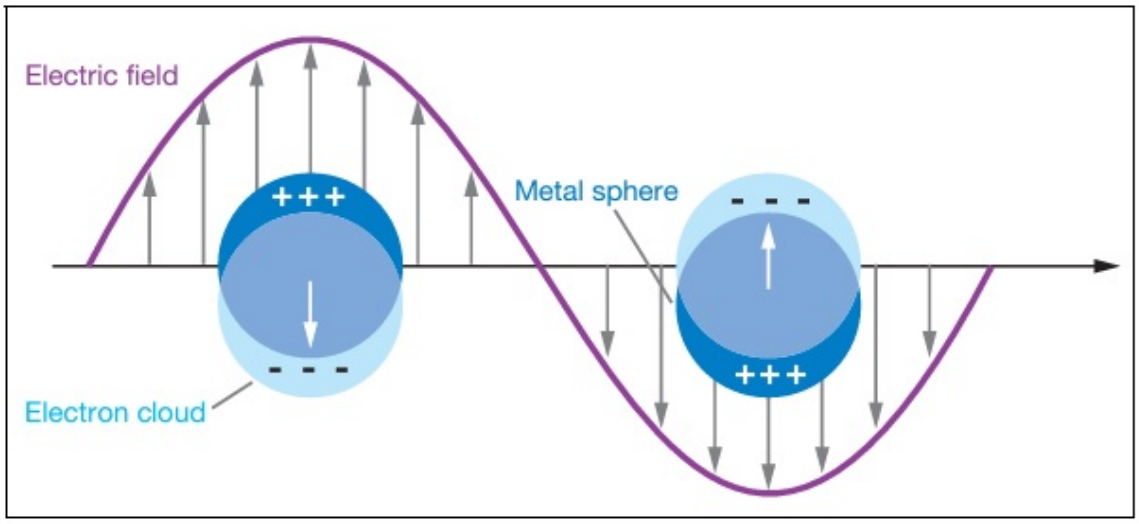

Figure 1.3: Scheme of surface plasmon resonance [93].

Local surface plasmon resonance

The optical properties of composite materials have been the subject of numerous studies during the last few decades [101]. The collective oscillation of electrons on the surface of metallic nanostructures in response to incident light is known as local surface plasmon resonance (LSPR). The "local"denotes that the plasmon resonance only applies to a small region close to the metal's surface. Hence, the LSPR describes the collective oscillation of the conduction electrons in metal nanostructures connected to an electromagnetic field on the metal-dielectric interface [102]. The nonlinearities of such materials may be strongly enhanced relative to bulk samples of the same materials, and intrinsic bistability may arise in them under certain conditions. These effects are the results of a possibly great enhancement of the electric within the particles. This enhancement can be produced by an appropriate ratio of the host to particle complex dielectric permittivity and modification of the field inside a given particle by neighboring particles. The quasistatics resonance is

an extreme manifestation of the so called local field effect.

In general, coherent oscillations of free electrons occur at the boundaries between metal and dielectric [103, 104]. Scientists may investigate the behavior of plasmons, by which they are similar in wave producing by the movement of electrons in metals, using surface plasmon resonance (SPR) and local surface plasmon resonance (LSPR) [93]. Because of this, both of them include using electromagnetic waves to excite these plasmons, in order to investigate their interactions with various materials. In scientific and medical applications, they are helpful for sensing things, determine the presence of particular chemicals or substances by detecting changes in light's behavior as it interacts with the metal structures [105].

But if we look at their distinctions, LSPR, which frequently refers to metallic nanoparticles, happens when the frequency of the incident photon is resonant with the collective oscillation of conduction electrons in metallic nanoparticles [43]. SPR is known as a phenomenon excited when the frequency of an evanescent electromagnetic wave propagating at the metal-dielectric interface is resonant with the oscillation of the surface conduction electrons in metal [106].

1.2.6 Plasmonic materials

The term "plasmonics"refers to the field's present concern in taking use of the collective oscillations of this plasma's conduction electrons [107]. A type of materials known as plasmonic materials exhibit significant nanoscale light interactions as a result of a phenomena called surface plasmon resonance (SPR). When a metal surface is stimulated by electromagnetic radiation, free electrons collectively oscillate, creating surface plasmons. However, plasmonics is a field of optical condensed matter physics that is used to investigate optical phenomena at the nanoscale in nanostructured metal systems [108, 109].

One noteworthy characteristic of these systems is their capacity to maintain the concentration of optical energy at the nanoscale, which is attributed to modes known as surface plasmons (SPs) [110]. The existence of SPs depends entirely on the fact that dielectric function ε_m has a negative real part, $Re[\varepsilon_m] < 0$. The SPs are well pronounced as resonances when the losses are small enough, i.e., $Im[\varepsilon_m] << Re[\varepsilon_m]$ [111]. This is a recognized characteristic of a high-quality plasmonic metal, such as silver throughout the majority of the visible spectrum. When two characteristics are present, a material is considered a good plasmonic metal. A type of materials known as plasmonic materials has remarkable light-interacting properties at the nanoscale because of plasmons, which are collective oscillations of free electrons [103]. These materials are usually metals, like aluminum, silver, and gold, which exhibit special optical qualities due to the way their conduction electrons behave.

Light can couple to the collective oscillations of electrons when it interacts with plasmonic materials, producing a range of fascinating effects. Plasmonic materials have uses in photonics, optoelectronics, sensing, imaging, and other domains by manipulating and controlling light behavior at the nanoscale [108, 112, 113]. The capacity of plasmonic materials to sustain surface plasmons collective electron oscillations that take place at the interface between a plasmonic material and a dielectric substance is one of their main qualities. By propagating along the surface after being activated by incident light, surface plasmons can limit electromagnetic energy to subwavelength lengths.

Because of the extreme confinement and intensification of electromagnetic fields at the nanoscale, plasmonic materials have special features like ability to concentrate light into small volumes, which can result in improved interactions between light and matter. This characteristic has been used in applications like surface-enhanced Raman spectroscopy (SERS), where the Raman signal of molecules in the vicinity can be significantly amplified

by the presence of plasmonic materials. Additionally, they are employed in the creation of nanophotonic devices, including nanoantennas, sensors, and waveguides [114–116]. All things considered, plasmonic materials have special chances for directing and modifying light at the nanoscale, opening up new possibilities in a number of industries where exact control over light-matter interactions is important.

1.2.7 Core-shell nanocomposites

Core-shell nanocomposites (CSNCs) are unique materials consisting of a shell surrounding the core. They consist of several materials, each with unique characteristics. In this manner, the nanocomposite's core and shell combine to provide new and enhanced characteristics. We may regulate and modify the material's properties by changing the size, thickness, and makeup of the shell and core [117].

There are numerous useful uses for these CSNCs [118–120]. Using a core material that is effective at catalyzing processes and a shell material that helps to maintain and protect the core, for instance, can be utilized to create better catalysts in the field of catalysis. CSNCs can be engineered to distribute and release medications in a regulated way. The core contains the medications, and it has been covered in a protective shell. Also, CSNCs have the potential to enhance supercapacitors and batteries in the energy storage sector. The shell material aids with charge movement and stability while the core material can store a significant amount of energy. The shell changes the surface and increases the sensitivity or selectivity of the sensor to particular chemicals, whereas the core functions as a sensing element. Finally, CSNCs are employed in optics to produce materials with distinct optical characteristics. The shell aids in controlling and manipulating light, whereas the core may have unique optical properties.

Researchers employ a variety of methods, such as surface modification and chemical

synthesis, to create CSNCs. By using these techniques, they are able to precisely regulate the dimensions, makeup, and structure of the shell and core, producing materials with certain qualities. All things considered, CSNCs are fascinating materials which combine various constituents to produce novel and enhanced qualities. They have a wide range of applications in various fields, where their unique properties can be harnessed to solve real-world problems and create innovative technologies [121, 122]. The characteristics and behaviors of CSNCs can be strongly influenced by size, shape, chemistry, and other factors [119]. Therefore, the following influence are related to these NCs factors:

Effects of size

Size of the core and shell materials can affect the overall size and surface area of the nanocomposite. Small core size can result in a higher surface-to-volume ratio, leading to increased reactivity or enhanced sensing properties. Size matching between the core and shell can promote better interface contact and facilitate efficient charge or energy transfer [123, 124].

The optical properties of CSNCs can be adjusted according on the size of the materials used in the shell and core. Quantum confinement effects in semiconductor core-shell nanoparticles can cause a shift in the absorption and emission wavelengths when the core size is changed. It is possible to accurately tailor the absorption and emission spectra by adjusting the size ratio between the core and shell. Furthermore, the electrical conductivity of CSNCs made of conductive materials can be influenced by the core's size. Reduced core sizes can improve electrical conductivity by promoting shorter electron transport channels and more connection. To further improve the overall conductivity, a conductive shell may also act as a barrier to stop the core nanoparticles from collecting together.

Ellipsoid-effects of shape

The optical properties of core-shell nanoparticles can be influenced by their shape. Different shapes can exhibit unique plasmonic resonances, where the localized surface plasmon resonances (LSPRs) are strongly dependent on the geometry [125]. Because of this, core-shell nanocomposites' absorption, scattering, and emission spectra can be adjusted by changing their shape, thereby opening up new possibilities for optical devices, imaging, and colorimetric sensing. A lot of work has gone into creating shape-controlled metal colloidal nanoparticles with unique chemical and physical properties in recent years [126]. The shape of the core and shell can influence the overall morphology and packing of the NCs [127, 128].

Generally, modern materials chemistry requires the ability to control a metal nanocrystal's morphology since modifying its shape and size can readily and broadly adjust its chemical and physical properties [129]. Therefore, when NCs combined appropriately, the metal nanocrystals with specific functions show great promise for a broad range of applications in electronics, photonics, catalysis, sensing, imaging, and medicine. Shape controlling metal nanocrystals is crucial in most of these applications to fully realize the potential of these amazing nanoscale materials and to optimize their performance. Anisotropic core - shell shapes, such as rods, wires, or plates, can introduce directional properties or alignment within the nanocomposite [130].

1.3 Research Questions

The main questions asked in this dissertation are:

1. What is the effect of local field on the enhancement factor in core-shell NCs in passive and active dielectric cores?

2. How the induced optical bistability can be investigated in the core-shell spheroidal NCs in passive and active dielectric cores?

3. To what extent bistability domain range found in core-shell spheroidal NCs in passive and active dielectric cores?

4. What is the effects interfacial layer on local field enhancement factor of spheroidal core-shell nanocomposite in passive and active host matrix?

1.4 Objectives

1.4.1 General objective

The general objective of the dissertation is to investigate analytically and numerically the propagation of light in spheroidal core-shell nanocomposites with passive and active dielectric cores embedded in a host matrix.

1.4.2 Specific objectives

The specific objectives of the dissertation are:

1. to study the effects of depolarization factor, metal fraction, and host matrix on the local field enhancement factor in core-shell spheroidal nanocomposites with passive and active dielectric cores.

2. to investigate the effects of depolarization factor, metal fraction, and host matrix on the induced optical bistability and bistability domain of spheroidal core-shell nanocomposites with passive and active dielectric cores.

3. to investigate the effects of interfacial layer on local field enhancement factor of spheroidal core-shell nanocomposite in passive and active host matrix.

1.5 Significance of the Study

In this dissertation, we discussed how spheroidal core-shell nanocomposite (CSNCs) with dielectric cores can have significant implications in the field of nanophotonics, particularly in obtaining local field enhancement factors and inducing optical bistability. Here are some key aspects of their significance:

In local field enhancement factor (LFEF), the depolarization factor, metal fraction, interfacial layer, and host matrix of nanoparticles influence their interaction with incident light. Spheroidal CSNCs can exhibit localized surface plasmon resonances (LSPRs), leading to enhanced electromagnetic fields in their vicinity. The LFEF quantifies the increase in the electromagnetic field strength at the nanoparticle surface. Spheroidal core-shell structures can be engineered to achieve high local field enhancement, which is crucial for various applications, including sensing, spectroscopy, and enhanced light-matter interactions [114].

Also, induced optical bistability (IOB) of core-shell nanoparticles can exhibit nonlinear optical properties, where the response of the material to light becomes dependent on the light intensity. This can lead to optical bistability, a phenomenon where the optical properties of the material depend on the history of the incident light. Optical bistability is essential for the development of devices such as optical switches and memory elements. The ability to induce and control optical bistability in spheroidal CSNCs can have applications in all-optical signal processing and information storage [131], quantum computing and communications [132–134].

In summary, the significance of this study lies in the exploration of core-shell nanoparticles, which offer superior qualities compared to single-composition nanomaterials. The potential applications of these nanoparticles span a wide range of fields, and the investigation into enhancing the local electric field and inducing optical bistability holds promise

for advancing technologies such as sensors, optical switching, and quantum computing.

1.6 Scope of the Study

The scope of this study involves the application of Drude-Sommerfeld models and quasistatic approximations to formulate electric potential equations governing the electric field distribution within spheroidal nanoparticles. The solutions to these equations are obtained by considering boundary conditions based on the shape characteristics of spheroidal core-shell nanocomposites (CSNCs) and involve considerations of Maxwell's equations. Furthermore, the study encompasses the integration of dielectric constants, depolarization factor, metal fraction, and host matrix, along with other optical properties of both passive and active materials, into the theoretical model. The ultimate goal within this scope is to derive expressions for key parameters such as the local field enhancement factor, induced optical bistability, and the bistability domain. These expressions are obtained through a theoretical model that incorporates the specified parameters. The outcome of this derivation is anticipated to contribute to the formulation of equations describing the intricate interaction of light with the nanocomposite.

Therefore, due to time constraints, the study is limited to the theoretical analysis and calculation of the local field enhancement factor, induced optical bistability, and bistability domain for the spheroidal core-shell nanocmposite with passive and active dielectric cores.

1.7 Limitations of the Study

In this dissertation study, the spheroidal form of the passive and active dielectric cores was examined in order to determine LFEF, IOB, and BD. Additionally, the passive and active host matrix were examined in order to determine LFEF. These investigations revealed a

number of constraints. Notably, the obtained result includes the metal (shell) medium's encapsulation in the host matrix, the interfacial layer between the host matrix and metal, and the encapsulation of dielectric cores in metals. To achieve results from the core-sheel, and interfacial layers, it all takes time. Consequently, the primary limitation of this study was the time constraints imposed during the analysis, hypothesis formulation, and manuscript preparation for publication. As a consequence of this time constraint, we did not extend our investigation to include other shapes, such as cylindrical, and others within both passive and active dielectric cores.

1.8 Structure of the Dissertation

The dissertation consists of 5 chapters. It is organized as follows:

- Chapter 2: Investigates the effects of depolarization factor, metal fraction, and permittivity of the host matrix on the local field enhancement factor of spheroidal core-shell nanocomposites with passive and active dielectric cores. Under this chapter, we also investigate the effects of depolarization factor, metal fraction, and dielectric function host matrix of the core on LFEF of core-shell NCs.

- Chapter 3: Discusses the effects of depolarization factor, metal fraction, and permittivity of the host matrix on induced optical bistability and bistability domain in spheroidal core-shell NCs with passive and active dielectric cores. We also describe the impacts of depolarization factor, metal fraction, and dielectric function host matrix of the core on IOB and BD of core-shell NCs.

- Chapter 4: Describes the effects of interfacial layer on enhancement factor of local field in spheroidal core-shell NCS in passive and active host matrix. Additionally,

the consequence of thickness, radius, metal fractions, and depolarization factorwith or without an interfacial layer on LFEF in spheroidal NCs in passive and active host matrix was investigated.

- Chapter 5: This chapter provides an overview of all the study findings and suggests areas for further investigation in the future.

Chapter 2

Local Field Enhancement Factor of Spheroidal Core-Shell Nanocomposite with Passive and Active Dielectric Cores

This chapter is based on published article in Materials Research Express:

> *Hirpha, Tolasa Tamasgen et al., "Local Field Enhancement Factor of Spheroidal Core-Shell Nanocomposite with Passive and Active Dielectric Cores", Mater. Res. Express 10(4), 045005: 1-8. https://doi.org/10.1088/2053-1591/accb2d.*

2.1 Introduction

Recently, the study of nanoparticles have attracted the attention of many scientists worldwide. When light interacts with such nanoparticles, their optical properties are considerably different from their corresponding bulk structures [135]. The optical responses of metal coated core-shell nanoparticles are governed by oscillations of the surface electrons in the electrical potential made by the positively charged ionic core [136]. It has been shown that metals have fast and strong nonlinear response [137, 138], and if combined with dielectrics

[139, 140], they are good candidates for various applications in different fields of science and technology [141, 142] such as nonlinear optics [143]. Furthermore, many innovative concepts and applications of such nanocomposite materials have been developed over the past few years [118, 119, 144, 145]. To control light by light in the systems, combining metals with dielectrics has two main purposes[146]. One is allowing light to enter more deeply into metals, and this can be achieved by canceling reflections at interference. The other is achieving light localization which in turn leads to an enhanced nonlinear response [64, 147, 148].

During the last three decades, the optical properties of nanoparticles have been widely studied in various ways. Among these, core-shell NCs are found to have vast applications in different fields of science and technology [149]. It is also found that the optical properties of dielectric core-metallic shell NCs are strongly dependent on the size, metal fraction, spatial distribution of the core-shell structure, and the embedding medium [150–153]. Other research evidences further demonstrated that although size and embedding medium are important parameters, the surface plasmon resonances of the core-shell nanoparticles depend much more sensitively on the particle shapes [32, 154, 155]. Hence, changing the shape of core-shell NCs is an alternative way to tune the resonances of surface plasmons and hence their optical properties. Due to their geometric shape providing tunability of their optical properties, spheroidal core-shell NCs have attracted significant interest [156, 157]. Since such geometry supports plasmon resonances, spheroidal core-shell NCs composed of a dielectric core coated by a metallic shell is one of the most useful structure for wider tunability range from the visible to infrared regions of electromagnetic spectrum [158, 159].

However, many of the studies conducted so far focused on spherical and cylindrical core-shell NCs [160, 161]. In other studies, researchers investigated plasmonic properties of

spheroidal core-shell nanoparticles such as extinction, absorption, scattering cross sections, and field enhancement factor as a function of parameters angle, wavelength, and distance from the center [45]. For coated spheroidal NCs, the effect of depolarization factor and the surrounding dielectric constant on the optical bistability and absorption spectra has been studied [47, 162]. To the best of our knowledge, the effect of passive and active dielectric cores on local field enhancement factor (LFEF) has not been largely investigated for spheroidal core-shell NCs. Thus, in the present study, we theoretically and numerically investigated the effects of passive and active dielectric cores, metal fraction, and host matrices on the LFEF of dielectric core-metallic shell spheroidal NCs.

2.2 Theoretical Models and Calculations

We considered spheroidal core-shell nanocomposite in the quasistatic approximation. To investigate its effect on LFEF, the dielectric function of the core was taken to be either passive or active. The dielectric function, ε_d of the core is called passive or active depending on the response of the material to the applied electric field. This dielectric function can be written as [163]:

$$\varepsilon_d = \varepsilon_d^{'} + i\varepsilon_d^{''}, \tag{2.2.1}$$

where $\varepsilon_d^{'}$ and $\varepsilon_d^{''}$ are the real and imaginary parts of the dielectric function of the core material, respectively. When $\varepsilon_d^{''} = 0$, the core's dielectric function will be passive and when $\varepsilon_d^{''} < 0$, it will be active. In this study, both components of the dielectric functions were separately considered.

2.2.1 Electric potential distribution in spheroidal core-shell nanocomposite

Using spheroidal core-shell NCs, it is possible to investigate spherical and cylindrical core-shells by limiting cases [164]. However, our approach in the present work is the reverse of this. By applying boundary conditions and solving the Laplace's equations for spherical core-shell NCs, the electric potential distributions in the core, shell, and host matrix were obtained. Then, by employing the depolarization factors, we obtained the corresponding equations for a system of spheroidal nanocomposites.

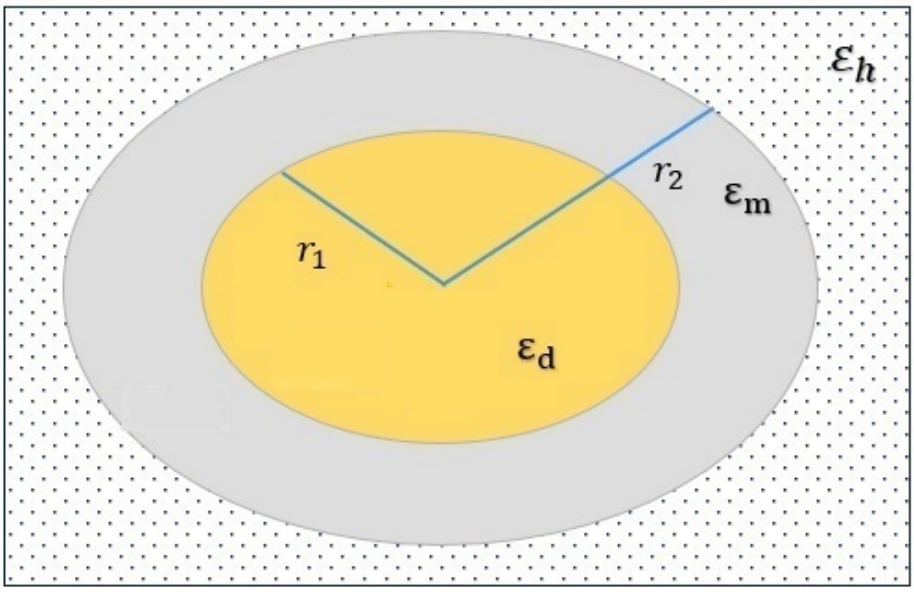

Figure 2.1: Schematic representation of spheroidal core-shell NCs. The dielectric constants of the core (active or passive), shell, and host matrix are denoted by ε_d, ε_m, ε_h, respectively.

Consider the core-shell nanocomposite shown in Fig. 2.1, where the dielectric core has a radius r_1 and dielectric permittivity ε_d. The shell is characterized by the radius r_2 and dielectric permittivity ε_m (where $r_1 < r_2$). The host material has an electric permittivity ε_h. Then, the electric potential distribution in the dielectric core (Φ_d), metallic shell (Φ_m),

and host matrix (Φ_h) are, respectively, given by [42]:

$$\Phi_d = -E_0 A r \cos\theta, \quad r \leq r_1, \tag{2.2.2}$$

$$\Phi_m = -E_0 \left(Br - \frac{C}{r^2} \right) \cos\theta, \quad r_1 \leq r \leq r_2, \tag{2.2.3}$$

$$\Phi_h = -E_0 \left(r - \frac{D}{r^2} \right) \cos\theta, \quad r > r_2, \tag{2.2.4}$$

where E_0 is the applied electric field, r and θ are the spherical coordinates of the observation point (the z-axis, chosen along the vector E_0), A, B, C, and D are unknown coefficients to be calculated using the continuity equations of the electric potential and displacement vector at the boundaries between core-shell and shell-host matrix interfaces. At the boundary between the dielectric core and the metallic shell, the potentials must satisfy the following boundary conditions [43]:

$$\Phi_d = \Phi_m \mid_{r=r_1} . \tag{2.2.5}$$

Substituting Eqns. (2.2.2) and (2.2.3) into Eqn. (2.2.5), and simplifying, we obtain:

$$A = B - \frac{C}{r_1^3}. \tag{2.2.6}$$

Similarly, at the boundary between the metallic shell and the host matrix, the equation for the potentials can be written as:

$$\Phi_m = \Phi_h \mid_{r=r_2} . \tag{2.2.7}$$

Now, substituting Eqns. (2.2.3) and (2.2.4) into Eqn. (2.2.7), we found the expression which relates the coefficients B, C, and D as follows:

$$B - \frac{C}{r_2^3} = 1 - \frac{D}{r_2^3}. \tag{2.2.8}$$

The continuity equations for the displacement vector at the interfaces are given by

$$\frac{1}{r_1}\frac{\partial \Phi_d}{\partial \theta}\bigg|_{r=r_1} = \frac{1}{r_1}\frac{\partial \Phi_m}{\partial \theta}\bigg|_{r=r_1}, \tag{2.2.9}$$

$$\frac{1}{r_2}\frac{\partial \Phi_m}{\partial r}\bigg|_{r=r_2} = \frac{1}{r_2}\frac{\partial \Phi_h}{\partial \theta}\bigg|_{r=r_2},$$

$$\varepsilon_d \frac{1}{r_1}\frac{\partial \Phi_d}{\partial r}\bigg|_{r=r_1} = \varepsilon_m \frac{1}{r_1}\frac{\partial \Phi_m}{\partial \theta}\bigg|_{r=r_1}, \tag{2.2.10}$$

$$\varepsilon_m \frac{1}{r_2}\frac{\partial \Phi_m}{\partial r}\bigg|_{r=r_2} = \varepsilon_h \frac{1}{r_2}\frac{\partial \Phi_h}{\partial \theta}\bigg|_{r=r_2},$$

By substituting Eqns. (2.2.2)-(2.2.4) into Eqns. (2.2.9) and (2.2.10) and simplifying, we obtain

$$A\varepsilon_d = \varepsilon_m\left(B + 2\frac{C}{r_1^3}\right), \tag{2.2.11}$$

and

$$\varepsilon_m\left(B + \frac{2C}{r_2^3}\right) = \varepsilon_h\left(1 + \frac{2D}{r_2^3}\right). \tag{2.2.12}$$

By introducing the depolarization factor L into equations of spherical shape, i.e., Eqns. (2.2.11) and (2.2.12), the equivalent equations for spheroidal shape can respectively be given by

$$LA\varepsilon_d = \varepsilon_m\left[LB + (1-L)\frac{C}{r_1^3}\right], \tag{2.2.13}$$

and

$$L\varepsilon_m B + \varepsilon_m(1-L)\frac{C}{r_2^3} = \varepsilon_h\left[L + (1-L)\frac{D}{r_2^3}\right]. \tag{2.2.14}$$

Now, by substituting Eqn. (2.2.6) into Eqn. (2.2.13), the expression for B is obtained to be

$$B = \frac{C}{r_1^3}\frac{(1-L)\varepsilon_m + L\varepsilon_d}{L(\varepsilon_d - \varepsilon_m)}, \tag{2.2.15}$$

If we substitute the expression for B in Eqn. (2.2.15) into Eqn. (2.2.8), the equation that relates C and D can be written as

$$\frac{C}{r_1^3}\frac{L\varepsilon_d + \varepsilon_m(1-L) - (1-p)(L\varepsilon_d - L\varepsilon_m)}{L(\varepsilon_d + \varepsilon_m)} = 1 - \frac{D}{r_2^3}, \tag{2.2.16}$$

where $p = 1 - (r_1/r_2)^3$.

Furthermore, by substituting Eqn. (2.2.15) into Eqn. (2.2.14), we obtain

$$\frac{C}{r_1^3}\frac{\varepsilon_m^2 L(1-L) + L^2\varepsilon_m\varepsilon_d + L(\varepsilon_d + \varepsilon_m)(1-L)(1-p)\varepsilon_m}{L(\varepsilon_d + \varepsilon_m)} = L\varepsilon_h + \varepsilon_h(1-L)\frac{D}{r_2^3}, \tag{2.2.17}$$

The ratio of eqns. (2.2.16) and (2.2.17) leads to

$$\frac{\varepsilon_m + Lp(\varepsilon_d - \varepsilon_m)}{(L)\varepsilon_d\varepsilon_m(1-p) + Lp\varepsilon_m(\varepsilon_d - \varepsilon_m) + p\varepsilon_m^2} = \frac{1 - \frac{D}{r_2^3}}{L\varepsilon_h + \varepsilon_h(1-L)\frac{D}{r_2^3}}. \tag{2.2.18}$$

Hence, the expressions for the unknown coefficients A, B, C, and D of Eqns. (2.2.2)-(2.2.4) can be summarized as follows:

$$A = \frac{\varepsilon_h\varepsilon_m}{La + b\varepsilon_h(1-L)}, \tag{2.2.19}$$

$$B = \frac{\varepsilon_h\big(L\varepsilon_d + \varepsilon_m(1-L)\big)}{La + b\varepsilon_h(1-L)}, \tag{2.2.20}$$

$$\frac{C}{r_1^3} = \frac{(\varepsilon_d - \varepsilon_m)\varepsilon_h L}{La + b\varepsilon_h(1-L)}, \tag{2.2.21}$$

$$\frac{D}{r_2^3} = \frac{(a - b\varepsilon_h)L}{La + b\varepsilon_h(1-L)}, \tag{2.2.22}$$

where

$$a = \varepsilon_m\varepsilon_d - p\varepsilon_m(\varepsilon_d - \varepsilon_m) + Lp\varepsilon_m(\varepsilon_d - \varepsilon_m) \quad \text{and} \quad b = \varepsilon_m + Lp(\varepsilon_d - \varepsilon_m).$$

From the Drude-Sommerfeld model, the dielectric function of the metal (ε_m) is given by [165]:

$$\varepsilon_m = \varepsilon_\infty - \frac{1}{z(z+i\gamma)}, \tag{2.2.23}$$

where ε_∞ describes the contribution of bound electrons to polarizability, $z = \omega/\omega_p$, $\gamma = \nu/\omega_p$ (ω_p and ω are the plasma frequency of the bulk and the frequency of the incident radiation, respectively), ν is the electron damping constant. Moreover, the real and imaginary parts of ε_m can be rewritten as

$$\varepsilon_m = \varepsilon_m^{'} + i\varepsilon_m^{''}, \tag{2.2.24}$$

where

$$\varepsilon_m^{'} = \varepsilon_\infty - \frac{1}{z^2+\gamma^2} \quad \text{and} \quad \varepsilon_m^{''} = \frac{\gamma}{z(z^2+\gamma^2)}.$$

2.2.2 Local field enhancement factor of spheroidal core-shell nanocomposite

Since we are using the quasi-static approach, the electric field E_0 (assumed to be directed along the z-axis) is uniform. Then, by using the relation $E = -\nabla\Phi$, the local field in the dielectric core E_d of the spheroidal nanocomposite can be written as [166]:

$$E_d = -\nabla\Phi_d = AE_0, \tag{2.2.25}$$

where A is the complex function given by Eqn. (2.2.19). The real quantity, $|A|^2$, is known as the local field enhancement factor (LFEF). If we substitute Eqn. (2.2.24) into Eqn. (2.2.19), squaring it and simplifying, we find the LFEF in the dielectric core to be:

$$\mid A \mid^2 = \frac{\varepsilon_h^2(\varepsilon_m^{'2} + \varepsilon_m^{''2})}{\Big(La_1 + a_3\varepsilon_h(1-L)\Big)^2 + \Big(La_2 + a_4\varepsilon_h(1-L)\Big)^2}, \tag{2.2.26}$$

where

$a_1 = \varepsilon_m^{'}\varepsilon_d^{'}(1-p+Lp) + [\varepsilon_m^{'2} - \varepsilon_m^{''2}](p-Lp),$

$a_2 = \varepsilon_m^{''}\varepsilon_d^{''}(1-p+Lp) + 2\varepsilon_m^{'}\varepsilon_m^{''}(p-Lp),$

$a_3 = \varepsilon_m^{'}(1-Lp) + Lp\varepsilon_d^{'}$

$a_4 = \varepsilon_m^{''}(1-Lp) + Lp\varepsilon_d^{''}.$

2.3 Results and Discussions

We studied the effect of passive and active dielectric cores on LFEF of spheroidal core-shell NCs by varying the depolarization factor (L), metal fraction (p), and dielectric function of the host matrix (ε_h). The observed effects of those parameters and findings of the study were discussed accordingly and presented below. For numerical evaluations, the following parameter values are used: (i) for the host matrix $\varepsilon_h = 1$ [166], (ii) for the silver shell ($\varepsilon_\infty = 4.5$, $\omega_p = 1.45 \times 10^{16}\ rad/s$, $\nu = 1.67 \times 10^{14}\ rad/s$ [86, 167]), and (iii) for the dielectric core $\varepsilon_d^{'} = 2.25$, $\varepsilon_d^{''} = 0$ (for passive) and $\varepsilon_d^{''} = -0.13866$ (for active) [41].

2.3.1 The effect of dielectric function of the core on LFEF of core-shell nanocomposite

To investigate the effect of passive and active dielectric core on the LFEF of spheroidal core-shell NCs, all other parameters such as depolarization factor, metal fraction, dielectric constants of the metallic shell, and that of the host matrix were kept constant, we plot using Eqn. (2.2.26). Then, to see the effect, the dielectric function of the core was made passive and active alternately. Under these conditions, the study shows that the LFEF of the spheroidal core-shell NCs posses two peaks with the passive dielectric cores whereas only one peak is observed with active dielectric core (Figs. 2.2(a) and (b)). As the depolarization

factor increases from 0.34 to 0.42 equally in both passive and active core, the first set of peaks (counted from left to right) of LFEF of the spheroidal core-shell NCs show similar patterns both in passive and active dielectric core. However, all peaks of LFEF were more pronounced in the passive dielectric core than its corresponding active core. This may indicate that passive dielectric core is preferable to the active one when higher and two sets of peaks of local filed enhancement factors are required.

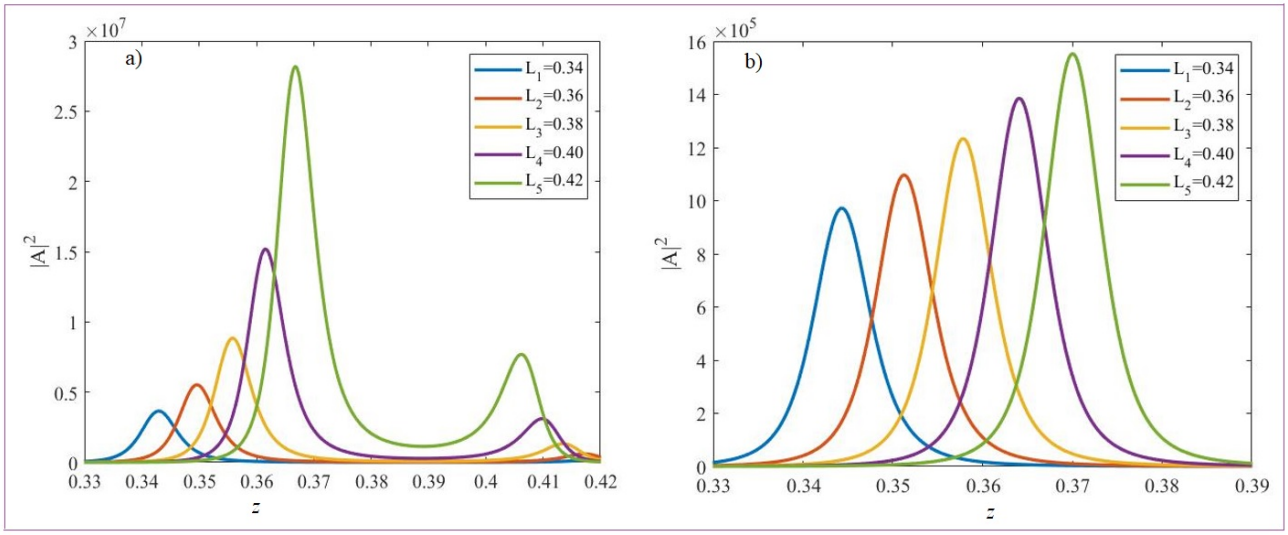

Figure 2.2: LFEF of the spheroidal core-shell NCs: (a) in passive dielectric core and (b) in active dielectric core with $\varepsilon_h = 1$, $p = 0.99$, $\varepsilon_\infty = 4.5$, $\varepsilon_d^{'} = 2.25$, $\varepsilon_d^{''} = -0.13866$, and $\gamma = 0.0115$.

The nanocomposite with passive dielectric core, although the first and the second sets of the corresponding peaks of LFEF increase with increase in depolarization factor, the intensities of the first peaks are comparatively larger (Fig. 2.2(a)). This might be attributed to the case that the core holds the applied field as the field passes from the metallic shell to the dielectric core. From this figure, it is observed that with an increase in the depolarization factor, the first and the second sets of peaks are blue shifted (towards larger z or shorter λ) and red shifted (towards smaller z or longer λ), respectively. This caused

the horizontal positions between the corresponding peaks of the LFEF to become closer to each other. It is worth noting that our findings on Fig. 2.2(a) is similar to the previous study showing that LFEF possesses two peaks when the dielectric core with real dielectric function (passive) is considered in metal coated spheroidal core-shell NCs [164]. Hence, the

Table 2.1: Effects of depolarization factor, (L) and its LFEF value for of spheroidal core-shell NCs in passive core (PC) and active core (AC).

	Approximate value of $\chi\|E_h\|^2$	
Depalization factor, L	$1^{st}$and 2^{nd} peak in PC ($\times 10^6$)	in AC ($\times 10^6$)
0.34	3.630 (0.2226)	0.9700
0.36	5.496 (0.5877)	1.096
0.38	8.838 (1.332)	1.233
0.40	15.17 (3.169)	1.381
0.42	28.10 (7.650)	1.550

number and the intensities of peaks of LFEF of spheroidal core-shell NCs vary greatly in the same material when its core is made passive and active dielectric.

2.3.2 The effect of metal fraction on LFEF of spheroidal core-shell NCs

Next, we considered the effect of metal fraction on the LFEF core-shell NCs. For the same parameters, the LFEF of spheroidal core-shell NCs vary with the metal concentration both with passive and active dielectric cores were plotted using Eqn. (2.2.26), as shown in (Figs. 2.3(a) and (b)). It shows that when the metal fraction of spheroidal core-shell NCs with passive dielectric core increases, the intensities of peaks of the first set of LFEF increases and are blue shifted. Similarly, the peaks of the second set also increases in intensity, however, they are slightly red shifted (Fig. 2.3(a)).

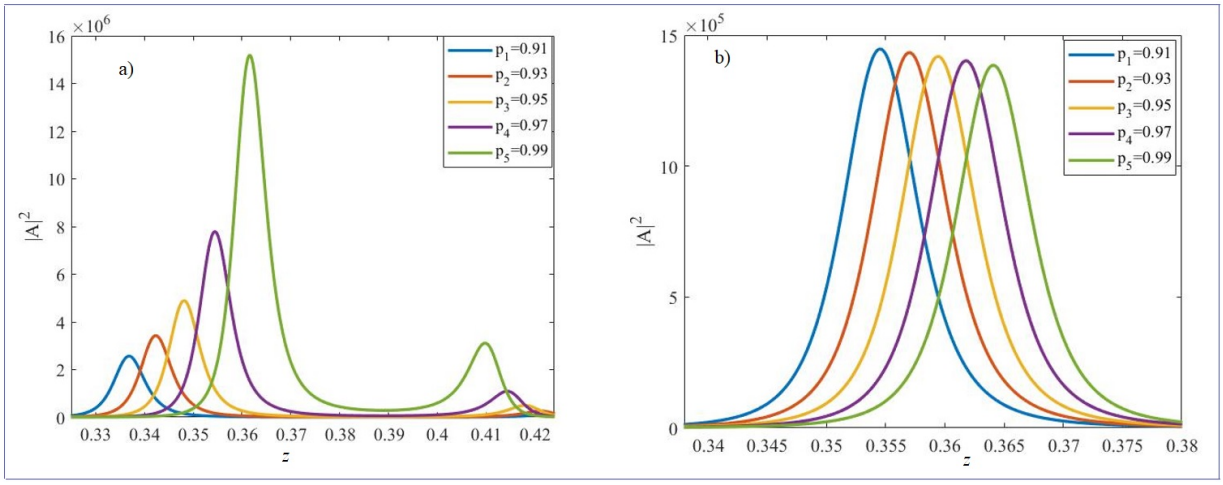

Figure 2.3: The effect of the metal fraction on LFEF of spheroidal core-shell NCs: (a) in passive dielectric core and (b) in active dielectric core with $\varepsilon_h = 1$, $L = 0.40$, $\varepsilon_\infty = 4.5$, $\varepsilon_d^{'} = 2.25$, $\varepsilon_d^{''} = -0.13866$, and $\gamma = 0.0115$.

We have seen that for a constant metal fraction ($p = 0.99$) and the same change in depolarization factor, peaks of LFEF varies in number and intensities in NCs with passive dielectric core (Fig. 2.2(a)). On the other hand, when the metal fraction p is changed uniformly from 0.91 to 0.99 for the same depolarization factor ($L = 0.40$), the patterns of the LFEF observed in Fig. 2.3(a) is similar to the pattern observed in Fig. 2.2(a), but their intensities were about ten times larger in Fig. 2.2(a). Similarly, when Figs. 2.2(b) and 3(b) are compared, the patterns of the LFEF observed seem to be similar. Yet, larger intensities were noticed when the depolarization factor increases than does the metal fraction. When the depolarization factor changes, obviously the geometry of the spheroidal core-shell NCs also changes. This might indicate that the change in the geometry of the spheroidal core-shell NCs has larger effect in increasing the LFEF than the metal concentration. These results are in agreement with that reported in Ref. [168].

Furthermore, when the dielectric core becomes active (perturbed by an incident field),

Table 2.2: Effects of metal fraction, (p) and its LFEF value for of spheroidal core-shell NCs in passive core (PC) and active core (AC).

	Approximate value of $\chi\|E_h\|^2$	
Metal fraction, p	$1^{st}$and 2^{nd} peak in PC ($\times 10^6$)	in AC ($\times 10^6$)
0.91	2.553 (0.1396)	1.447
0.93	3.422 (0.2556)	1.433
0.95	4.884 (0.4915)	1.416
0.97	7.783 (1.072)	1.402
0.99	15.18 (3.101)	1.385

the peak values of the LFEF in the core-shell structure increase with increase in the depolarization factor provided that the metal fraction is kept constant (Fig. 2.2(b)). However, when the metal fraction increases at constant depolarization factor, the peak values tend to decrease (Fig. 2.3(b)). Hence, it is observed that the depolarization factor and the metal fraction show different effects on the LFEF of spheroidal core-shell NCs with active dielectric core. Moreover, for the system of nanocomposites considered, whether the depolarization or metal fraction varies, only a single peak is observed when the core is active dielectric.

Hence, we found that when the core of the metallic shell of the spheroidal core-shell NCs is made active, it seems that the whole system behaves like a metal nanoparticle. However, when the dielectric core is passive, two peaks of the LFEF were observed for spheroidal core-shell NCs.

2.3.3 The effect of the host matrix on LFEF of spheroidal core-shell NCs

Finally, by using Eqn. (2.2.26), we investigated the effect of the dielectric function of the host matrix on the LFEF of the spheroidal core-shell NCs with passive and active dielectric

cores. For, the NCs with passive dielectric core, it is observed that the intensities of the LFEF decrease with increase in the dielectric function of the host matrix (Fig. 2.4(a)).

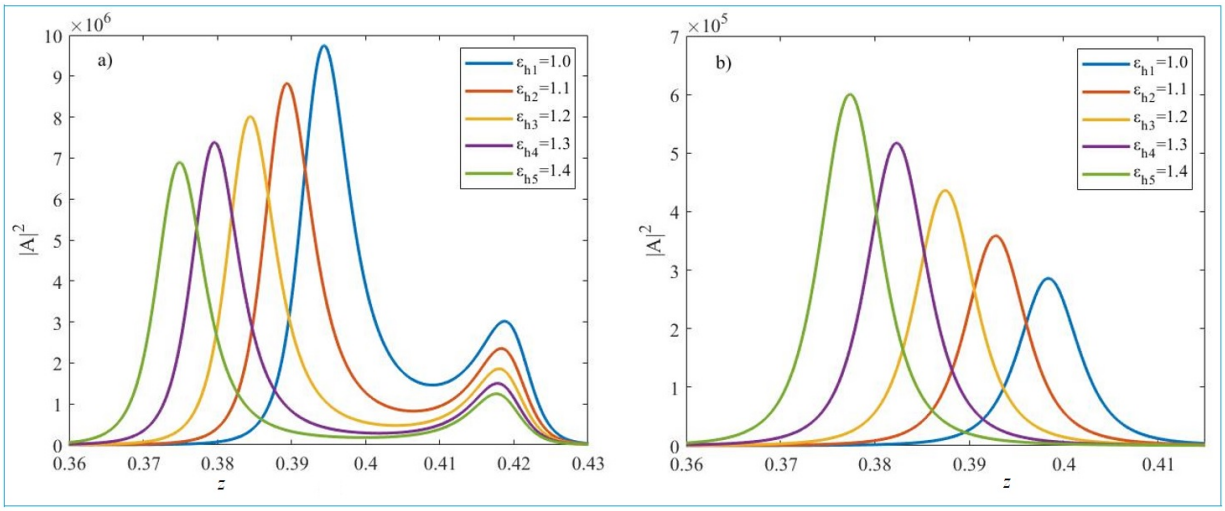

Figure 2.4: The effect of the host matrix on LFEF of spheroidal core-shell NCs: (a) in passive dielectric core and (b) in active dielectric core with $L = 0.36$, $p = 0.99$, $\varepsilon_\infty = 4.5$, $\varepsilon_d^{'} = 2.25$, $\varepsilon_d^{''} = -0.1386$, and $\gamma = 0.0115$.

Moreover, for the same increase in the dielectric function of the host material, the first set of peaks (counted from left to right) of LFEF were red shifted, while the second peaks show no shifts (Fig. 2.4(a)). When the dielectric function of the host matrix increases while L and p are kept constant, the peaks of the LFEF are red shifted (Fig. 2.4(b)). The result also show that the effect of dielectric function of the host material on the LFEF is different in passive and active dielectric core of the spheroidal core-shell NCs. That is, for the same increase in the dielectric function of the host matrix, the intensity of LFEF, respectively, decreases and increases when the dielectric core is made to be passive and active (Figs. 2.4(a) and (b)). Comparing Figs. 2.3(a) with 2.4(a), and 2.3(b) with 2.4(b), it is seen that the metal fraction and dielectric function of the host matrix have reverse effects on the LFEF of spheroidal core-shell NCs. Generally, the results agree with other

Table 2.3: Effects of host matrix, (ε_h) and its LFEF value for of spheroidal core-shell NCs in passive core (PC) and active core (AC).

	Approximate value of $\chi\|E_h\|^2$	
Permitivity of host matrix, ε_h	$1^{st}$and 2^{nd} peak in PC ($\times 10^6$)	in AC ($\times 10^5$)
1.0	9.726 (3.014)	2.858
1.1	8.823 (2.343)	3.585
1.2	8.017 (1.853)	4.356
1.3	7.381 (1.499)	5.161
1.4	6.893 (1.254)	6.004

research findings in that varying the dielectric functions of the surrounding medium plays an important role in determining the resonance positions of the field emissions in core-shell nanostructures [169–171].

2.4 Conclusions

We investigated the effect of passive and active dielectric cores on the LFEF of spheroidal core-shell NCs by varying L, p, and ε_h. The results show that whether L, p, or ε_h vary or kept constant, the LFEF of the spheroidal core-shell NCs possesses two sets of peaks in NCs with passive dielectric core whereas only one set of peak is observed in the NCs with active dielectric core. In addition, the two peaks observed in spheroidal core-shell with passive dielectric core, the first set of peaks are more pronounced than the second, indicating that passive dielectric core is preferable to the active one when higher and two sets of peaks of LFEF are required. We also found that as L increases, the peaks of LFEF are increased and blue shifted in both passive and active dielectric cores.

Moreover, when p in the passive dielectric core increases, the intensities of the peaks of the first set of LFEF increases and are blue shifted. Similarly, the second set of peaks also increases in intensity, however, they are slightly red shifted. Yet, larger intensities were

noticed when L increases than does p, indicating that change in the geometry of spheroidal core-shell NCs has larger effect in increasing the LFEF than the metal concentration.

Furthermore, with an increase in ε_h, the intensity of the LFEF decreases when the dielectric core is passive and increases when the core is active. Moreover, when ε_h increases while keeping L and p constant, the peaks of the LFEF are red shifted in the spheroidal NCs with both types of dielectric cores. For the same increase in ε_h, the intensity of the LFEF decreases and increases when the dielectric core is passive and active, respectively. For spheroidal core-shell NCs with active dielectric core, increasing L and ε_h increases the peak intensities of the LFEF, however, the peak positions are reversed. Moreover, p and ε_h have reverse effects on the LFEF of the spheroidal core-shell NCs. We found that the peak values of the LFEF of the spheroidal core-shell NCs can be tuned by changing the depolarization factor, metal fraction, and dielectric function of the host medium of the NCs. Moreover, the number and the intensities of these peaks vary significantly when its dielectric core is made passive than active. Hence, by changing these parameters and types of dielectric cores, adjustable LFEF of spheroidal core-shell NCs could be obtained and used for applications in optical sensing, nonlinear optics, and quantum optics.

Chapter 3

Investigation of Optical Bistability in Spheroidal Core-Shell Nanocomposites with Passive and Active Dielectric Cores

This chapter is based on published article in AIP Advances:

> *Hirpha, Tolasa Tamasgen et al., "Investigation of Optical Bistability in Spheroidal Core-Shell Nanocomposites with Passive and Active Dielectric Cores", AIP Advances 14, 015037: 1-9. https://doi.org/10.1063/5.0180907.*

3.1 Introduction

One of the most rapidly developing areas of condensed matter physics and nanotechnology nowadays is the control of light at the nanoscale [172]. Devices of nonlinear optics are one of the various types of nanosized particles, and induced optical bistability (IOB) is one of them. IOB is particularly fascinating since it can be applied to optical computers, quantum information, optical detectors, optical transistors, and other applications [37]. Moreover,

IOB refers to the circumstance in which two distinct output intensities are obtained for a given input intensity. Additionally, IOB can be used to monitor light by the light itself. This implies that, depending on whether an optical property is caused by the intrinsic properties of the optical device or by external feedback, it may have two different values at high incidence intensities [173]. Furthermore, the observed bistability effects may be caused by a significant enhancement of the electric field within the particles, which can be brought about by a suitable ratio of the host to particle dielectric permittivity, modification of the field within a particular particle by its environment, and surface plasmon resonance [174, 175]. Hence, it is desirable to investigate and comprehend the optical bistable properties of nanoscale optical devices before designing them for real-world applications.

To address this, IOB in nanostructures has been studied and investigated theoretically and experimentally by different scholars [36, 46, 176, 177]. It was also shown that nanoparticles with metallic shell coatings display optical bistability over a wider range of incident light intensities [178]. Moreover, the size, spatial distribution, and makeup of the surrounding host matrix can all affect the properties of nanoparticles [179]. IOB also largely depends on the geometry of the shell-coated nanoparticle, particularly the volume fraction of the metallic core [42]. Careful monitoring and design over these parameters can make nanocomposites (NCs) a promising medium for the development of novel nonlinear materials in nanodevices and optical elements. [150].

To study the effects of shape, size, composition structure, and spatial distributions of NCs on the IOB, wide ranging researches have been conducted [86, 180–182]. However, the majority of these researches focused on spherical or cylindrical core-shell NCs and no enough spheroidal core-shell geometry were considered. Even where the IOB property of ellipsoidal core-shell nanocomposite was investigated [183], the effects of active and passive

dielectric cores were given no attention. Previous studies show that the dielectric material as a core coated with metals are used to study the optical bistabllity property of core-shell NCs [37, 184–186]. By the utilization of electromagnetic field enhancement effects, noble metals such as silver has been used to study the bistable response and the nonlinear effects of NCs [109]. Hence, using dielectric function (passive and active) as a core and silver metal as a shell in different external embedding medium, we investigated the effects of depolarization factor (L), metal fraction (p), and dielectric permittivity (ε_h) of host matrix on induced optical bistability (IOB) and bistability domains (BD) of spheroidal core-shell NCs in active and passive dielectric cores.

3.2 Theoretical Model and Calculations

Based on the quasistatic approach [187], we proposed a model shown in Fig. 3.1 and investigated its OB theoretically and numerically. To obtain the optical bistable behavior [185], we considered a spheroidal core-shell NCs with dielectric core of radius r_1 and dielectric permittivity ε_d. The shell (Ag) has a radius r_2 and a field dependent dielectric permittivity ε_m. The whole nanocomposite is embedded in a dielectric host matrix of dielectric function ε_h and is illuminated with incident electromagnetic radiations. The dielectric function, ε_d, of the core is called passive or active depending on the response of the material to the applied electric field. This dielectric function can be written as [163]:

$$\varepsilon_d = \varepsilon_d^{'} + i\varepsilon_d^{''}, \tag{3.2.1}$$

where $\varepsilon_d^{'}$ and $\varepsilon_d^{''}$ are the real and imaginary parts, respectively. If $\varepsilon_d^{'} > 0$ and $\varepsilon_d^{''} = 0$, the dielectric is passive; whereas $\varepsilon_d^{'} = 0$ and $\varepsilon_d^{''} < 0$, is active dielectric function.

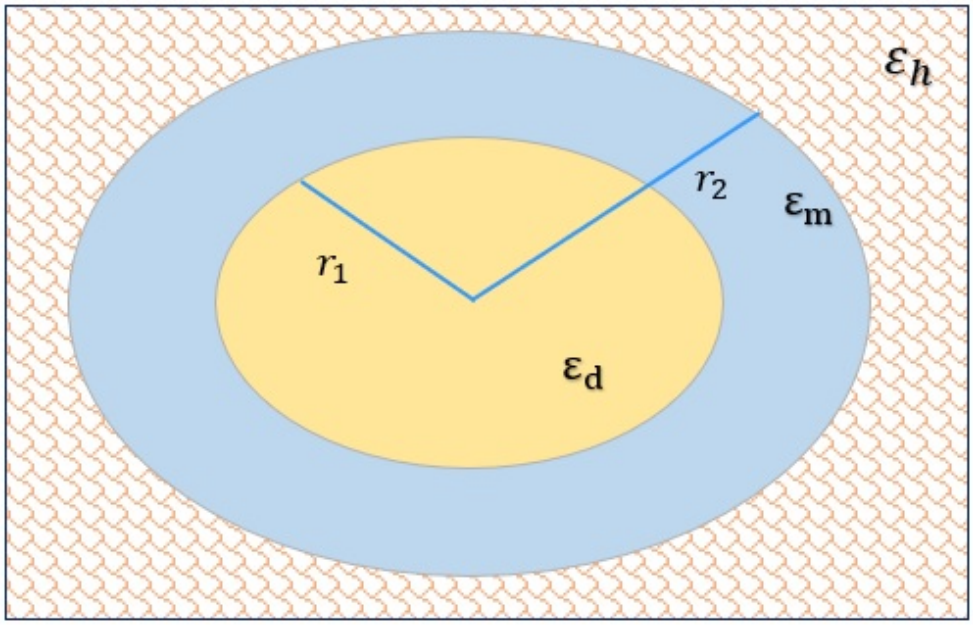

Figure 3.1: Schematic representation of spheroidal core-shell NCs.

3.2.1 Induced optical bistability of spheroidal core-shell nanocomposites

To investigate the IOB of spheroidal core-shell NCs, it is worth considering the electric potential distributions in the different regions of the nanocomposite. Referring to Fig. 3.1, the electric potential distribution in the dielectric core (Φ_d), metallic shell (Φ_m), and host matrix (Φ_h) are, respectively, given by [78, 188]:

$$\Phi_d = -E_h A r \cos\theta, \quad r \leq r_1, \tag{3.2.2}$$

$$\Phi_m = -E_h \left(Br - \frac{C}{r^2} \right) \cos\theta, \quad r_1 \leq r \leq r_2, \tag{3.2.3}$$

$$\Phi_h = -E_h \left(r - \frac{D}{r^2} \right) \cos\theta, \quad r > r_2, \tag{3.2.4}$$

where E_h is the external incident electromagnetic field, r and θ are the spherical coordinates (the z-axis, chosen along the vector E_h), A, B, C, and D are unknown coefficients to be determined using the appropriate boundary conditions at the interfaces. Hence, it can be shown that [189]:

$$A = \frac{\varepsilon_h \varepsilon_m}{La + b\varepsilon_h(1-L)}, \tag{3.2.5}$$

$$B = \frac{\varepsilon_h\big(\varepsilon_m + L(\varepsilon_d - \varepsilon_m)\big)}{La + b\varepsilon_h(1-L)}, \tag{3.2.6}$$

$$C = \frac{(\varepsilon_d - \varepsilon_m)\varepsilon_h L}{La + b\varepsilon_h(1-L)} r_2^3, \tag{3.2.7}$$

$$D = \frac{(a - b\varepsilon_h)L}{La + b\varepsilon_h(1-L)} r_2^3, \tag{3.2.8}$$

where

$$a = \varepsilon_m\varepsilon_d - p\varepsilon_m(\varepsilon_d - \varepsilon_m) + Lp\varepsilon_m(\varepsilon_d - \varepsilon_m), \tag{3.2.9}$$

$$b = \varepsilon_m + Lp(\varepsilon_d - \varepsilon_m), \tag{3.2.10}$$

where $p = 1 - (r_1/r_2)^3$ is the metal fraction. It is worth noting that Eqns. (3.2.2) - (3.2.10) are general equations derived for spheroidal core-shell nanoparticles, but can be adapted to be used for the description of the electric potential distribution of spherical and cylindrical core-shell nanoparticles by setting $L = 1/3$ and $L = 1/2$ [190, 191], in Eqns. (3.2.2) - (3.2.10), respectively.

The local electric field E_1 induced in the dielectric core of the spheroidal NCs is related to the incident electric field E_h is given by [166]:

$$E_1 = A|E_h|. \tag{3.2.11}$$

Also, we considered the nonlinear form of the dielectric constant of the core to be given by [173]:

$$\tilde{\varepsilon}_d = \varepsilon_d + \chi(\omega)|E_1|^2, \tag{3.2.12}$$

where $\chi(\omega)$ is the complex Kerr coefficient, and E_1 is the local electric field in the core.

Using the Drude-Lorentz model, the electric permittivity of the metallic shell, ε_m, is given by [160]:

$$\varepsilon_m = \varepsilon_\infty - \frac{1}{z(z+i\rho)}, \tag{3.2.13}$$

where ε_∞ describes the contribution of bound electrons to polarizability, $z = \omega/\omega_p$, $\rho = \nu/\omega_p$ (ω_p and ω are the plasmon frequency of the bulk and the incident radiation frequencies, respectively), ν is the electron damping constant [188].

Moreover, the real and imaginary parts of ε_m can be rewritten as

$$\varepsilon_m = \varepsilon_m^{'} + i\varepsilon_m^{''}, \tag{3.2.14}$$

where

$$\varepsilon_m^{'} = \varepsilon_\infty - \frac{1}{z^2+\rho^2}, \qquad \varepsilon_m^{''} = \frac{\rho}{z(z^2+\rho^2)}.$$

To derive the expression for IOB in the core-shell spheroidal NCs, we considered the nonlinear dielectric core coated with linear metallic shell and then the whole nanocomposite placed in linear host matrix. Based up on this, we substituted Eqn. (3.2.14) and the first part of Eqn. (3.2.12) into Eqn. (3.2.9) and (3.2.10), and finally, inserting into Eqn. (3.2.5) we obtained the reduced LFEF.

Further multiplication and simplification of Eqn. (3.2.5), one can get

$$|A|^2 = \frac{\varepsilon_h^2\left(\varepsilon_m^{'2} + \varepsilon_m^{''2}\right)}{\alpha X^2 + \beta X + \gamma}, \tag{3.2.15}$$

where

$$\alpha = \left[L\delta(\varepsilon_d^{'}\varepsilon_m^{'} - \varepsilon_d^{''}\varepsilon_m^{''}) + L\zeta(\varepsilon_m^{'2} - \varepsilon_m^{''2})\right]^2 + \left[L\varepsilon_m^{''}\delta\right]^2,$$

$$\beta = 2\Big\{\big[L\delta(\varepsilon_d^{'}\varepsilon_m^{'} - \varepsilon_d^{''}\varepsilon_m^{''}) + L(\varepsilon_m^{'2} - \varepsilon_m^{''2})\zeta\big] \times \big(L\varepsilon_m^{'}\delta + \varepsilon_h(1-L)Lp\big) + \big[L\delta(\varepsilon_d^{'}\varepsilon_m^{''} + \varepsilon_d^{'}\varepsilon_m^{'}) + 2\varepsilon_m^{'}\varepsilon_m^{''}L\zeta + \big(\varepsilon_m^{''}\xi + \varepsilon_d^{''}Lp\big) \times \big\{\varepsilon_h(1-L)\big\}\big] \times \big(L\varepsilon_m^{''}\delta\big)\Big\},$$

and

$$\gamma = \big[L\delta(\varepsilon_d^{'}\varepsilon_m^{'} - \varepsilon_d^{''}\varepsilon_m^{''}) + L(\varepsilon_m^{'2} - \varepsilon_m^{''2})\zeta\big]^2 + \big[L\delta(\varepsilon_d^{'}\varepsilon_m^{''} + \varepsilon_d^{'}\varepsilon_m^{'}) + 2\varepsilon_m^{'}\varepsilon_m^{''}L\zeta + \big(\varepsilon_m^{''}\xi + \varepsilon_d^{''}Lp\big) \times \big(\varepsilon_h(1-L)\big)\big]^2,$$

where $\delta = 1 - p + Lp$, $\zeta = p(1-L)$, $\xi = 1 - Lp$.

To find the expression for IOB, first let us square both sides of Eqn. (3.2.11) and multiply by χ. From this, we get

$$X = |A|^2 Y, \tag{3.2.16}$$

where $X = \chi|E_1|^2$ and $Y = \chi|E_h|^2$. Then, by substituting Eqn. (3.2.15) into (3.2.16), the IOB, Y we obtain:

$$Y\eta = \alpha X^3 + \beta X^2 + \gamma X. \tag{3.2.17}$$

where $\eta = \big(\varepsilon_m^{'2} + \varepsilon_m^{"2}\big)\varepsilon_h^2$.

3.2.2 Bistability domain of spheroidal core-shell nanocomposites

The bistability domain of spheroidal core-shell NCs in the plane $(z, |E_h|^2)$ can be found from the analysis of roots of the cubic equation presented in Eqn. (3.2.17), where the root location can be indicated by using Routh-Hurwitz theorem as referenced in [192–194]. Hence, from this analysis, the bistability domain (BD) of the spheroidal core-shell NCs in the plane $(z, \chi|E_h|^2)$ can be given as

$$\frac{dY}{dX} = 0. \tag{3.2.18}$$

Here, by examining the core-shell spheroidal BD in the plane $(z, \chi|E_h|^2)$, and we can get its solution by analyzing the roots of the Eqn. (3.2.17) it becomes:

$$Y\eta = \frac{1}{9\alpha}\left[\frac{(-2\beta^2 + 6\alpha\gamma)(-\beta \pm \sqrt{(\beta^2 - 3\alpha\gamma)}}{3\alpha} - \gamma\beta\right]. \tag{3.2.19}$$

Eqn. (3.2.19) is called the bistability domain (BD).

3.3 Results and Discussions

We investigated the effects of varying L, p, and ε_h on the IOB and BD of spheroidal core-shell NCs in passive and active dielectric cores. The model considered in the study, specifically consists a dielectric core (passive and active), a silver (Ag) shell, and different host materials. The parameters used for numerical evaluations are [41, 86, 166, 167]: $\varepsilon_d^{'} = 2.3$ and $\varepsilon_d^{''} = 0$ (for passive core), $\varepsilon_d^{'} = 0$ and $\varepsilon_d^{"} = -0.13866$ (for active core), $\varepsilon_\infty = 4.5$, $\omega_p = 1.45 \times 10^{16}\ rad/s$, $\rho = 1.15 \times 10^{-2}$, $\nu = 1.67 \times 10^{14}\ rad/s$, and $z = 0.2$.

3.4 Induced Optical Bistability of Spheroidal of Core-Shell NPs

Among the parameters that affect the induced optical bistability in spheroidal core-shell nanoparticles with passive and active dielectric cores are the depolarization factor (L), the metal fraction (p), and the permittivity of the embedding host matrix (ε_h). The numerical results and the corresponding discussions are presented in the following subsections.

3.4.1 The effect of depolarization factor on IOB of core-shell nanocomposite

Depolarization factor is one of the parameters that affects the optical properties of spheroidal NCs. For a fixed metal fraction (p), the IOB can only be observed when the depolarization factor (L) is larger than a certain critical value [195, 196]. Larger L values above the critical value indicate that the NC is disk-like, which enhances surface plasmon resonance effects on the metallic shell; smaller L values indicate that the NC is needle-like, and thus the plasmonic effects as well as the optical bistability property may not be observed [196, 197]. By using Eqn. (3.2.17), we plotted and investigated the graphs of IOB and how it changes in passive and active dielectric cores with changes in L at constants p and ε_h, as shown in Figs. 3.2(a) and (b). When we slowly increase the value of L from 0.34 to 0.42, we observe an $S-$like shape of IOB produced in both in passive and active dielectric cores of spheroidal NCs.

Although there are the same change in L generally resulted in similar patterns of stable states of IOB of spheroidal core-shell NCs in both passive and active cores. With the same values of L, p, ε_h, and composition of spheroidal core-shell NCs, the switching-up threshold is achieved at lower applied field in the passive dielectric core than the active one. Whether the dielectric core is either passive or active, it could be observed that bistability is obtained by changing the intensity of incident electromagnetic field.

In both types of dielectric cores, the switching-up and switching-down threshold points of OB for varying L are achieved nearly at equal values of applied fields. That is, the switching-up and switching-down threshold points do vary significantly with changes in depolarization factor. However, when L increases, the bistable region of OB increases leading to wider range of incident electromagnetic fields between the onset and offset points

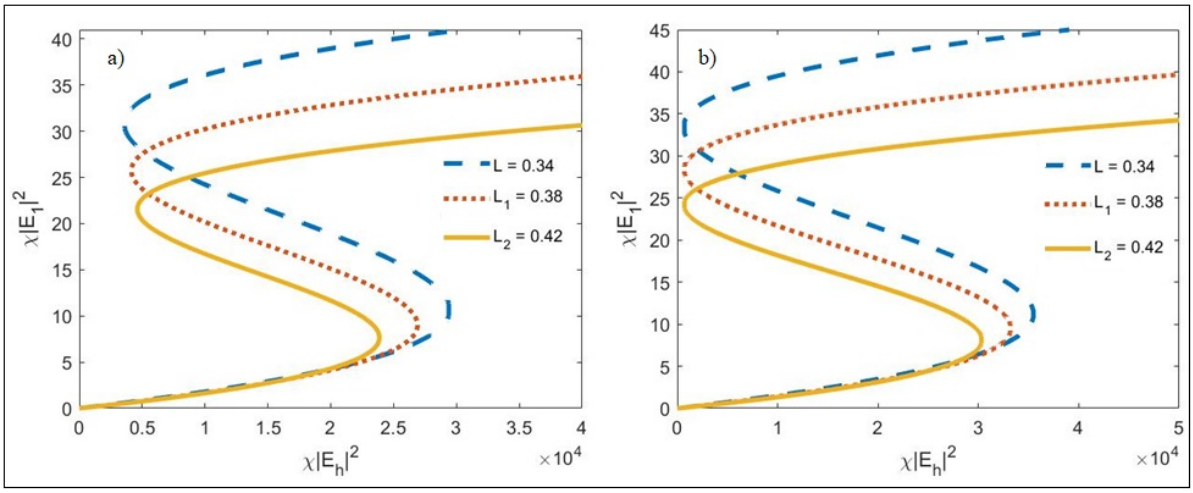

Figure 3.2: IOB of spheroidal core-shell (Ag) NCs (a) in passive dielectric core and (b) in active dielectric core with parameters: $\varepsilon_d^{'} = 2.3$ and $\varepsilon_d^{''} = 0$ (for passive dielectric core), $\varepsilon_d^{'} = 0$ and $\varepsilon_d^{''} = -0.13866$ (for active dielectric core), $\varepsilon_\infty = 4.5$, $\gamma = 1.15 \times 10^{-2}$, $\omega_p = 1.45 \times 10^{16}\ rad/s$, $\nu = 1.67 \times 10^{14}\ rad/s$, $\varepsilon_h = 1.5$, $p = 0.9$, $z = 0.2$, and different values of L.

as shown in Table 3.1. Our finding well agrees with previous study [44].

When we compare the bistability region for IOB in passive and active dielectric cores, we find that the region is narrower in the passive and broader in the active dielectric core (Fig. 3.2(a) and (b)). However, in both cores, the local field in the nonlinear core increases as the incident field increases. When the applied field amplitude reaches the upper threshold field, the local field amplitude in the core discontinuously jumps to the top stable branch.

Table 3.1: Depolarization factor (L) and switching-up and down incident field value for IOB of spheroidal core-shell NCs in passive core (PC) and active core (AC).

	Approximate value of $\chi\|E_h\|^2$	
Depalization factor, L	Onset ($\times 10^4$) (offset) in PC	Onset ($\times 10^4$) (offset) in AC
0.34	2.945 (3,593)	3.550 (632.7)
0.38	2.689 (4,172)	3.321 (757.3)
0.42	2.388 (4,726)	3.036 (767.3)

If the incident field is reduced from a large value, the local field in the core first decreases continuously, and then jumps down to the lower stable branch. This is in agreement with previous findings on OB [34].

3.4.2 Effect of metal fraction on IOB

When we vary the metal fraction in nanocomposites, their optical bistability properties shows some interesting phenomena. In particular, increasing the metal fraction enhances their ability to interact with electromagnetic waves, reduces the interparticle distances as well as the power needed to operate, and makes them more flexible to tune their material properties [80, 197, 198]. Therefore, next we studied the effect of increasing or decreasing the metal fraction on the IOB of spheroidal core-shell NCs with passive and active dielectric cores. It is shown that fixing the values of L and ε_h using the derived Eqn. (3.2.17) and changing the metal fraction by the same amount produces different peaks and bistability regions of IOB in passive and active dielectric cores (Fig. 3.3(a) and (b)). When the metal fraction increases, the incident field required at each switching-up threshold points also increases both in passive and active dielectric cores (Table 3.2). However, the switching-down points for various values of p occur at nearly the same incident electromagnetic field. Further, comparison of the results from Fig. 3.3 that shows the value of $\chi|E_h|^2$ at which switching-up of IOB occurs for each value of the increase in p is larger in active dielectric core.

When the radius of the core increases, i.e., when the p value decreases, the bistable threshold of spheroidal core-shell NCs decreases leading to smaller bistable outputs as shown in Table 3.2. On the other hand, when the metal fraction increases, the switching-up threshold field increases and the bistable region produced gets wider. Hence, it could

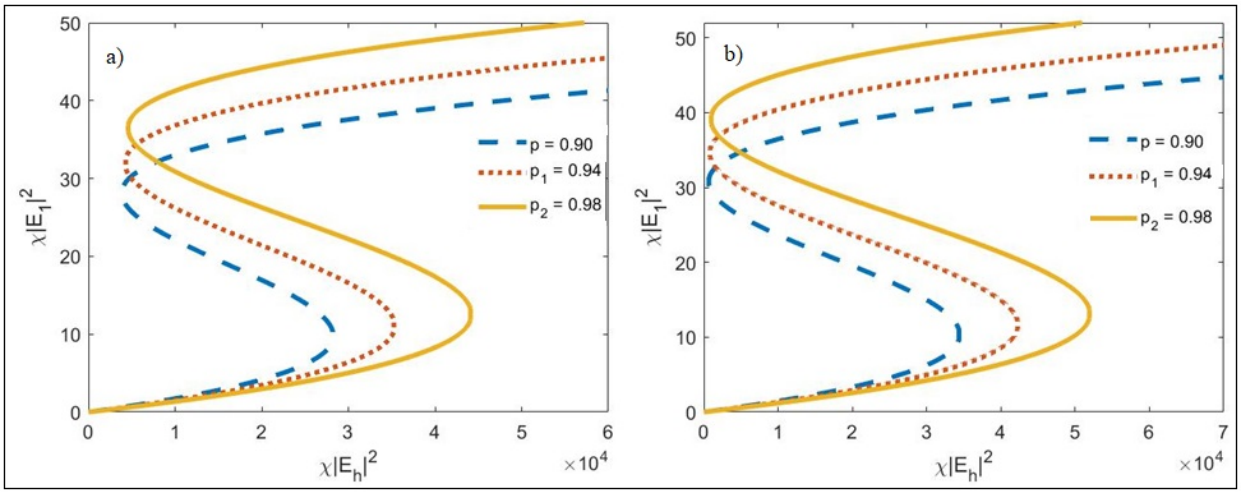

Figure 3.3: IOB of spheroidal core-shell (Ag) NCs (a) in passive dielectric core and (b) in active dielectric core with parameters: $\varepsilon_d^{'} = 2.3$ and $\varepsilon_d^{''} = 0$ (for passive dielectric core), $\varepsilon_d^{'} = 0$ and $\varepsilon_d^{''} = -0.13866$ (for active dielectric core), $\varepsilon_\infty = 4.5$, $\gamma = 1.15 \times 10^{-2}$, $\omega_p = 1.45 \times 10^{16}\ rad/s$, $\nu = 1.67 \times 10^{14}\ rad/s$, $L = 0.36$, $\varepsilon_h = 1.5$, $z = 0.2$, and different values of p.

be said that the OB in the passive and active dielectric core can be controlled by adjusting the metal fraction or size of the core-shell NCs. We can see from our findings the effect of metal fraction is in good agreement with previous findings on OB [176, 199].

Table 3.2: Metal fraction in passive core (PC) and active core (AC) and switching-up/down incident field value for IOB of spheroidal core-shell NCs.

	Approximate value of $\chi\|E_h\|^2$	
Metal fraction, p	Onset (($\times 10^4$)) (offset) in PC	Onset (($\times 10^4$)) (offset) in AC
0.90	2.826 (3,882)	3.445 (674.9)
0.94	3.537 (4,255)	4.232 (805.3)
0.98	4.421 (4,551)	5.200 (920.9)

3.4.3 Effect of embedding medium on IOB

Permittivity of the embedding host matrix is one of the parameters that affects the IOB of nanoparticles. The IOB response is sensitive to changes in the permittivity of the embedding host matrix. Increasing the permittivity of the host medium enhances electromagnetic wave interaction with the NC, improves signal quality and stability and provides a means to control the switching-up and switching-down thresholds of the IOB; while decreasing the permittivity weakens light interactions, limits the operating threshold values of the IOB, and makes the NC sensitive to external factors [178, 200]. Hence, in the design and fabrication of bistability systems, these effects must be considered. In this section,by using Eqn. (3.2.17), we studied the effect of varying the permittivity of the host matrix in spheroidal core-shell NCs with passive and active dielectric cores. We used different values

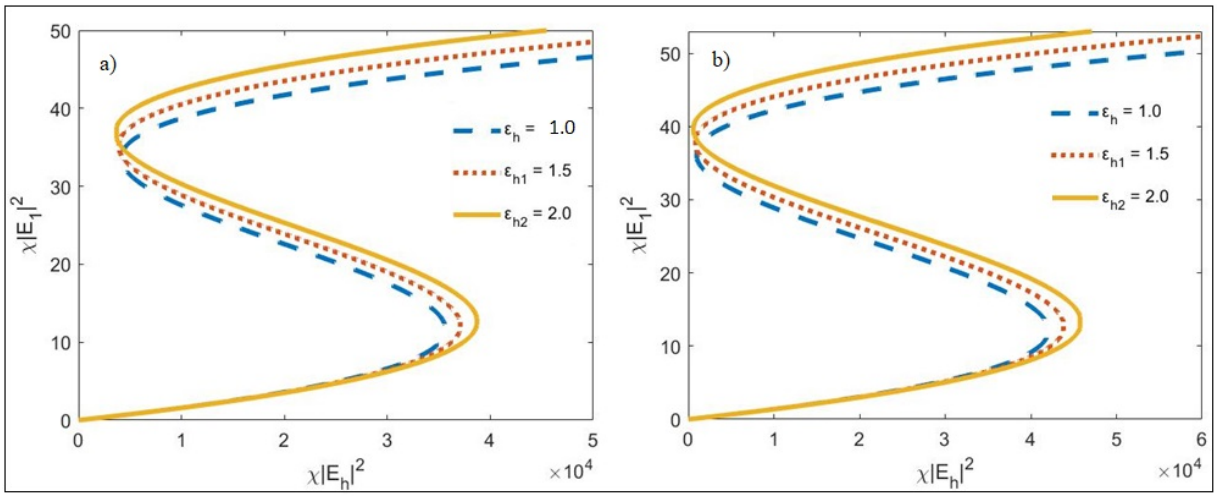

Figure 3.4: IOB of spheroidal core-shell (Ag) NCs (a) in passive dielectric core and (b) in active dielectric core with parameters: $\varepsilon_d^{'} = 2.3$ and $\varepsilon_d^{''} = 0$ (for passive dielectric core), $\varepsilon_d^{'} = 0$ and $\varepsilon_d^{''} = -0.13866$ (for active dielectric core), $\varepsilon_\infty = 4.5$, $\gamma = 1.15 \times 10^{-2}$, $\omega_p = 1.45 \times 10^{16}\ rad/s$, $\nu = 1.67 \times 10^{14}\ rad/s$, $L = 0.34$, $p = 0.94$, $z = 0.2$, and different values of ε_h.

of ε_h at constant values of L and p and investigated the result for spheroidal core-shell NCs

in passive and active dielectric cores, as shown in Fig. 3.4. The result shows that when the value of ε_h increases, the switching-up threshold field also increases in both types of cores. When the value of $\varepsilon_h = 1.0$, the values of $\chi|E_h|^2$ are nearly 3.65×10^4 and 4.207×10^4 in passive and active dielectric cores, respectively. When ε_h value is increased to 2.0, the corresponding switching-up threshold fields increase to 3.873×10^4 and 4.588×10^4 in passive and active dielectric cores, respectively (Table 3.3). Hence, for large values of ε_h, the switching-up threshold of IOB of spheroidal core-shell NCs also occurs at large values of incident field.

Moreover, it could be observed that increasing the dielectric constant of the embedding medium decreases of the bistable region of IOB in both passive and active dielectric cores of spheroidal core-shell NCs. Additionally, one can observe that increasing the surrounding dielectric constant produces no change in the switching-down threshold field, especially in the active dielectric core.

Table 3.3: Permittivity of host matrix and switching-up incident field value for IOB of spheroidal core-shell NCs.

	Approximate value of $\chi\|E_h\|^2$	
Permitivity of host matrix, ε_h	Onset ($\times 10^4$) (offset) in PC	Onset (($\times 10^4$)) (offset) in AC
1.0	3.565 (4,203)	4.207 (1005)
1.5	3.712 (4,118)	4.388 (840.6)
2.0	3.873 (3,685)	4.588 (575)

In conclusion, the IOB of spheroidal core-shell NCs in passive and active dielectric core is sensitive to the changes in L, p and ε_h. Changing those parameters under different conditions can lead to the possibility of tuning the bistable thresholds and the bistable regions which enables one to design various types of nanodevices for practical applications in nonlinear optics.

3.5 Bistability Domain of Spheroidal Core-Shell NCs

We have also studied the characteristics of bistability domain (BD) in the $z-Y$ plane using eqn. (3.2.19). Then, eqn. (3.2.19) represented by (f_1, f_2) is called curves of BD, where f_1 and f_2 are the curves for switching up and down of BD, respectively. Particularly, we investigated effects of depolarization factor L, metal fraction p, and dielectric permittivity of host medium ε_h, on the BD of spheroidal core-shell NCs in active and passive dielectric cores. The results obtained from the investigation are presented as follows.

3.5.1 Effect of depolarization factor on BD

To see the effect of depolarization factor on the BD of the spheroidal core-shell NCs, we used two different values of L (i.e., $L = 0.34$ and $L = 0.36$) at constant p and ε_h. By setting $z = 0.2$, the plots of the OB and the BD of the NCs for active and passive dielectric cores are as shown in Figs. 3.5(a) and (b). From Fig. 3.5(a), the BD region for passive dielectric core are found at 4778 and 3.185×10^4 offset and onset points, respectively. For the active dielectric core, the offset and the onset points of the BD are found at 1251 and 3.62×10^4, respectively (Fig. 3.5(b)). This shows that the ranges of BD are relatively wider in the active dielectric core than the passive one, indicating that the type of dielectric core material (being passive or active) affects the BD of the spheroidal core-shell NCs. However, whether the dielectric core is passive or active, the points of BD are confined within the IOB regions.

In both passive and active dielectric cores, f_1 and f_2 are the in set regions of the BD of spheroidal core-shell NCs (Fig. 3.5). This reveals that when the value of the depolarization factor changes, the region of BD also changes in both types of cores.

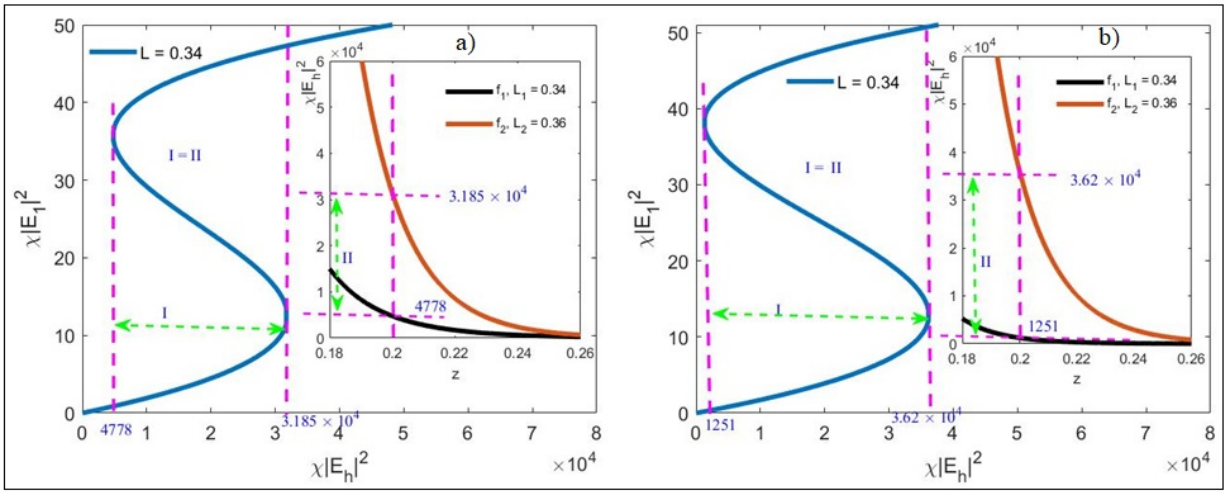

Figure 3.5: BD of spheroidal core-shell(Ag) NCs: (a) in passive dielectric core and (b) in active dielectric core with parameters $L = 0.34, 0.36$, $\varepsilon_h = 1.5$, $p = 0.99$, $\varepsilon_d^{'} = 2.3$, $\varepsilon_d^{''} = 0$, and $z = 0.2$, where the rest of parameters are the same as in Fig. 3.2.

3.5.2 Effect of metal fraction on BD

By keeping the values of $L = 0.34$ and $\varepsilon_h = 1.5$ constant, we investigated how the BD of spheroidal core-shell NCs changes with the change in metal fraction, p. The analysis shows that change in BD is observed for different frequencies in both passive and active dielectric cores (Fig. 3.6). In particular at $z = 0.2$ one can clearly see that the regions of BD are found between 4684 and 2.792×10^4 points for the passive dielectric core. Similarly, the regions of BD for the active dielectric core are found between the 1241 and 3.199×10^4 points (Fig. 3.6). Comparing the results of Fig. 3.6 with that of Fig. 3.5, wider regions of BD are observed in both passive and active dielectric cores when the depolarization factor varies rather than varying the metal fraction.

Further observation of Fig. 3.6 shows that the BD regions of the NCs vanish after 0.26 and 0.28 in the passive and active dielectric cores, respectively. When electric field $\chi|E_h|^2 = 4684$ is applied to the passive dielectric core spheroidal NCs system, the BD

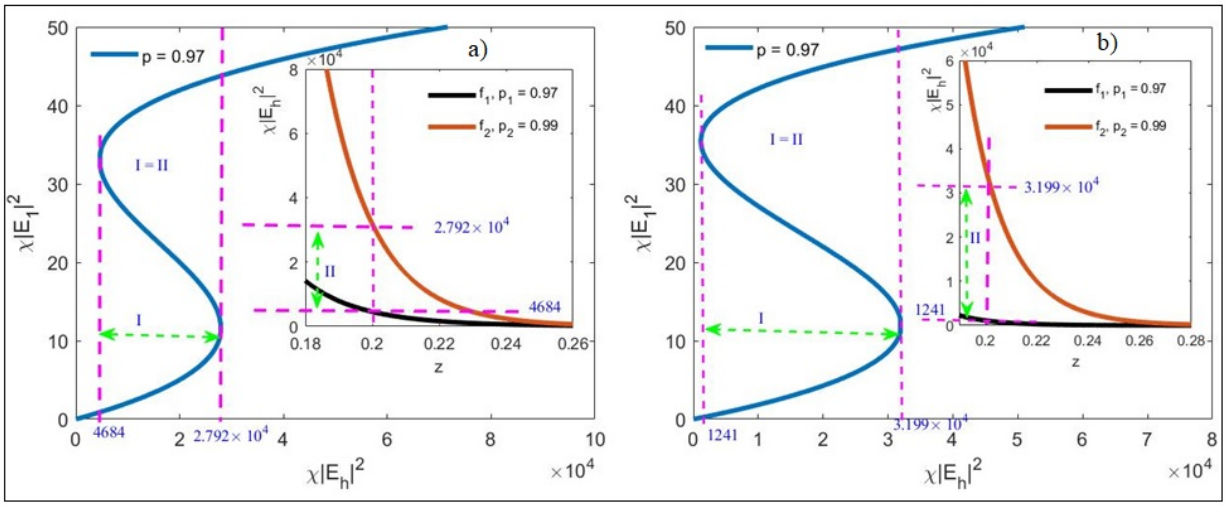

Figure 3.6: BD of spheroidal core-shell(Ag) NCs: (a) in passive dielectric core and (b) in active dielectric core with parameters: $\varepsilon_h = 1.5$, $L = 0.36$, $z = 0.2$, and varying metal fraction, p, where the rest of parameters are the same as in Fig. 3.2.

regions I and II confined between f_1 and f_2 are formed, where the negative root started emerging from $\chi|E_h|^2 = 2.792 \times 10^4$, as shown in Fig. 3.6(a). As shown by black and red color line on Fig. 3.6(b), the BD in the active dielectric core system bends up and open widely as the value of z decreases from 0.26 to 0.2 for positive and negative roots. When the two lines overlap at about $z = 0.26$, no BD is observed in both passive and active spheroidal core-shell NCs. This means that the BD region decreases gradually as the frequency exceeds $z = 0.2$ and finally merges after $z = 0.26$. Further observation again shows that the inset regions of BD are comparatively narrower in passive dielectric core than the active core (Figs. 3.6(a) and (b)). Generally, changing the value of p in both passive and active dielectric cores causes the BD to vanish or emerge. There are also other previous studies that support this finding [86, 201].

3.5.3 Effect of embedding medium on BD

We also investigated how the change in the dielectric permittivity of the surrounding medium (ε_h) affects the BD of spheroidal core-shell NCs of passive and active dielectric cores. At constant values of $L = 0.34$ and p=*0.99*, we changed the value of ε_h from 1.1 to 1.5. From the analysis, we observed that there are two separate peaks in both types of dielectric cores, with each of the peaks showing their own characteristics (Figs. 3.7(a) and (b)). Moreover, the inset regions of the BD merges after the frequency reaches about $z = 0.24$ and $z = 0.26$ in the passive and active dielectric cores, respectively. As observed

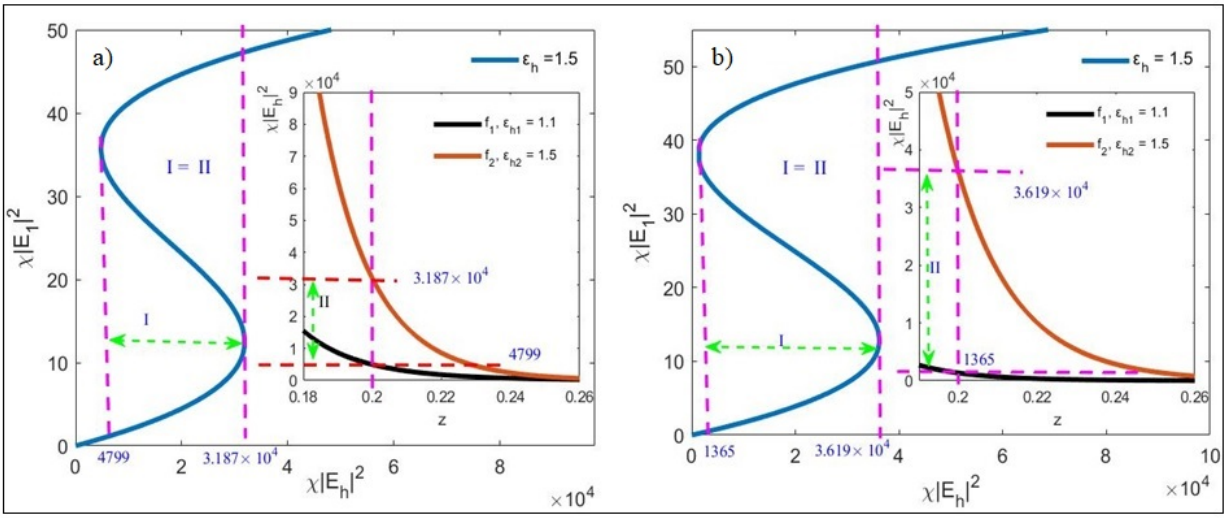

Figure 3.7: BD of spheroidal core-shell(Ag) NCs: (a) in passive dielectric core and (b) in active dielectric core with parameters: $p = 0.99$, $L = 0.34$, $z = 0.2$, and $\varepsilon_h = 1.1, 1.5$, where the rest of parameters are the same as in Fig. 3.2.

in the cases of L and p, the variation in ε_h also produces wider offset and the onset region of the BD in active dielectric core than in the passive core. Generally, the BD is clearly displayed between f_1 and f_2 regions with red and black color lines resulted from the root analysis of Eqn. (3.2.19). As the permittivity of the embedding medium changes, BD ranges are observed in the OB regions in both passive and active dielectric cores.

From this, it could be said that the change in the value of the dielectric permittivity of the embedding medium ε_h affects the BD of the spheroidal core-shell NCs both in passive and active dielectric cores. Hence, managing this parameter helps to acquire the IOB domain for the spheroidal core-shell NCs. This finding agrees with the results of the previous studies [86, 202, 203].

3.6 Conclusions

By changing the values of L, p, and ε_h and using the root analysis approach, we examined how the IOB and BD of spheroidal core-shell NCs change in passive and active dielectric cores. The findings show that the IOB of the spheroidal core-shell NCs is attained at a lower applied field in the passive dielectric core than the active one, regardless of the changes in L, p, or ε_h. The study also reveals that for the same change in the values of L, the stable states of IOB of spheroidal core-shell NCs in both passive and active cores show similar patterns. Particularly, for the same change in L, the switching-up and switching-down threshold points of the IOB are obtained at comparable values for applied fields in both types of cores. However, the IOB region is relatively narrower in the passive and broader in the active dielectric cores. When the metal fraction increases, the incident field required at each switching-up threshold points also increases in both passive and active dielectric cores and the bistable region produced also gets wider. However, the switching-down points for various values of p occur at nearly the same incident electromagnetic field. When the value of p decreases, the bistable threshold of spheroidal core-shell NCs also decreases leading to smaller bistable outputs. This concludes that the OB in the passive and active dielectric core can be controlled by adjusting the metal fraction of the core-shell NCs. The study also indicates that at larger values of ε_h, the switching-up threshold of IOB of spheroidal

core-shell NCs also occurs at larger value of incident field. However, the increase in ε_h the of the surrounding medium produces no change in the switching-down threshold field, especially in the active dielectric core. In conclusion, the IOB of spheroidal core-shell NCs in passive and active dielectric core is sensitive to the changes in L, p and ε_h.

The study also reveals that when the value of the depolarization factor changes, the region of BD also changes in both types of cores. However, the ranges are relatively wider in the active dielectric core than the passive one, indicating that the type of dielectric core material (being passive or active) affects the BD of the spheroidal core-shell NCs. Moreover, wider regions of BD are observed in both passive and active dielectric cores when the depolarization factor varies rather than varying the metal fraction. Similarly, the BD ranges are observed in the OB regions in both passive and active dielectric cores. In conclusion, it could be said that varying the values of depolarization factor, metal fraction, and host medium leads to the possibility of controlling the ranges of BD in spheroidal core-shell NCs both in passive and active dielectric cores. These possibilities could enable one to use such NCs in practical applications such as optical circuit, logic operations, and optical memory.

Chapter 4

Effects of Interfacial Layer on Enhancement Factor of Spheroidal Metal/dielectric Nanocomposites in Passive and Active Host Matrix

This chapter is based on submitted article to a journal:

> *Tolasa Tamasgen Hirpha and Belayneh Mesfin Ali, "Effects of Interfacial Layer on Enhancement Factor of Spheroidal Metal/dielectric Nanocomposites in Passive and Active Host Matrix", submitted and is accepted for publication (October 2023).*

4.1 Introduction

Recent developments in nanocomposites (NCs), and nanotechnology have made it possible to create reliable, extremely sensitive, and focused detection techniques that are intended to overcome some shortcomings in traditional detection systems [2]. Within this context, remarkable optical phenomena that are revealed by light's interaction with NCs of spheroidal metal/dielectric NPs can create a unique optical capabilities. As a result, the

optical characteristics of NPs have been well investigated throughout the past century, and metal/dielectric NPs have found a number of applications like in the development of next-generation ultrafast communications, signal processing systems, photonics, chemical sensing, and microelectronic devices [204]. Surface plasmon resonance (SPR), controls the optical characteristics of metal probing with thin dielectric nanoparticles, at interfaces enhanced evanescent field and heated regions emerging on the particle's surface [97, 205, 206]. The NCs of metal/dielectric NPs consist of one and two layers i.e. the surface layer, and the shell layer [207]. Hence, a unique structure with distinct qualities is produced by the combination of various constituent materials in NCs material, leading to a distinct structure. Consequently, NPs may include a unit nanomaterial or perhaps it consist of a combination of many materials [208]. The dielectric function of host mediums' can be separately considered as passive and active. The active layer of the medium are more favorable because the field that passes through the medium are increase light absorption without affecting charge transport to the electrodes [209]. Therefore, it is desirable to research and comprehend the properties of their enhancing field in order to construct nanoscale optical devices for real-world applications.

In order to deal with it, the local field enhancement factor (LFEF) was thoroughly experimentally and theoretically researched by many scholars [23, 205, 210–212]. Applying spheroidal model, the numerical simulations and calculations are carried out to determine the local field enhancement factor. Moreover, the properties of NPs as well rely on spatial distribution, size, and the types of embedding host matrix [179, 210, 213]. Furthermore, the LFEF seriously depends on the shapes of the shell-covered nanoparticle, particularly the depolarization factors, metal fraction, interfacial factor, thickness and surface dielectric function is considered [214].

To investigate the effects of shape, size, composition structure, and spatial distributions of NCs on the local field enhancement factor, (LFEF) wide ranging researches have been conducted [86, 212, 215]. However, much of this research focused on spherical or cylindrical metal/dielectric NCs [167, 216]. Prior studies show that the LFEF at the core of cylindrical and spherical metal/dielectric NP inclusions in the presence of applied NPs is sensitive to changes in shape, size, and others in the dielectric host matrix were studied [167, 217]. Noble metals like silver (Ag) have been utilized to explore the enhanced response and the nonlinear effects of NCs by applying electromagnetic field enhancement effects [109]. To the best of our knowledge, we investigated the effects of the depolarization factor (L), thickness (t), radius (r), metal fraction (p), interfacial factor (I), and surface dielectric permittivity (ε_s) medium on the local field enhancement factor (LFEF) of spheroidal metal/dielectric NCs in active and passive dielectric host mediums using silver (Ag) metal as a shell.

4.2 Theoretical Model and Calculation of NCs in Passive and Active Host Matrix

We considered spheroidal shell nanocomposite in the passive and active host mediums using the quasistatic approximation. The dielectric function of the embedding medium was regarded as either passive or active to explore its results on LFEF. Depending on how the externally applied field affects the medium, the host medium's embedding dielectric function, ε_h, is referred to as passive or active. Hence, this embedding dielectric function can be written as $\varepsilon_h = \varepsilon_h^{'} + i\varepsilon_h^{''}$, where the real and imaginary parts of the host media are denoted by the variables $\varepsilon_h^{'}$ and $\varepsilon_h^{''}$, respectively. The embedding dielectric function is passive when $\varepsilon_h^{'} > 0$ and $\varepsilon_h^{''} = 0$, but an active embedding dielectric function is when $\varepsilon_h^{'} = 0$ and $\varepsilon_h^{''} < 0$. In the present study, each component of the dielectric function was

considered separately.

Considering the application of the Drude-Sommerfeld concept, ε_m, of the metallic shell's electric permittivity [160, 165], is given by:

$$\varepsilon_m = \varepsilon_\infty - \frac{1}{z(z+i\gamma)}, \tag{4.2.1}$$

where ε_∞ describes how confined electrons influence polarizability, $z = \omega/\omega_p$, $\gamma = \nu/\omega_p$ (ω_p and ω are the Plasmon frequency of the bulk and the incident radiation frequencies, respectively), ν is the electron damping constant.

Moreover, the real and imaginary parts of ε_m can be rewritten as

$$\varepsilon_m = \varepsilon_m^{'} + i\varepsilon_m^{''}, \tag{4.2.2}$$

where $\varepsilon_m^{'}$, and $\varepsilon_m^{''}$ are the real and imaginary parts of the metal's-dielectric functions.

4.3 Electric Potential Distribution in Spheroidal Shell Nanocomposite in Host Matrix

4.3.1 Enhancement factor for pure metal nanocomposite

An electromagnetic wave that is embedded in the host matrix and has the shape of a spheroidal impact is a metal/dielectric nanoparticles (NPs). So let's take a look at the spheroidal metal/dielectric NCs model illustrated in Fig. 4.1 that consists of ε_m enclosed at the core of the host matrix, ε_h. Therefore, the given electrical potential equations [176], are given as

$$\Phi_m = -E_h A r\cos\theta, \qquad r_1 \le r \tag{4.3.1}$$

$$\Phi_h = -E_h\left(r - \frac{B}{r^2}\right)\cos\theta, \qquad r \ge r_1, \tag{4.3.2}$$

where, Φ_m and Φ_h are electrical potential and host matrix respectively.

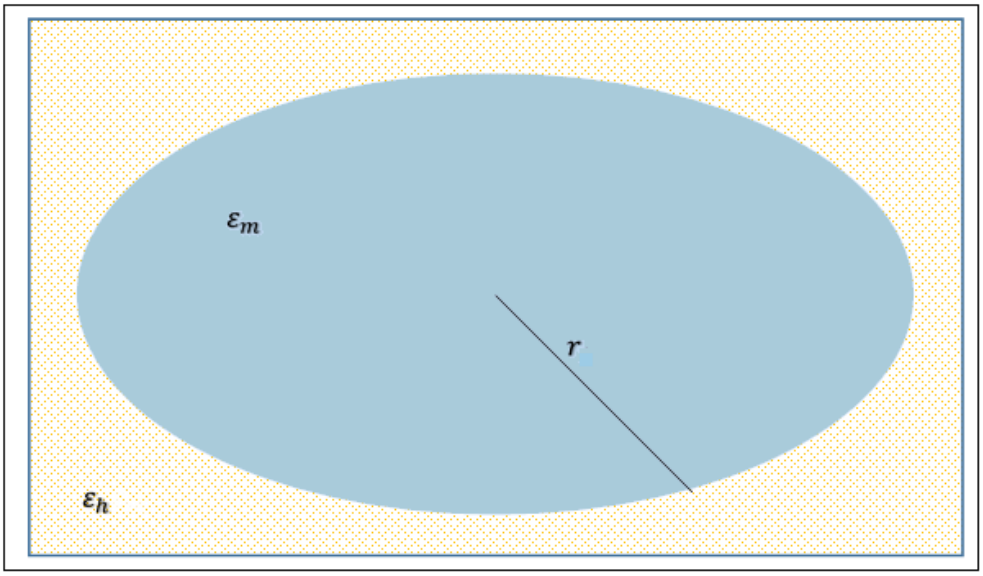

Figure 4.1: Schematic representation of spheroidal shell-host NCs.

At the boundary between the dielectric core and the metallic shell, the potentials must satisfy the following boundary conditions [43]:

$$\begin{aligned} \Phi_m &= \Phi_h|_{r=r_1}, \\ D_m &= D_h|_{r=r_1}, \end{aligned} \tag{4.3.3}$$

Using quasistatic approaches, Eqn. (4.3.1) and (4.3.2) we obtained as:

$$A = \left(1 - \frac{B}{r_1^3}\right). \tag{4.3.4}$$

Applying the displacement vector at the interface mediums using Eqn. (4.3.1) and (4.3.2), and then, introducing depolarization L, we acquired:

$$L\varepsilon_m A = \varepsilon_h \left[1 + (1-L)\frac{B}{{r_1}^3}\right], \tag{4.3.5}$$

Therefore, the unknown coefficients A, and B of Eqns. (4.3.1 - 4.3.2) expression can be summarized as follows:

$$A = \frac{\varepsilon_h}{\varepsilon_m L + \varepsilon_h (1-L)}, \tag{4.3.6}$$

$$B = \left[\frac{L(\varepsilon_m - \varepsilon_h)}{L\varepsilon_m + \varepsilon_h(1-L)}\right] r_1^3, \tag{4.3.7}$$

4.3.2 Local field enhancement factor of spheroidal of shell nanocomposites in host matrix

To find LFEF for metal/dielecdtric composite of ellipsoidal nanoparticles by using the complex host matrix and Eqn. (4.2.2) into Eqn. (4.3.6) and squaring it we get:

$$\mid A \mid^2 = \frac{\varepsilon_h^{'2} + \varepsilon_h^{''2}}{\left[L\varepsilon_m^{'} + \varepsilon_h^{'}(1-L)\right]^2 + \left[L\varepsilon_m^{''} + \varepsilon_h^{''}(1-L)\right]^2}, \tag{4.3.8}$$

where

$$\varepsilon_m^{'} = \varepsilon_\infty - \frac{1}{z^2+\gamma^2}, \qquad \varepsilon_m^{''} = \frac{\gamma}{z(z^2+\gamma^2)}.$$

Equation (4.3.8) is called local field enhancement factor of spheroidal metal/dielectric NPs in passive and active host matrix.

4.4 The Electric Potential Distribution of Spheroidal Shell NCs with Interfacial Layers

4.4.1 Enhancement factor of pure metal NCs with interfacial layer

Once more, in this section we take into account a spheroidal metal/dielectric NPs system, as illustrated in Fig. 4.2, which includes a metal as a shell, ε_m, the embedding permittivity of a dielectric as a host matrix, ε_h, and finally, the interface layer between the two media, ε_s. The distribution of the electric potential in the system is described by the following expressions

$$\Phi_m = -E_h A r\cos\theta, \quad r \le r_1, \tag{4.4.1}$$

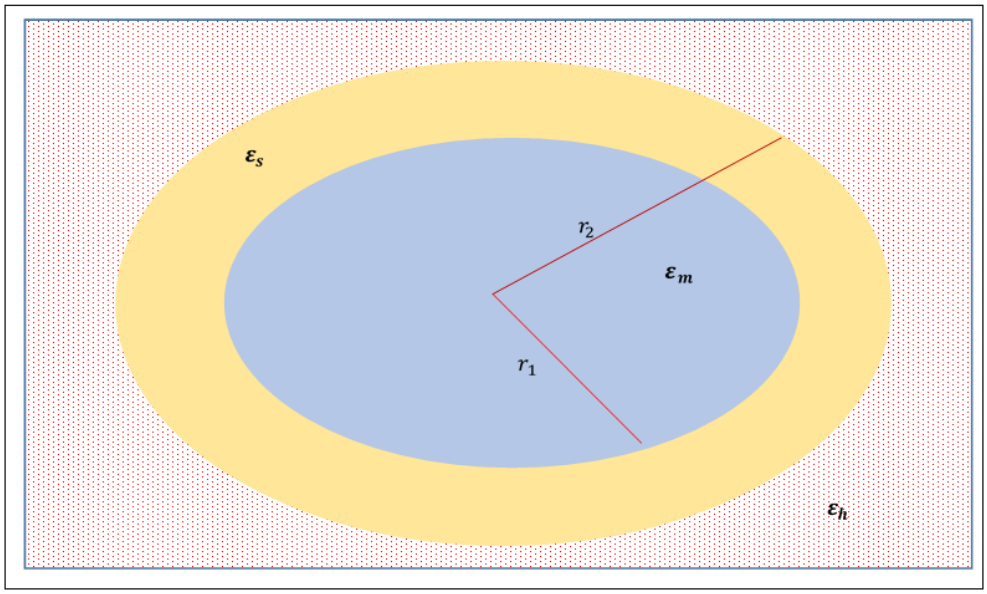

Figure 4.2: Schematic representation of spheroidal core-interfacial-host NCs.

$$\Phi_s = -E_h\left(Br - \frac{C}{r^2}\right)\cos\theta, \quad r_1 \leq r \leq r_1 + t, \tag{4.4.2}$$

$$\Phi_h = -E_h\left(r - \frac{D}{r^2}\right)\cos\theta, \quad r \geq r_1 + t, \tag{4.4.3}$$

where Φ_m, Φ_s and Φ_h is metal dielectric, dielectric interfacial layer, and host medium electric potential function respectively.

By using the condition given in Eqn. (4.3.3), and from Eqns. (4.4.1) and (4.4.2) we get

$$A = B - \frac{C}{r_1^3}, \tag{4.4.4}$$

And also considering Eqn. (4.3.3) for the displacement vector at boundary using Eqn. (4.4.1) and (4.4.2), and introducing depolarization factor, we obtain

$$L\varepsilon_m A = \varepsilon_s\left[LB + (1-L)\frac{C}{r_1^3}\right]. \tag{4.4.5}$$

Again, equating Φ_s and Φ_h, given in Eqn. (4.4.3), and (4.4.4) simplifying we find:

$$B - \frac{C}{(r_1+t)^3} = 1 - \frac{D}{(r_1+t)^3}. \tag{4.4.6}$$

Using the definition of displacement vector at boundary condition given in Eqn. (4.3.3), and applying depolarization factor, we get:

$$\varepsilon_s\left[LB+(1-L)\frac{C}{(r_1+t)^3}\right]=\varepsilon_h\left[L+(1-L)\frac{D}{(r_1+t)^3}\right]. \tag{4.4.7}$$

Hence, by rearranging and simplifying the expressions for the unknown coefficients A, B, C, and D of Eqns. (4.4.1) - (4.4.3) we get:

$$A=\frac{\varepsilon_h\varepsilon_s}{Lb+a\varepsilon_h(1-L)}, \tag{4.4.8}$$

$$B=\frac{\varepsilon_h(L\varepsilon_m+\varepsilon_s)+\varepsilon_s(1-L)}{Lb+a\varepsilon_h(1-L)}, \tag{4.4.9}$$

$$C=\frac{L\varepsilon_h(\varepsilon_m-\varepsilon_s)}{Lb+a\varepsilon_h(1-L)}r_1^3 \tag{4.4.10}$$

$$D=\frac{b-a\varepsilon_h L}{Lb+a\varepsilon_h(1-L)}(r_1+t)^3, \tag{4.4.11}$$

where

$$a=L\varepsilon_m(1-p)+\varepsilon_s(1-L+Lp),$$

and

$$b=\varepsilon_m(p+Lp)+L\varepsilon_m\varepsilon_s+p\varepsilon_s(1-L)+\varepsilon_s^2(1-L).$$

4.4.2 Local field enhancement factor of spheroidal in nanocomposite with interfacial layer

Since we are using the quasistatic approach, the electric field E_h (assumed to be directed along the z-axis) is uniform. Then, by using the relation $E=-\nabla\Phi$ the local field in the metal dielectric and interfacial layer at ε_s of the spheroidal nanocomposite can be written as

$$E_s=AE_s. \tag{4.4.12}$$

where A is the complex function given by Eqn. (4.4.12).

Now, the enhancement factor for a metal/dielectric composite of spheroidal obtained at the interface mediums of the interfacial layer can be obtained by substituting the values of a and b given under Eqns. (4.4.8)-(4.4.11), we acquired

$$A = \frac{\varepsilon_h \varepsilon_s}{\varepsilon_m a_1 + \varepsilon_m \varepsilon_h a_2 + a_3 \varepsilon_h + a_4}, \tag{4.4.13}$$

where

$a_1 = L(p + L\varepsilon_s)$, $a_2 = L[1 - L - p(1 - L)]$, $a_3 = \varepsilon_s[1 - 2L + Lp(1 - L) + L^2]$, and $a_4 = \varepsilon_s L[Lp + \varepsilon_s(1 - L)]$.

where $\varepsilon_s = I/3t$, and $p = 1 - (r_1/r_2)^3$.

By substituting the complex embedding mediums and Eqn. (4.3.1) into Eqn. (4.4.13), and then, squaring and simplifying it, we find the LFEF of dielectric host mediums.

Finally, squaring Eqn. (4.4.13) we get the LFEF equation as:

$$|A|^2 = \frac{\left(\varepsilon_h^{'2} + \varepsilon_h^{''2}\right)\varepsilon_s^2}{\left(a_1\varepsilon_m^{'} + a_2\varepsilon_m^{'}\varepsilon_h^{'} - a_2\varepsilon_m^{''}\varepsilon_h^{''} + a_3\varepsilon_h^{'} + a_4\right)^2 + \left(a_1\varepsilon_m^{''} + a_2\varepsilon_m^{'}\varepsilon_h^{''} + a_2\varepsilon_m^{''}\varepsilon_h^{'} + a_3\varepsilon_h^{''}\right)^2}. \tag{4.4.14}$$

Equation (4.4.14) is called LFEF of spheroidal in metal/dielectric NPs - interfacial layer in the passive and active host medium.

4.5 Results and Discussions

We discussed how changing the parameters L, p, I, t, ε_s, and ε_h affect the LFEF of NCs with spheroidal shells and interfacial layers in host medium dielectrics. The model taken into consideration in the study is made up of a silver (Ag) shell, a dielectric embedded in metal, and an embedding host matrix that is (a) a passive medium, when $\varepsilon_h^{'} = 2.25$ and $\varepsilon_h^{''} = 0$; (b) active medium, when $\varepsilon_h^{'} = 0$ it is passive and active when $\varepsilon_h^{''} = -0.13886$.

In this section, we investigated the effects of host and interfacial layer on LFEF of spheroidal shell-interfacial layer NCs by varying the values L, I, r, t, p, and ε_s.

4.5.1 The effects of depolarization factor on LFEF

In this subsection, we discussed the effects of host medium dielectric function on the LFEF of spheroidal NCs when the depolarization factor is varied, while the rest of the parameters, such as interfacial factor, thickness, and radius, remained fixed in passive and active host mediums. The plots of $|A|^2$ versus z when the values of L is varied between 0.34 and 0.42, while other parameters are left unchanged, is illustrated in Figs. 4.3(a) and (b). The blue-shifted LFEF was observed as the value of the depolarization factor, L, is gradually increased from 0.34 to 0.42, as shown in 4.3(a), and plotted by using Eqn. (4.3.8).

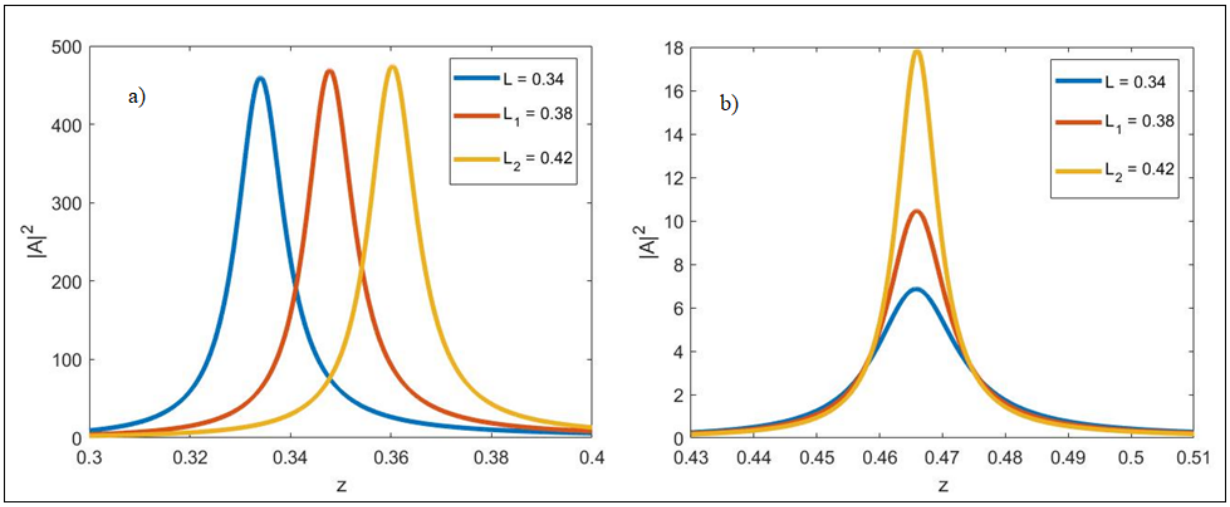

Figure 4.3: The effect of the depolarization factor on LFEF of spheroidal shell NCs: a) in passive dielectric shell and b) in active dielectric shell with $\varepsilon_h^{'} = 2.25$, $\varepsilon_h^{''} = -0.13866$, $\varepsilon_\infty = 4.5$, $\gamma = 0.0115$, $\omega = 1.45 \times 10^{16}\ rad/s$, and different values of L.

Also, as shown in Fig. 4.3(b), the LFEF peaks rise with a similar upward trend as the medium becomes active. In active embedded mediums, the LFEF steadily rises for each value of L one over the other, whereas, the LFEF obtained in the passive dielectric

medium is blue-shifted and it is slowly increased with an increase in L values, as shown in Fig. 4.3(a). However, in the active embedding mediums, $\varepsilon_h^{''} < 0$, with a gradually increased L, the LFEF peaks are observed to increase, with no shift in position. We investigated the impacts of the depolarization factor on LFEFs as they are changed, and as can be observed in Fig. 4.4(a), their output peaks show no significant shifts in the passive host medium. The best position, however, is indicated by the LFEF with $L_2 = 0.42$, which is at $z = 0.36$. As a result, when an applied field impinged on the metal/dielectric nanocomposite medium, the LFEF grew progressively one after another in the specified frequency with a single peak. Additionally, we obtained symmetrical pattern peaks when the embedding host medium is decreased, for example, in passive $\varepsilon_h^{'} = 1.3$ and $\varepsilon_h^{''} = 0$, while $\varepsilon_h^{'} = 0$ and $\varepsilon_h^{''} = -0.13886$ for active host mediums. However, when L increased, the peaks gradually decreased, as shown in Fig. 4.4(a), compared with that in Fig. 4.3(a) by using Eqn. (4.3.8).

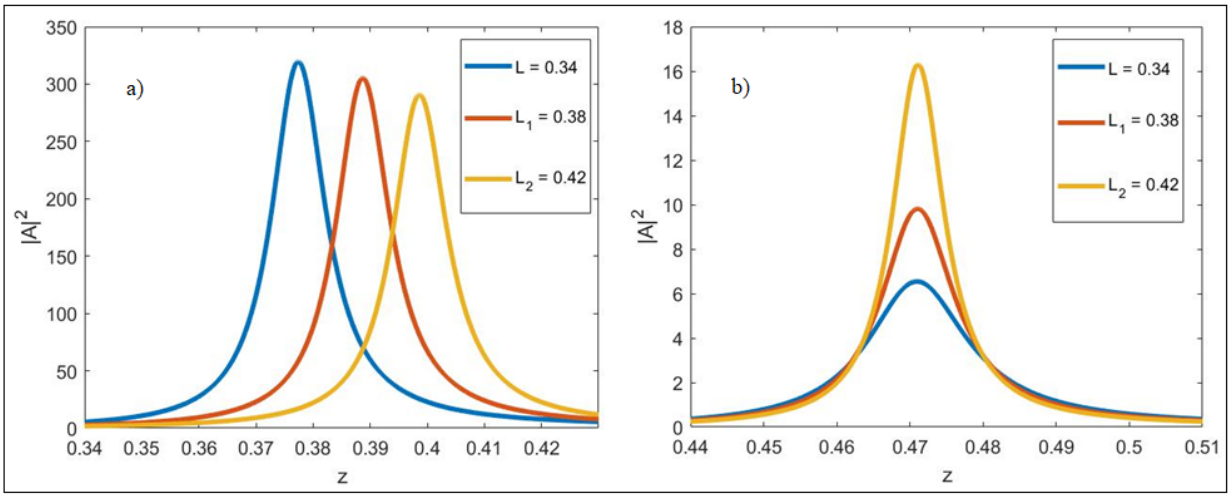

Figure 4.4: Effects of depolarization factor on LFEF of spheroidal shell (Ag) NCs (a) in passive dielectric and (b) in active dielectric host mediums with parameters: $\varepsilon_h = 1.3$, $\varepsilon_\infty = 4.5$, $\omega = 1.45 \times 10^{16}\ rad/s$, $\nu = 1.67 \times 10^{14}\ rad/s$, $\gamma = 1.15 \times 10^{-2}$, and different depolarization factor.

Finally, we draw the conclusion that the LFEF of spheroidal metal-dielectric NPs can

be influenced by the passive and active host matrix permittivity. As the dielectric function of the host medium is decreased from $\varepsilon_h^{'} = 2.25$ to $\varepsilon_h^{'} = 1.3$, the peaks of the LFEF is decreased significantly for a system with passive host, whereas it remains constant for a system with active host, as seen in Figs. 4.3(a) and 4.4(a).

4.5.2 The effects of depolarization factor on LFEF with interfacial layer

In this section, we investigated the LFEF of a composite of spheroidal nanoparticles made of metal/dielectric with an interfacial layer embedded in the passive and active host matrix. By changing the depolarization factor while keeping constant the other variables, the LFEF under investigation is simulated in this case by using Eqn. (4.4.14).

According to the model (Fig. 4.2), the interfacial medium is the space between the metal-dielectric and the spheroidal host matrix medium NCs. As a result, Figs. 4.5(a) and (b) illustrate the impact of depolarization factor on the effects of LFEF. The LFEF in the passive host medium is blue-shifted as the L is raised. Although the LFEFs active embedding medium is shown in Fig. 4.5(b).

We also analyze the impact of the interfacial layer, I, via the limit where the interfacial factor, or $t \to 0$, is laid on the surface of two medium interfaces. Due to the medium's tendency to have zero thickness, this parameter may also have an impact on the LFEF of a spheroidal shell. According to Eqn. (4.4.14), the only meaningful quantity is $t\varepsilon_s$. Here, the I is given to explain passing of fields using the following equation:

$$I = \lim_{t \to 0,\ \varepsilon_s \to \infty} t\varepsilon_s \tag{4.5.1}$$

From this Eqn. (4.5.1), when t approaches 0, the $I = 0$, and in the normal condition of the electric displacement at the interface there is no jump between metallic and host dielectric

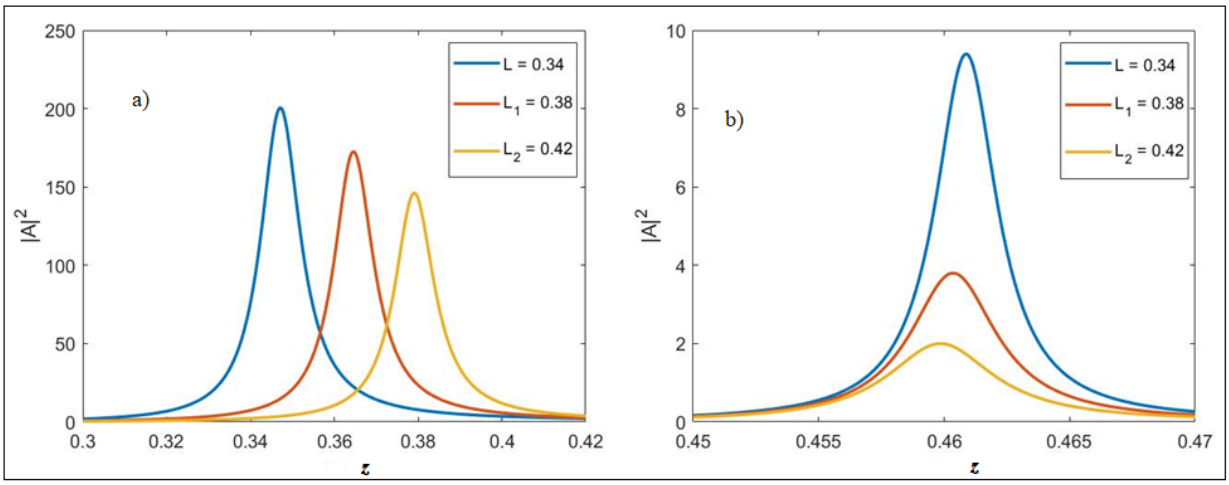

Figure 4.5: The Effect of depolarization factor on LFEF of spheroidal shell (Ag) NCs a) in passive dielectric and b) in active dielectric host mediums with interfacial layer parameters: $\omega_p = 1.45 \times 10^{16}\ rad/s$, $\varepsilon_\infty = 4.5$, $\gamma = 0.0115$, $I = 1.8$, $r_1 = 1.25$, $t = 0.75$, and different depolarization factor.

functions; whereas, for imperfect interface denoted by $I \neq 0$, the electric displacement passes across the interface mediums. Hence, managing the space of mediums between metallic and host dielectric function, I accordingly helps to obtain the LFEF of spheroidal NPs.

We studied the effects of L at the interfaces between metal-like, passive and active host matrices, by keeping parameters constant: where (I is 1.8, t is 0.75, r_1 is 1.25, the LFEF peaks are reduced. Hence, in constant thickness, interfacial factor, and radius of the interfaces as the depolarization factor increased, the LFEF peaks decreases slowly as shown in Fig. 4.5(a). However, the active host medium of the interfaces can have less LFEF as seen from its output results. Also the peaks of the active host medium decreased as the parameters like I, t, r, and L are increased.

4.5.3 Effects of interfacial factor on the LFEF

Next, we looked at how interfacial layer, I, affected the LFEF while the other parameters remained constant. Using the parameters $I = 2.25, I_1 = 2.5$, and $I_2 = 2.75$, the LFEF increased in the provided interfacial layer, as it is observed in (Figs. 4.6(a) and (b)) by using derived Eqn. (4.4.14). According to these findings, the interfacial layer was one of the elements that contributed to the LFEF rising as the interfacial magnitude at the interface rose. As it is seen in Figs. 4.6(a) and (b), it is considerably higher in passive host mediums compared to active host mediums. This demonstrated how crucial it is to have a close-fitting interfacial layer between the mediums, such as the active host matrix in a metal/dielectric nanocomposite, in order to achieve high LFEF at a specific frequency.

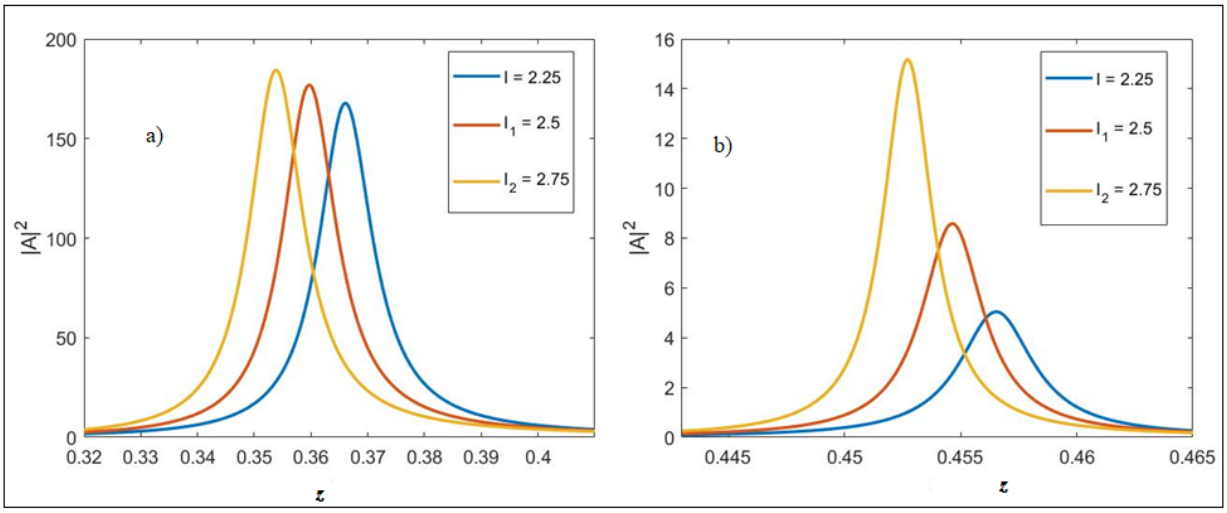

Figure 4.6: The effects of interfacial on LFEF of spheroidal shell NCs in passive and active host medium: $\omega = 1.45 \times 10^{16}\ rad/s$, $\gamma = 0.0115$, $\varepsilon_\infty = 4.5$, $L = 0.42$, $t = 0.75$, $r_1 = 1.25$ and different interfacial factor.

Generally, for the fixed values of L, t, and r,, we are able to get a higher output of LFEF in passive medium, while less output value in active embedding media as shown in Figs. 4.6(a) and (b), respectively. Also, the parameters present in ε_s of NCs in passive and

active host media can also affect the LFEF. Therefore, as I is increased, the peaks of the LFEF also increases and red-shifted. This is in agreement with that reported by Wu [218].

4.5.4 Effects of thickness on LFEF of NCs

Here, we are able to create a slowly growing LFEF by adjusting the thickness of spheroidal metal/dielectric NCs, t, by fixing the following parameters constant: $L = 0.36$, $I = 1.8$, and $r_1 = 1.25$, as shown in Figs. 4.7(a) and (b). When the depolarization factor, thickness, interfacial layer, and radius were used, the effects of thickness on the LFEF were clearly investigated as shown Fig. 4.7. However, when the mediums thickness were raised in both passive and active dielectric host mediums, the LFEF peaks are found to increase.

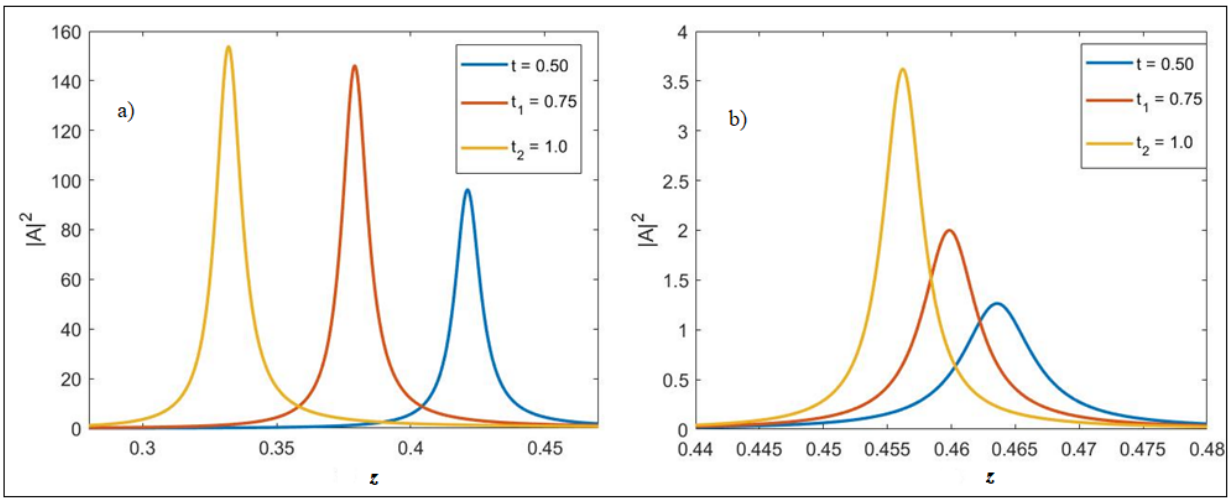

Figure 4.7: The effect of thickness on LFEF of spheroidal shell NCs in a) passive and b) active host medium: $\omega = 1.45 \times 10^{16}\ rad/s$, $\gamma = 0.0115$, $L = 0.42$, $I = 1.8$, $r_1 = 1.25$, and different thickness.

Further, as the thickness increase, the LFEF of the NCs spheroidal shell in passive and active dielectric host mediums gradually moves to the left, as seen in Fig. 4.7. In the LFEF in passive host media, there are noticeable small LFEF peaks in thin thickness at the interface mediums. However, as the thickness is varied, the LFEF in the active host

medium likewise shows a red-shift and increased symmetrically as thickness increased as shown in Fig. 4.7(b). As a result, in passive embedding host mediums, the enhancement factor with high thickness has a high peak, while in perturbed host mediums, it slowly decreases.

Likewise, in both passive and active embedding mediums the LFEFs can be affected by varying the thickness of the spheroidal metal/dielectric composite with the interfacial layer and red-shifted in both passive and active host matrix. As shown in both Figs. 4.7(a) and (b), changing the numerical values of the thickness in the medium may result in distinct LFEF outcomes.

4.5.5 Effect of radius on the LFEF of NCs

In this section, we investigated the effects of radius, r_1, on the LFEF of spheroidal metal/dielectric NPs, by fixing all the other parameters. As shown in both Figs. 4.8(a) and (b), the effect of radius on spheroidal NCs in passive and active host mediums greatly influenced the LFEF. However, the peaks of the LFEF are almost constant but blue-shifted as the radius increases in NCs with passive embedding materials as shown in Fig. 4.8(a). In contrast, the effects of radius on the LFEF is varied as the radius is increased in NCs with active medium; its peaks increases sequentially and slightly red-shifted, as shown in Fig. 8(b). Therefore, as shown in Figs. 4.8(a) and (b), the radius in spheroidal metal/dielectric NPs has an impact on the LFEF of spheroidal NCs. As illustrated in Fig. 4.8(a), increasing the radius can raise the LFEF, which is a peak that occurs at the metal/dielectric interface.

In general, when the incident field is applied to spheroidal metal-dielectric NPs in passive and active host matrix mediums, the field moves slowly in a thick medium and swiftly in a thin one. This can show us that the output result of the enhancement factor

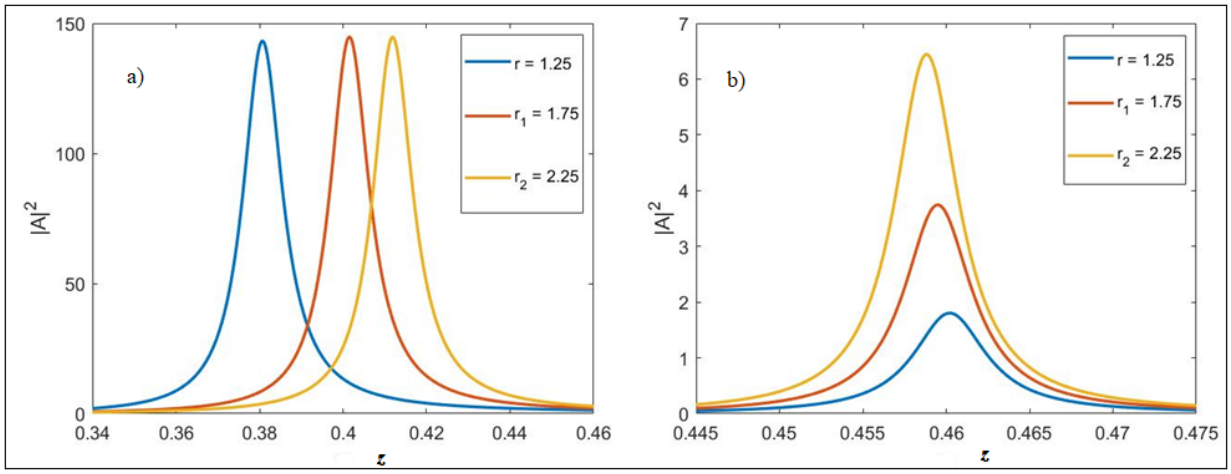

Figure 4.8: The effect of radius on LFEF of spheroidal shell NCs in a) passive and b) active host medium:$\omega = 1.45 \times 10^{16}\ rad/s$, $\gamma = 0.0115$, $\varepsilon_\infty = 4.5$, $L = 0.42$, $I = 1.75$, $t = 0.75$, and different radii.

reduces, and applied fields can pass through the composite medium more easily in less dense mediums. Therefore, in order to achieve the LFEF results, we must control the parameters in the spheroidal metal/dielectric NCs with passive and active host mediums such as the parameters L, I, t, and, r_1 employed in the spheroidal shell.

4.5.6 The effects of metal fraction on LFEF with interfacial layer

Next, keeping the remaining parameters constant, we examined how the metal proportion affected the LFEF of spheroidal metal/dielectric NPs using Eqn. (4.4.14). We calculated the LFEF of spheroidal metal-dielectric NPs embedded in passive and active host matrix using different values of $p = 0.85, 0.92, 0.99$, while $L = 0.36$, $I = 2.75$, $t = 0.75$, and $r_1 = 1.25$ can affect it. This illustrates that due to the incident electromagnetic, the output intensities of the peaks of the LFEF slightly decreases as the metal fraction increases in the passive embedding medium accompanied with a red-shift, as shown in Fig. 4.9(a). In the NCs with active medium, the LFEF peaks increases and is blue-shifted as the metal

fraction increases, as shown in Fig. 4.9(b).

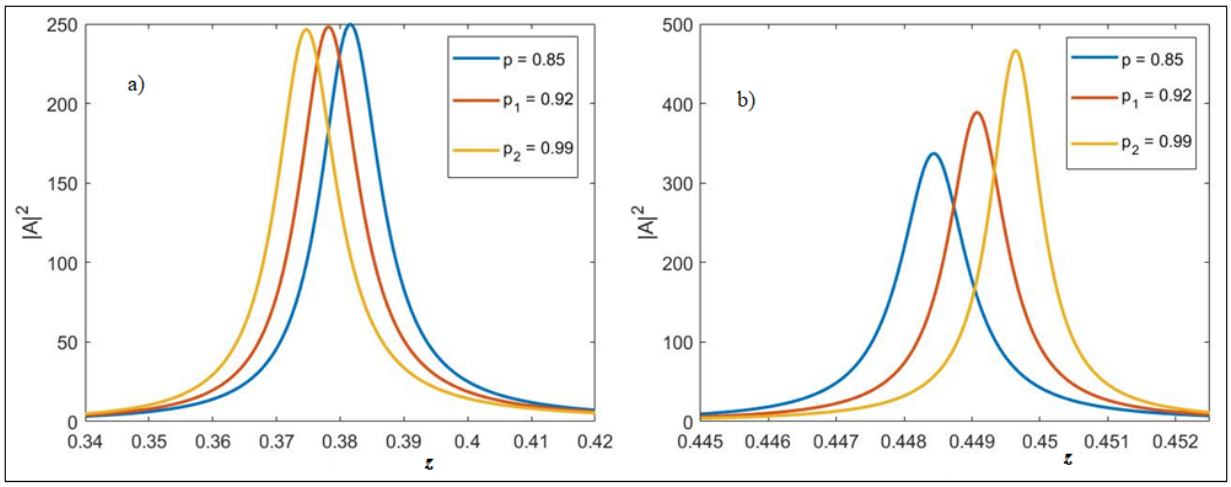

Figure 4.9: Effects of metal fraction on LFEF of spheroidal shell (Ag) NCs a) in passive dielectric and b) in active dielectric host mediums with parameters: $\omega = 1.45 \times 10^{16}\ rad/s$, $\gamma = 0.0115$, $\varepsilon_\infty = 4.5$, $L = 0.36$, $I = 2.75$, $t = 0.75$, and $r_1 = 1.25$, and different values of metal fraction.

Furthermore, as shown in Fig. 4.9(b), the peak values of the LFEF in the NCs increase with an increase in the metal content when the dielectric host medium becomes active and is perturbed by an incident field. The peak values, however, have a tendency to decline as the metal proportion rises in NCs with passive dielectric (Fig. 4.9(a)). Thus, we can see that the metal content in an active dielectric host medium has a significant impact on the LFEF of spheroidal shell NPs and causes a rise in its value.

Additionally, the peaks of the LFEF in NCs with active host medium is almost double compared to that in NCs with passive host matrix, as shown in Figs. 4.9(a) and (b). In both the passive and active dielectric host matrices, just one peak is visible. In general, the computational results demonstrate that the effects of metal fraction on the local field enhancement factor of spheroidal metal/dielectric NC inclusions can be significantly influenced, as shown in Fig. 4.9, and both of them displayed a single peak.

4.6 Conclusions

We studied the effect of passive and active permittivity of host matrix on the LFEF of spheroidal metal/dielectric NCs by varying L, p, I, t, and r. The findings demonstrate that in both passive and active host matrices, a single set of peaks is observed in the LFEF of the spheroidal metal/dielectric NCs with passive and active host matrices, regardless of how much L, p, I, and t vary or are kept constant. Furthermore, as the depolarization factor increases, the peaks seen in spheroidal metal/dielectric with passive and active host matrix gradually become less prominent. This demonstrates that when greater output values and a single LFEF peak is required, the spheroidal metal/dielectric NCs with passive host dielectric function is preferred to the active one. Additionally, we discovered that in the passive host matrix, the LFEF peaks are reduced and blue-shifted as L grows, while they decreased in the active host dielectric matrix. The peaks of LFEF are raised, and the blue shift is observed in both the passive and active host matrix as L grows. Moreover, the initial set of LFEF's peaks has red-shifted intensities as t in the passive host matrix increases. But as I grew above t, high intensities were observed, suggesting that altering the interface mediums of the geometry of spheroidal metal/dielectric NCs has a greater impact on raising the LFEF than altering the thickness of the medium at the interface.

Additionally, while the host matrix is passive, a rise in r_1 causes the LFEF's intensity to slightly increase, whereas the LFEF's intensity increases when the core is active. Furthermore, the examined LFEF peaks are both blue-shifted in the spheroidal NCs with passive host matrix, when r_1 increases while holding L, I, t, and p constant; in contrast, they are prominent in the active host matrix. Also, we discovered that by adjusting the metal fraction that is blue-shifted in the active host matrix and red-shifted in the passive host matrix, the LFEF of the spheroidal metal/dielectric NCs may be modified. Moreover,

the intensity of this peak varies significantly when its host matrix is active rather than passive. Hence, by changing these parameters and types of dielectric cores, adjustable LFEF of spheroidal metal/dielectric NCs could be obtained and used for applications in optical detection and imaging, nonlinear optics, and optical sensing.

Chapter 5

Summary

In this dissertation, we studied the effects of depolarization factor (L), metal fraction (p), permittivity of the host matrix (ε_h), and interfacial layer on the local field enhancement factor (LFEF), induced optical bistability (IOB), and bistability domain (BD) of spheroidal core-shell nanocomposites (NCs) that consists of a passive or active dielectric cores. The analysis is carried out by employing the Drude-Lorentz dielectric function model and Laplace's equation under quasistatic approximation. The overall analysis consists of three parts. Accordingly, the main results of the investigations are summarized below:

I. For local field enhancement factor (LFEF)

In the first part of the study, we investigated the effects of L, p, and ε_h on the local field enhancement factor (LFEF) of the spheroidal core-shell NCs with passive or active dielectric cores.

- It is shown that the graph of the LFEF versus wavelength possesses two sets of peaks for NCs with passive dielectric cores, while only one set of peaks is observed in NCs with active dielectric cores, regardless the specific values of L, p, or ε_h.

- For NCs with passive cores, when the parameters, i.e., L, p or ε_h are varied, it is found that the first set of peaks have higher intensities the second set of peas. In addition, with passive dielectric core as L or p increases, the intensity of the first set of LFEF's peaks increases accompanied with a blue shift. On the other hand, the intensity of the second set of peaks also increases in a similar manner, but they exhibit a red shift. However, higher intensities were seen when L increases instead of p, suggesting that altering the geometry of spheroidal CSNCs has a greater impact on the LFEF of the NCs than varying the metal fraction, p.

- Similarly, the intensity of the LFEF increases with an increase in ε_h when the dielectric core is active and decreases when it is passive. Furthermore, in the spheroidal NCs with both kinds of dielectric cores, the peaks of the LFEF are red-shifted when ε_h is increased while keeping L and p to be constant. The peak intensities of the LFEF for spheroidal CSNCs with an active dielectric core are increased by increasing L and ε_h, but the peak positions are reversed.

II. Induced optical bistabity (IOB) and bistability domain (BD)

In the second part of the investigation, we considered how induced optical bistability (IOB) and bistability domain (BD) of spheroidal core-shell nanocomposites (NCs) are affected by L, p, and ε_h. The NCs are composed of passive and active dielectric cores coated with a metallic shell and embedded in host matrices. The main results are:

- The IOB of the NCs is attained at a lower applied field in the passive dielectric core than the active one, regardless of how L, p, or ε_h vary. In both passive and active dielectric cores, the switching-up and switching-down threshold points of IOB for the depolarization factor, L, are obtained essentially at similar values of the applied fields,

and for the given values of L, the stable states of IOB display the same patterns. In addition, the IOB regions are narrow in the NCs with passive cores, while it is broad for those with active dielectric core. In a similar way, keeping L and ε_h constant while changing p results in "S-like"bistability regions in both passive and active dielectric cores. However, when p increases, so does the incident field required at each switching-up threshold point, in both passive and active dielectric cores. The other parameter which affects the IOB is ε_h, Increasing ε_h, also increases the switching-up threshold of IOB in both types of cores. For a larger value of ε_h, the switching-up threshold of the IOB of spheroidal CSNCs can be obtained at a smaller value of the incident field.

- In addition, we looked at the positive and negative roots from the IOB equations and observed that the bistability domain (BD) lies on the $z - Y$ plane. The BD is limited within the inset regions of the extremum points f_1 and f_2, resulting in a series of maxima and minima in the $z - Y$ plane. As a result, when the maxima of the positive and minima of the negative root points of the curves f_1 and f_2 merge, the bistability domain vanishes. In general, we observed that by varying the depolarization factor, metal fraction, and host medium, it is possible to control the values of BD in spheroidal core-shell NCs in each region.

III. The effects interfacial layer on LFEF

In the third part of the work, we considered a system that consists of spheroidal shell nanocomposite embedded in a host matrix and analyzed it using the quasistatic approximation. The dielectric function of the embedding medium was regarded as either passive or active to explore its effects on the LFEF.

- The findings demonstrate that in both passive and active host matrices, a single set

of peaks is observed in the spectra of the LFEF of the spheroidal metal/dielectric NCs regardless of how we vary L, p, I, or t. Furthermore, as the depolarization factor rises, the peaks seen in spheroidal metal/dielectric with passive and active host matrix gradually become less prominent. The peaks with passive dielectric core are very larger compared with that using active core, demonstrating that NCs with passive host is preferred to the active one for potential applications.

- It is also observed that in NCs with passive host matrix, the LFEF peaks are reduced and blue-shifted as L increases, while there is no shift in the peak positions for NCs with active host matrix. However, when the interfacial layer is taken into account and L increases, the peaks of the LFEF are found to increase and red shifted in both NCs with passive and active host matrix.

- Moreover, the initial set of LFEFs peaks have red-shifted intensities as t in the passive host matrix increases. But, as I is increased above t, relatively high intensities were observed, suggesting that altering the geometry of spheroidal metal/dielectric NCs has a greater impact on raising the LFEF than altering the thickness of the medium at the interface.

- In addition, when the host matrix is passive, an increase in r causes the LFEFs the intensity to increase only slightly, whereas the LFEFs intensity increases significantly when the core is active. Furthermore, we observed that the LFEF peaks are red-shifted in both spheroidal NCs with passive and active host matrices when r is increased while keeping the other parameters constant. Also, increasing the metal fraction, p, results to blue-shift in the active host matrix and red-shift in NCs with passive host matrix.

Bibliography

[1] Suravi Pandit, Debaprotim Dasgupta, Nazneen Dewan, and Ahmed Prince. Nanotechnology based biosensors and its application. *The Pharma Innovation*, 5(6, Part A):18, 2016.

[2] Carlos Caro, Paula M. Castillo, Rebecca Klippstein, David Pozo, and Ana P Zaderenko. Silver nanoparticles: sensing and imaging applications. *Silver nanoparticles*, 201, 2010.

[3] Samer Bayda, Muhammad Adeel, Tiziano Tuccinardi, Marco Cordani, and Flavio Rizzolio. The history of nanoscience and nanotechnology: from chemical–physical applications to nanomedicine. *Molecules*, 25(1):112, 2019.

[4] T Pradeep. *Nano: the essentials: understanding nanoscience and nanotechnology*. McGraw-Hill Education, 2007.

[5] George M Whitesides. Nanoscience, nanotechnology, and chemistry. *Small*, 1(2):172–179, 2005.

[6] Mihail C Roco, Chad A Mirkin, and Mark C Hersam. Nanotechnology research directions for societal needs in 2020. *Retrospective and Outlook. National Science Foundation (Sponsor)*, 2010.

[7] Erik T Thostenson, Chunyu Li, and Tsu-Wei Chou. Nanocomposites in context. *Composites science and technology*, 65(3-4):491–516, 2005.

[8] Freddy C Adams and Carlo Barbante. Nanoscience, nanotechnology and spectrometry. *Spectrochimica Acta Part B: Atomic Spectroscopy*, 86:3–13, 2013.

[9] Gabor L Hornyak, Joydeep Dutta, Harry F Tibbals, and Anil Rao. *Introduction to nanoscience*. CRC press, 2008.

[10] Herbert Gleiter. Nanostructured materials: basic concepts and microstructure. *Acta materialia*, 48(1):1–29, 2000.

[11] K Lance Kelly, Eduardo Coronado, Lin Lin Zhao, and George C Schatz. The optical properties of metal nanoparticles: the influence of size, shape, and dielectric environment, 2003.

[12] Jaison Jeevanandam, Ahmed Barhoum, Yen S Chan, Alain Dufresne, and Michael K Danquah. Review on nanoparticles and nanostructured materials: history, sources, toxicity and regulations. *Beilstein journal of nanotechnology*, 9(1):1050–1074, 2018.

[13] Shawn Y Stevens, LeeAnn M Sutherland, and Joseph S Krajcik. *The big ideas of nanoscale science and engineering*. NSTA press, 2009.

[14] Chan Zheng, Jiaxin Huang, Li Lei, Wenzhe Chen, Haiyan Wang, and Wei Li. Nanosecond nonlinear optical and optical limiting properties of hollow gold nanocages. *Applied Physics B*, 124:1–8, 2018.

[15] Viktoriia E Babicheva. Optical processes behind plasmonic applications. *Nanomaterials*, 13(7):1270, 2023.

[16] Rui Xiong, Jingyi Luan, Saewon Kang, Chunhong Ye, Srikanth Singamaneni, and Vladimir V Tsukruk. Biopolymeric photonic structures: design, fabrication, and emerging applications. *Chemical Society Reviews*, 49(3):983–1031, 2020.

[17] Hao Jing, Li Zhang, and Hui Wang. Geometrically tunable optical properties of metal nanoparticles. In *UV-VIS and Photoluminescence Spectroscopy for Nanomaterials Characterization*, pages 1–74. Springer, 2013.

[18] Chao Wang, Vignesh Murugadoss, Jie Kong, Zhenfeng He, Xianmin Mai, Qian Shao, Yanjun Chen, Li Guo, Chuntai Liu, Subramania Angaiah, et al. Overview of carbon nanostructures and nanocomposites for electromagnetic wave shielding. *Carbon*, 140:696–733, 2018.

[19] Biao Zhao, Mahdi Hamidinejad, Shuai Wang, Pengwei Bai, Renchao Che, Rui Zhang, and Chul B Park. Advances in electromagnetic shielding properties of composite foams. *Journal of Materials Chemistry A*, 9(14):8896–8949, 2021.

[20] Junxi Zhang and Lide Zhang. Nanostructures for surface plasmons. *Advances in Optics and Photonics*, 4(2):157–321, 2012.

[21] Junxi Zhang, Lide Zhang, and Wei Xu. Surface plasmon polaritons: physics and applications. *Journal of Physics D: Applied Physics*, 45(11):113001, 2012.

[22] Yi Ding and Mingwei Chen. Nanoporous metals for catalytic and optical applications. *MRS bulletin*, 34(8):569–576, 2009.

[23] Tapan K Sau, Andrey L Rogach, Frank Jäckel, Thomas A Klar, and Jochen Feldmann. Properties and applications of colloidal nonspherical noble metal nanoparticles. *Advanced Materials*, 22(16):1805–1825, 2010.

[24] Jun Lu, Yao Xue, and Nicholas A Kotov. Emerging trends in chiral inorganic nanostructures. *Israel Journal of Chemistry*, 61(11-12):851–862, 2021.

[25] Isabel Pastoriza-Santos, Calum Kinnear, Jorge Pérez-Juste, Paul Mulvaney, and Luis M Liz-Marzán. Plasmonic polymer nanocomposites. *Nature Reviews Materials*, 3(10):375–391, 2018.

[26] Mehdi Keshavarz Hedayati, Franz Faupel, and Mady Elbahri. Review of plasmonic nanocomposite metamaterial absorber. *Materials*, 7(2):1221–1248, 2014.

[27] Pavel I Geshev, Stefan Klein, Tobias Witting, Klaus Dickmann, and Michael Hietschold. Calculation of the electric-field enhancement at nanoparticles of arbitrary shape in close proximity to a metallic surface. *Physical Review B*, 70(7):075402, 2004.

[28] Martin Moskovits, Li-Lin Tay, Jody Yang, and Thomas Haslett. Sers and the single molecule. In *Optical properties of nanostructured random media*, pages 215–227. Springer, 2002.

[29] George C Schatz and Richard P Van Duyne. Electromagnetic mechanism of surface-enhanced spectroscopy, 2002.

[30] PW Barber, RK Chang, and He Massoudi. Electrodynamic calculations of the surface-enhanced electric intensities on large ag spheroids. *Physical Review B*, 27(12):7251, 1983.

[31] A Wokaun. Surface enhancement of optical fields: mechanism and applications. *Molecular Physics*, 56(1):1–33, 1985.

[32] Wen-Hui Yang, George C Schatz, and Richard P Van Duyne. Discrete dipole approximation for calculating extinction and raman intensities for small particles with arbitrary shapes. *The Journal of chemical physics*, 103(3):869–875, 1995.

[33] M Futamata, Y Maruyama, and M Ishikawa. Local electric field and scattering cross section of ag nanoparticles under surface plasmon resonance by finite difference time domain method. *The Journal of Physical Chemistry B*, 107(31):7607–7617, 2003.

[34] WJ Yu, H Sun, and L Gao. Optical bistability in core-shell magnetoplasmonic nanoparticles with magnetocontrollability. *Optics Express*, 24(19):22272–22281, 2016.

[35] YR Shen. Recent advances in optical bistability. 1982.

[36] R Neuendorf, M Quinten, and U Kreibig. Optical bistability of small heterogeneous clusters. *The Journal of chemical physics*, 104(16):6348–6354, 1996.

[37] Nader Daneshfar and Tayebeh Naseri. Switching between optical bistability and multistability in plasmonic multilayer nanoparticles. *Journal of Applied Physics*, 121(2):023111, 2017.

[38] Russell J Gehr and Robert W Boyd. Optical properties of nanostructured optical materials. *Chemistry of materials*, 8(8):1807–1819, 1996.

[39] Yachen Gao and Deigui Kong. Nonlinear optical response of noble metal nanoparticles. *Laser Technology and its Applications*, page 43, 2019.

[40] KM Leung. Optical bistability in the scattering and absorption of light from nonlinear microparticles. *Physical Review A*, 33(4):2461, 1986.

[41] VN Mal'nev and Sisay Shewamare. Slow and fast light in metal/dielectric composites with passive and active host matrices. *Physica B: Condensed Matter*, 426:52–57, 2013.

[42] OA Buryi, LG Grechko, VN Mal?nev, and S Shewamare. Induced optical bistability in small metal and metal coated particles with nonlinear dielectric functions. *Ukrainian Journal of Physics*, 56(4):311–311, 2011.

[43] Craig F Bohren and Donald R Huffman. *Absorption and scattering of light by small particles*. John Wiley & Sons, 2008.

[44] Tayebeh Naseri and Fatemeh Pourkhavari. Impact of geometry and magneto-optical properties on field enhancement and optical bistability in core–shell nanoparticles. *Journal of Theoretical and Applied Physics*, 13:23–29, 2019.

[45] Mina Piralaee, A Asgari, and V Siahpoush. Plasmonic properties of spheroid silicon-silver nanoshells in prolate and oblate forms. *Optik*, 172:1064–1068, 2018.

[46] JW Haus, N Kalyaniwalla, Ramarao Inguva, and CM Bowden. Optical bistability in small metallic particle composites. *Journal of applied physics*, 65(4):1420–1423, 1989.

[47] Jian Zhu and Shu-min Zhao. Plasmonic refractive index sensitivity of ellipsoidal al nanoshell: Tuning the wavelength position and width of spectral dip. *Sensors and Actuators B: Chemical*, 232:469–476, 2016.

[48] Riad Haidar. Famous optician: James clerk maxwell. *Photoniques*, pages 16–18, 2018.

[49] Frederick Seitz. James clerk maxwell (1831-1879); member aps 1875. *Proceedings of the American Philosophical Society*, 145(1):1–44, 2001.

[50] James Clerk Maxwell. Viii. a dynamical theory of the electromagnetic field. *Philosophical transactions of the Royal Society of London*, (155):459–512, 1865.

[51] Shun Lien Chuang. *Physics of photonic devices*. John Wiley & Sons, 2012.

[52] AG Astill. Material figures of merit for non-linear optics. *Thin Solid Films*, 204(1):1–17, 1991.

[53] Chuang-tian Chen and Guang-zhao Liu. Recent advances in nonlinear optical and electro-optical materials. *Annual Review of Materials Science*, 16(1):203–243, 1986.

[54] Sagadevan Suresh and Dakshanamoorthy Arivuoli. Nanomaterials for nonlinear optical (nlo) applications: a review. *Rev. Adv. Mater. Sci*, 30(3):243–253, 2012.

[55] A Primer. Linear and nonlinear polarizability. *i 1111ll Materials*, 455(9Q), 1991.

[56] McGraw-Hill. *McGraw-Hill encyclopedia of science and technology*. McGraw-Hill, New York, NY, 5th edn edition, 1993.

[57] R.W.Boyd. *Nonlinear Optics*. Academic Press, 1992.

[58] Robert W Boyd, Alexander L Gaeta, and Enno Giese. Nonlinear optics. In *Springer Handbook of Atomic, Molecular, and Optical Physics*, pages 1097–1110. Springer, 2008.

[59] M Bertolotti. 1962–2012: What does it mean fifty years in laser research? *Romanian Reports in Physics*, 65(3):619–637, 2013.

[60] Richard L Sutherland. *Handbook of nonlinear optics*. CRC press, 2003.

[61] D Arivuoli. Fundamentals of nonlinear optical materials. *Pramana*, 57:871–883, 2001.

[62] Thomas Schneider. *Nonlinear optics in telecommunications*. Springer Science & Business Media, 2004.

[63] Jerome V Moloney and Alan C Newell. Nonlinear optics. *Physica D: Nonlinear Phenomena*, 44(1-2):1–37, 1990.

[64] Zhen Chai, Xiaoyong Hu, Feifan Wang, Xinxiang Niu, Jingya Xie, and Qihuang Gong. Ultrafast all-optical switching. *Advanced Optical Materials*, 5(7):1600665, 2017.

[65] Vyacheslav A Trofimov, Alexey G Volkov, and Sheng Lan. Two-waves optical switching element based on layered nonlinear structure. In *Photonic Fiber and Crystal Devices: Advances in Materials and Innovations in Device Applications III*, volume 7420, pages 231–242. SPIE, 2009.

[66] Andrey K Sarychev and Vladimir M Shalaev. Electromagnetic field fluctuations and optical nonlinearities in metal-dielectric composites. *Physics Reports*, 335(6):275–371, 2000.

[67] WP Greene, HM Gibbs, A Passner, SL McCall, and TNC Venkatesan. Optical bistability: An undergraduate experiment. *Optics News*, 6(2):16–19, 1980.

[68] Luigi A Lugiato. Ii theory of optical bistability. In *Progress in optics*, volume 21, pages 69–216. Elsevier, 1984.

[69] N Peyghambarian and HM Gibbs. Optical bistability for optical signal processing and computing. *Optical Engineering*, 24(1):68–73, 1985.

[70] Toni Pérez, Alessandro Scirè, Guy Van der Sande, Pere Colet, and Claudio R Mirasso. Bistability and all-optical switching in semiconductor ring lasers. *Optics express*, 15(20):12941–12948, 2007.

[71] Michael Vasilyev, Yikai Su, and Colin J McKinstrie. Introduction to the special issue on nonlinear-optical signal processing. *Ieee Journal of Selected Topics in Quantum Electronics*, 14(3):527–528, 2008.

[72] Elsa Garmire. Introduction to bistable optical devices for optical signal processing. In *Devices and systems for optical signal processing*, volume 218, pages 27–32. SPIE, 1980.

[73] Hyatt Gibbs. *Optical bistability: controlling light with light*. Elsevier, 2012.

[74] A Asghari Nejad, H Ranjbar Askari, and HR Baghshahi. Optical bistability in coupled optomechanical cavities in the presence of kerr effect. *Applied Optics*, 56(10):2816–2820, 2017.

[75] Yaron Silberberg and Israel Bar-Joseph. Optical instabilities in a nonlinear kerr medium. *JOSA B*, 1(4):662–670, 1984.

[76] A-BMA Ibrahim and J Osman. Intrinsic optical bistability in kerr ferroelectric materials. *The European Physical Journal B*, 63:193–198, 2008.

[77] Govind P Agrawal. Nonlinear fiber optics. In *Nonlinear Science at the Dawn of the 21st Century*, pages 195–211. Springer, 2000.

[78] F. Bohren and D.R.Huffman. *Absorption and Scattering of Light by Small Particles*. Wiley, New York, 1983.

[79] Ineke Malsh. Biomedical Applications of Nanotechnology. *The Industrial physicists*, 8(3), 2002.

[80] Andrei Stalmashonak, Gerhard Seifert, Amin Abdolvand, Andrei Stalmashonak, Gerhard Seifert, and Amin Abdolvand. Optical properties of nanocomposites containing metal nanoparticles. *Ultra-Short Pulsed Laser Engineered Metal-Glass Nanocomposites*, pages 5–15, 2013.

[81] Luigi A Lugiato and René Lefever. Spatial dissipative structures in passive optical systems. *Physical review letters*, 58(21):2209, 1987.

[82] Raktim Haldar, Arkadev Roy, Partha Mondal, Vishwatosh Mishra, and Shailendra K Varshney. Free-carrier-driven kerr frequency comb in optical microcavities: Steady state, bistability, self-pulsation, and modulation instability. *Physical Review A*, 99(3):033848, 2019.

[83] Mustapha Tlidi, Paul Mandel, and René Lefever. Localized structures and localized patterns in optical bistability. *Physical review letters*, 73(5):640, 1994.

[84] Daniel Gruner, Raymond Kapral, and Anna Lawniczak. Nucleation, domain growth, and fluctuations in a bistable chemical system. *The Journal of chemical physics*, 99(5):3938–3945, 1993.

[85] Nick I Markevich, Jan B Hoek, and Boris N Kholodenko. Signaling switches and bistability arising from multisite phosphorylation in protein kinase cascades. *The Journal of cell biology*, 164(3):353–359, 2004.

[86] Sisay Shewamare and VN Mal'nev. Two optical bistability domains in composites of metal nanoparticles with nonlinear dielectric core. *Physica B: Condensed Matter*, 407(24):4837–4842, 2012.

[87] Luigi A Lugiato. Optical bistability. *Contemporary Physics*, 24(4):333–371, 1983.

[88] Anil K Maini. *Digital electronics: principles, devices and applications*. John Wiley & Sons, 2007.

[89] Mohommad T Fatehi, Kenneth C Wasmundt, and Stuart A Collins. Optical flip-flops and sequential logic circuits using a liquid crystal light valve. *Applied optics*, 23(13):2163–2171, 1984.

[90] Mohsin Ali Badshah, Na Yoon Koh, Abdul Wasy Zia, Naseem Abbas, Zahra Zahra, and Muhammad Wajid Saleem. Recent developments in plasmonic nanostructures for metal enhanced fluorescence-based biosensing. *Nanomaterials*, 10(9):1749, 2020.

[91] Nicolae C Panoiu, Wei EI Sha, DY Lei, and GC Li. Nonlinear optics in plasmonic nanostructures. *Journal of Optics*, 20(8):083001, 2018.

[92] Pietro Strobbia, Eric Languirand, and Brian M Cullum. Recent advances in plasmonic nanostructures for sensing: a review. *Optical Engineering*, 54(10):100902–100902, 2015.

[93] Katherine A Willets and Richard P Van Duyne. Localized surface plasmon resonance spectroscopy and sensing. *Annu. Rev. Phys. Chem.*, 58:267–297, 2007.

[94] Zheyu Fang and Xing Zhu. Plasmonics in nanostructures. *Advanced Materials*, 25(28):3840–3856, 2013.

[95] Yongdong Jin. Engineering plasmonic gold nanostructures and metamaterials for biosensing and nanomedicine. *Advanced Materials*, 24(38):5153–5165, 2012.

[96] Richard BM Schasfoort. *Handbook of surface plasmon resonance*. Royal Society of Chemistry, 2017.

[97] Rob PH Kooyman. Physics of surface plasmon resonance. *Handbook of Surface Plasmon Resonance*, 1, 2008.

[98] Pratim Biswas and Chang-Yu Wu. Nanoparticles and the environment. *Journal of the air & waste management association*, 55(6):708–746, 2005.

[99] VJ Mohanraj and YJTJOPR Chen. Nanoparticles-a review. *Tropical journal of pharmaceutical research*, 5(1):561–573, 2006.

[100] Lijun Li, Jingya Liu, and Ting Zhu. Study of plasmon resonance. In *IOP Conference Series: Materials Science and Engineering*, volume 381, page 012101. IOP Publishing, 2018.

[101] Laura L Beecroft and Christopher K Ober. Nanocomposite materials for optical applications. *Chemistry of materials*, 9(6):1302–1317, 1997.

[102] Lin Dong. *Optical properties of nanoparticles in composite materials*. PhD thesis, KTH Royal Institute of Technology, 2012.

[103] Stefan A Maier et al. *Plasmonics: fundamentals and applications*, volume 1. Springer, 2007.

[104] Yong Chen and Hai Ming. Review of surface plasmon resonance and localized surface plasmon resonance sensor. *Photonic Sensors*, 2:37–49, 2012.

[105] Robert Karlsson and Anders Fält. Experimental design for kinetic analysis of protein-protein interactions with surface plasmon resonance biosensors. *Journal of immunological methods*, 200(1-2):121–133, 1997.

[106] Heinz Reather. Surface plasmon on smooth and rough surfaces and on gratings. *Springer Tracts in Modern Physics*, 111, 1988.

[107] W Andrew Murray and William L Barnes. Plasmonic materials. *Advanced materials*, 19(22):3771–3782, 2007.

[108] Surbhi Lal, Stephan Link, and Naomi J Halas. Nano-optics from sensing to waveguiding. *Nature photonics*, 1(11):641–648, 2007.

[109] Martti Kauranen and Anatoly V Zayats. Nonlinear plasmonics. *Nature photonics*, 6(11):737–748, 2012.

[110] David J Bergman and David Stroud. Physical properties of macroscopically inhomogeneous media. In *Solid state physics*, volume 46, pages 147–269. Elsevier, 1992.

[111] Mark I Stockman. Nanoplasmonics: past, present, and glimpse into future. *Optics express*, 19(22):22029–22106, 2011.

[112] Harry A Atwater and Albert Polman. Plasmonics for improved photovoltaic devices. *Nature materials*, 9(3):205–213, 2010.

[113] Mark W Knight, Heidar Sobhani, Peter Nordlander, and Naomi J Halas. Photodetection with active optical antennas. *Science*, 332(6030):702–704, 2011.

[114] Jeffrey N Anker, W Paige Hall, Olga Lyandres, Nilam C Shah, Jing Zhao, and Richard P Van Duyne. Biosensing with plasmonic nanosensors. *Nature materials*, 7(6):442–453, 2008.

[115] Cecilia Noguez. Surface plasmons on metal nanoparticles: the influence of shape and physical environment. *The Journal of Physical Chemistry C*, 111(10):3806–3819, 2007.

[116] Ekmel Ozbay. Plasmonics: merging photonics and electronics at nanoscale dimensions. *science*, 311(5758):189–193, 2006.

[117] Nan Zhang, Siqi Liu, and Yi-Jun Xu. Recent progress on metal core@ semiconductor shell nanocomposites as a promising type of photocatalyst. *Nanoscale*, 4(7):2227–2238, 2012.

[118] Krishnendu Chatterjee, Sreerupa Sarkar, K Jagajjanani Rao, and Santanu Paria. Core/shell nanoparticles in biomedical applications. *Advances in colloid and interface science*, 209:8–39, 2014.

[119] Rajib Ghosh Chaudhuri and Santanu Paria. Core/shell nanoparticles: classes, properties, synthesis mechanisms, characterization, and applications. *Chemical reviews*, 112(4):2373–2433, 2012.

[120] Manoj B Gawande, Anandarup Goswami, Tewodros Asefa, Huizhang Guo, Ankush V Biradar, Dong-Liang Peng, Radek Zboril, and Rajender S Varma. Core–shell nanoparticles: synthesis and applications in catalysis and electrocatalysis. *Chemical Society Reviews*, 44(21):7540–7590, 2015.

[121] Pramod K Kalambate, Zhimei Huang, Yankai Li, Yue Shen, Meilan Xie, Yunhui Huang, Ashwini K Srivastava, et al. Core@ shell nanomaterials based sensing devices: A review. *TrAC Trends in Analytical Chemistry*, 115:147–161, 2019.

[122] Suying Wei, Qiang Wang, Jiahua Zhu, Luyi Sun, Hongfei Lin, and Zhanhu Guo. Multifunctional composite core–shell nanoparticles. *Nanoscale*, 3(11):4474–4502, 2011.

[123] Xiaoxia Ma, Yuxiang Li, Iftikhar Hussain, Ruiqi Shen, Guangcheng Yang, and Kaili Zhang. Core–shell structured nanoenergetic materials: preparation and fundamental properties. *Advanced Materials*, 32(30):2001291, 2020.

[124] Sheenam Thatai, Parul Khurana, Jyoti Boken, Surendra Prasad, and Dinesh Kumar. Nanoparticles and core–shell nanocomposite based new generation water remediation materials and analytical techniques: A review. *Microchemical Journal*, 116:62–76, 2014.

[125] Qiao Zhang, Ilkeun Lee, Ji Bong Joo, Francisco Zaera, and Yadong Yin. Core–shell nanostructured catalysts. *Accounts of Chemical Research*, 46(8):1816–1824, 2013.

[126] Hamed Ataee-Esfahani, Masataka Imura, and Yusuke Yamauchi. All-metal mesoporous nanocolloids: solution-phase synthesis of core–shell pd@ pt nanoparticles with a designed concave surface. *Angewandte Chemie*, 125(51):13856–13860, 2013.

[127] Kwangjin An and Gabor A Somorjai. Size and shape control of metal nanoparticles for reaction selectivity in catalysis. *ChemCatChem*, 4(10):1512–1524, 2012.

[128] Elad Gross, James M Krier, Lars Heinke, and Gabor A Somorjai. Building bridges in catalysis science. monodispersed metallic nanoparticles for homogeneous catalysis

and atomic scale characterization of catalysts under reaction conditions. *Topics in Catalysis*, 55:13–23, 2012.

[129] Byungkwon Lim and Younan Xia. Metal nanocrystals with highly branched morphologies. *Angewandte Chemie International Edition*, 50(1):76–85, 2011.

[130] Panikkanvalappil R Sajanlal, Theruvakkattil S Sreeprasad, Akshaya K Samal, and Thalappil Pradeep. Anisotropic nanomaterials: structure, growth, assembly, and functions. *Nano reviews*, 2(1):5883, 2011.

[131] Seyyed Hossein Asadpour and Abdullah Eslami-Majd. Controlling the optical bistability and transmission coefficient in a four-level atomic medium. *Journal of luminescence*, 132(6):1477–1482, 2012.

[132] AT Rosenberger, LA Orozco, and HJ Kimble. Observation of absorptive bistability with two-level atoms in a ring cavity. *Physical Review A*, 28(4):2569, 1983.

[133] DE Grant and HJ Kimble. Optical bistability for two-level atoms in a standing-wave cavity. *Optics Letters*, 7(8):353–355, 1982.

[134] HM Gibbs, SL McCall, and TNC Venkatesan. Differential gain and bistability using a sodium-filled fabry-perot interferometer. *Physical Review Letters*, 36(19):1135, 1976.

[135] Andrei Stalmashonak, Gerhard Seifert, and Amin Abdolvand. *Ultra-short pulsed laser engineered metal-glass nanocomposites*. Springer, 2013.

[136] Vincenzo Amendola, Roberto Pilot, Marco Frasconi, Onofrio M Maragò, and Maria Antonia Iatì. Surface plasmon resonance in gold nanoparticles: a review. *Journal of Physics: Condensed Matter*, 29(20):203002, 2017.

[137] NI Zheludev. Nonlinear optics on the nanoscale. *Contemporary Physics*, 43(5):365–377, 2002.

[138] Nick N Lepeshkin, Aaron Schweinsberg, Giovanni Piredda, Ryan S Bennink, and Robert W Boyd. Enhanced nonlinear optical response of one-dimensional metal-dielectric photonic crystals. *Physical review letters*, 93(12):123902, 2004.

[139] Vladimir M Shalaev and Satoshi Kawata. *Nanophotonics with surface plasmons*. Elsevier, 2006.

[140] Mark L Brongersma and Pieter G Kik. *Surface plasmon nanophotonics*, volume 131. Springer, 2007.

[141] M Righini, C Girard, and R Quidant. Light-induced manipulation with surface plasmons. *Journal of Optics A: Pure and Applied Optics*, 10(9):093001, 2008.

[142] Jun Wang and Werner J Blau. Inorganic and hybrid nanostructures for optical limiting. *Journal of Optics A: Pure and Applied Optics*, 11(2):024001, 2009.

[143] Andrey K Sarychev and Vladimir M Shalaev. Theory of nonlinear optical responses in metal?dielectric composites. In *Optical Properties of Nanostructured Random Media*, pages 169–186. Springer, 2002.

[144] Wolfgang Schärtl. Current directions in core–shell nanoparticle design. *Nanoscale*, 2(6):829–843, 2010.

[145] Mohammadreza Naeimirad, Ali Zadhoush, Richard Kotek, Rasoul Esmaeely Neisiany, Saied Nouri Khorasani, and Seeram Ramakrishna. Recent advances in core/shell bicomponent fibers and nanofibers: A review. *Journal of Applied Polymer Science*, 135(21):46265, 2018.

[146] Vladimir M Shalaev. *Optical properties of nanostructured random media*, volume 82. Springer Science & Business Media, 2002.

[147] Thomas Volz, Andreas Reinhard, Martin Winger, Antonio Badolato, Kevin J Hennessy, Evelyn L Hu, and Ataç Imamoğlu. Ultrafast all-optical switching by single photons. *Nature Photonics*, 6(9):605–609, 2012.

[148] Yu-xi Zhang and Yu-hua Wang. Nonlinear optical properties of metal nanoparticles: a review. *RSC advances*, 7(71):45129–45144, 2017.

[149] Ryan S Bennink, Young-Kwon Yoon, Robert W Boyd, and JE Sipe. Accessing the optical nonlinearity of metals with metal–dielectric photonic bandgap structures. *Optics Letters*, 24(20):1416–1418, 1999.

[150] Stephen Arnold, TR O?Keeffe, KM Leung, LM Folan, T Scalese, and A Pluchino. Optical bistability of an aqueous aerosol particle detected through light scattering: theory and experiment. *Applied optics*, 29(24):3473–3478, 1990.

[151] Lufsyi Mahmudin, Edi Suharyadi, Agung Bambang Setio Utomo, Kamsul Abraha, et al. Optical properties of silver nanoparticles for surface plasmon resonance (spr)-based biosensor applications. *Journal of Modern Physics*, 6(08):1071, 2015.

[152] AL Stepanov. Nonlinear optical properties of metal nanoparticles in silicate glass. In *Glass Nanocomposites*, pages 165–179. Elsevier, 2016.

[153] Daniel W Brandl and Peter Nordlander. Plasmon modes of curvilinear metallic core/shell particles. *The Journal of chemical physics*, 126(14):144708, 2007.

[154] Yu-Ying Yu, Ser-Sing Chang, Chien-Liang Lee, and CR Chris Wang. Gold nanorods: electrochemical synthesis and optical properties. *The Journal of Physical Chemistry B*, 101(34):6661–6664, 1997.

[155] I Lisiecki, F Billoudet, and MP Pileni. Control of the shape and the size of copper metallic particles. *The Journal of Physical Chemistry*, 100(10):4160–4166, 1996.

[156] Wei Lv, Patrick E Phelan, Rajasekaran Swaminathan, Todd P Otanicar, and Robert A Taylor. Multifunctional core-shell nanoparticle suspensions for efficient absorption. *Journal of solar energy engineering*, 135(2), 2013.

[157] VM Aroutiounian, KM Gambaryan, VG Harutyunyan, PG Soukiassian, T Boeck, J Schmidtbauer, and R Bansen. The ostwald ripening at nanoengineering of inassbp spherical and ellipsoidal quantum dots on inas (100) surface. *Journal of Contemporary Physics (Armenian Academy of Sciences)*, 48:37–42, 2013.

[158] Nader Daneshfar and Zeinab Noormohamadi. Optical surface second harmonic generation from plasmonic graphene-coated nanoshells: influence of shape, size, dielectric core and embedding medium. *Applied Physics A*, 126(1):55, 2020.

[159] Wenping Cui, Mingda Li, Zuyang Dai, Qingping Meng, and Yimei Zhu. Near-field optical effect of a core-shell nanostructure in proximity to a flat surface. *The Journal of Chemical Physics*, 140(4):044109, 2014.

[160] Garoma Dhaba Bergaga, Belayneh Mesfin Ali, and Teshome Senbeta Debela. Size dependent local field enhancement factor of cdse based core@ shell spherical nanoparticles. *Materials Research Express*, 9(4):045001, 2022.

[161] Nader Daneshfar and Khashayar Bazyari. Optical and spectral tunability of multilayer spherical and cylindrical nanoshells. *Applied Physics A*, 116:611–620, 2014.

[162] W Haus and N Kalyaniwal. a, r. inguva, and cm bowden. *J. App!. Phys*, 65:1420, 1989.

[163] Edward J Rothwell, Jonathan L Frasch, Sean M Ellison, Premjeet Chahal, and Raoul O Ouedraogo. Analysis of the nicolson-ross-weir method for characterizing the electromagnetic properties of engineered materials. *Progress In Electromagnetics Research*, 157:31–47, 2016.

[164] AA Ismail, AV Gholap, and YA Abbo. Enhancement of local electric field in core-shell orientation of ellipsoidal metal/dielectric nanoparticles. *arXiv preprint arXiv:1706.07271*, 2017.

[165] Uday K Chettiar and Nader Engheta. Internal homogenization: Effective permittivity of a coated sphere. *Optics express*, 20(21):22976–22986, 2012.

[166] Leta Jule, Vadim Mal'nev, Belayneh Mesfin, Teshome Senbeta, Francis Dejene, and Kittesa Rorro. Fano-like resonance and scattering in dielectric (core)–metal (shell) composites embedded in active host matrices. *physica status solidi (b)*, 252(12):2707–2713, 2015.

[167] YA Abbo, VN Mal'nev, and AA Ismail. Local field enhancement at the core of cylindrical nanoinclusions embedded in a linear dielectric host matrix. *arXiv preprint arXiv:1609.04700*, 2016.

[168] Debabrata Biswas. A universal formula for the field enhancement factor. *Physics of Plasmas*, 25(4):043113, 2018.

[169] Jian Zhu. Ellipsoidal core–shell dielectric-gold nanostructure: theoretical study of the tunable surface plasmon resonance. *Journal of Nanoscience and Nanotechnology*, 7(3):1059–1064, 2007.

[170] Jayanta K Majhi, Atis C Mandal, and Probodh K Kuiri. Theoretical calculation of optical absorption of noble metal nanoparticles using a simple model: effects of particle size and dielectric function. *Journal of Computational and Theoretical Nanoscience*, 12(10):2997–3005, 2015.

[171] Katsuaki Tanabe. Field enhancement around metal nanoparticles and nanoshells: a systematic investigation. *The Journal of Physical Chemistry C*, 112(40):15721–15728, 2008.

[172] Nader Daneshfar, Tayebeh Naseri, and Hamidreza Foroughi. Influence of anisotropy on optical bistability in plasmonic nanoparticles with cylindrical symmetry. *Plasmonics*, 13:385–392, 2018.

[173] Nader Daneshfar and Hamidreza Foroughi. Optical bistability in plasmonic nanoparticles: effect of size, shape and embedding medium. *Physica E: Low-dimensional Systems and Nanostructures*, 83:268–274, 2016.

[174] Uwe Kreibig, Michael Vollmer, Uwe Kreibig, and Michael Vollmer. Theoretical considerations. *Optical properties of metal clusters*, pages 13–201, 1995.

[175] Y Takeda, OA Plaksin, J Lu, K Kono, and N Kishimoto. Optical nonlinearity of cu: Srtio3 composite fabricated by negative ion implantation. *Nuclear Instruments and Methods in Physics Research Section B: Beam Interactions with Materials and Atoms*, 250(1-2):372–376, 2006.

[176] T Pan, JP Huang, and ZY Li. Optical bistability in metal/dielectric composite with interfacial layer. *Physica B: Condensed Matter*, 301(3-4):190–195, 2001.

[177] R Reinisch and G Vitrant. Optical bistability. *Progress in quantum electronics*, 18(1):1–38, 1994.

[178] Hongli Chen, Youming Zhang, Baile Zhang, and Lei Gao. Optical bistability in a nonlinear-shell-coated metallic nanoparticle. *Scientific reports*, 6(1):21741, 2016.

[179] Garoma Dhaba Bergaga, Belayneh Mesfin Ali, and Teshome Senbeta Debela. Effects of shape on the optical properties of cdse@ au core-shell nanocomposites. *AIP Advances*, 13(3):035331, 2023.

[180] Lei Gao, Hongli Chen, Youming Zhang, and Baile Zhang. Optical bistability in a nonlinear shell coated metallic nanoparticle. 2016.

[181] HL Chen, DL Gao, and L Gao. Effective nonlinear optical properties and optical bistability in composite media containing spherical particles with different sizes. *Optics express*, 24(5):5334–5345, 2016.

[182] Zhiping Wang and Benli Yu. Optical bistability and multistability in polaritonic materials doped with nanoparticles. *Laser Physics Letters*, 11(11):115903, 2014.

[183] N Kalyaniwalla, JW Haus, R Inguva, and MH Birnboim. Intrinsic optical bistability for coated spheroidal particles. *Physical Review A*, 42(9):5613, 1990.

[184] N Kalyaniwalla, JW Haus, MH Birnboim, R Inguva, and WP Ma. Enhanced nonlinear optical response of coated nanoparticles. *MRS Online Proceedings Library (OPL)*, 164, 1989.

[185] Lei Gao. Optical bistability in composite media with nonlinear coated inclusions. *Physics Letters A*, 318(1-2):119–125, 2003.

[186] Bintoro S Nugroho, Alexander A Iskandar, Victor A Malyshev, and Jasper Knoester. Plasmon-assisted two-photon absorption in a semiconductor quantum dot–metallic nanoshell composite. *Physical Review B*, 102(4):045405, 2020.

[187] Jonas Larsson. Electromagnetics from a quasistatic perspective. *American Journal of Physics*, 75(3):230–239, 2007.

[188] V.N.Mal'nev S.Shewamare, O.A.Buryi. Induced Optical Bistability In Small Metal And Metal Coated Particles With Nonlinear Dielectric Functions. *Ukr.J*, 56(4):657–660, 2012.

[189] Tolasa Tamasgen Hirpha, Garoma Dhaba Bergaga, Belayneh Mesfin Ali, and Sisay Shewamare Gebre. Local field enhancement factor of spheroidal core-shell nanocomposites with passive and active dielectric cores. *Materials Research Express*, 2023.

[190] Pei-Heng Zhou, Long-Jiang Deng, Bae-Ian Wu, and Jin Kong. Influence of scatterer's geometry on power-law formula in random mixing composites. *Progress In Electromagnetics Research*, 85:69–82, 2008.

[191] Ari Sihvola. Homogenization principles and effect of mixing on dielectric behavior. *Photonics and Nanostructures-Fundamentals and Applications*, 11(4):364–373, 2013.

[192] MA Palenberg and BU Felderhof. Local-field effects in nonlinear dielectrics. *Physical Review B*, 55(16):10326, 1997.

[193] Yves V Genin. Euclid algorithm, orthogonal polynomials, and generalized routh-hurwitz algorithm. *Linear algebra and its applications*, 246:131–158, 1996.

[194] Chyi Hwang and Shih-Feng Yang. The use of routh array for testing the hurwitz property of a segment of polynomials. *Automatica*, 37(2):291–296, 2001.

[195] Jian Zhu, Hai Liu, and Li-Qing Huang. Wall thickness dependent double optical bistability in gold nanotube: a physical mechanism based on local field enhancement. *Journal of Applied Physics*, 105(11), 2009.

[196] Lei Gao, Liping Gu, and Yanyan Huang. Effective medium approximation for optical bistability in nonlinear metal-dielectric composites. *Solid state communications*, 129(9):593–598, 2004.

[197] Elham Norouzi Afshar and Abdolrahman Namdar. Temperature dependence of the goos–hänchen shift in the nonlinear metal-dielectric nanocomposites. *Optical and Quantum Electronics*, 51:1–13, 2019.

[198] Shitong Fang, Shengxi Zhou, Daniil Yurchenko, Tao Yang, and Wei-Hsin Liao. Multistability phenomenon in signal processing, energy harvesting, composite structures, and metamaterials: A review. *Mechanical Systems and Signal Processing*, 166:108419, 2022.

[199] Tao Pan and Zhen-Ya Li. Optical bistability of metallic particle composites. *physica status solidi (b)*, 213(1):203–210, 1999.

[200] Pankaj K Das. *Optical signal processing: fundamentals*. Springer Science & Business Media, 2012.

[201] Hussein A Elsayed. Transmittance properties of one dimensional ternary nanocomposite photonic crystals. *Materials Research Express*, 5(3):036209, 2018.

[202] Leta Jule, Francis Dejene, and Kittessa Roro. Enhancing absorption in coated semiconductor nanowire/nanorod core–shell arrays using active host matrices. *Optics Communications*, 380:186–194, 2016.

[203] Bruno Sareni, Laurent Krähenbühl, Abderrahmane Beroual, and Christian Brosseau. Effective dielectric constant of random composite materials. *Journal of Applied Physics*, 81(5):2375–2383, 1997.

[204] Dentcho A Genov, Andrey K Sarychev, Vladimir M Shalaev, and Alexander Wei. Resonant field enhancements from metal nanoparticle arrays. *Nano Letters*, 4(1):153–158, 2004.

[205] Stefan A Maier and Harry A Atwater. Plasmonics: Localization and guiding of electromagnetic energy in metal/dielectric structures. *Journal of applied physics*, 98(1), 2005.

[206] Sanong Ekgasit, Chuchaat Thammacharoen, Fang Yu, and Wolfgang Knoll. Evanescent field in surface plasmon resonance and surface plasmon field-enhanced fluorescence spectroscopies. *Analytical chemistry*, 76(8):2210–2219, 2004.

[207] Mahyar Fazeli, Jennifer Paola Florez, and Renata Antoun Simão. Improvement in adhesion of cellulose fibers to the thermoplastic starch matrix by plasma treatment modification. *Composites Part B: Engineering*, 163:207–216, 2019.

[208] Ibrahim Khan, Khalid Saeed, and Idrees Khan. Nanoparticles: Properties, applications and toxicities. *Arabian journal of chemistry*, 12(7):908–931, 2019.

[209] Fahendri Fahendri, Ilham Perdana, Zulfi Abdullah, and Mulda Muldarisnur. Enhancement of light absorption in the active layer of organic solar cells using ag: Sio2 core-shell nanoparticles. *Jurnal Penelitian Pendidikan IPA*, 8(6):3121–3127, 2022.

[210] RA Dynich, AN Ponyavina, and VV Filippov. Local field enhancement near spherical nanoparticles in absorbing media. *Journal of Applied Spectroscopy*, 76:705–710, 2009.

[211] Tanya Hutter, Stephen R Elliott, and Sumeet Mahajan. Interaction of metallic nanoparticles with dielectric substrates: effect of optical constants. *Nanotechnology*, 24(3):035201, 2012.

[212] T Klar, M Perner, S Grosse, G Von Plessen, W Spirkl, and J Feldmann. Surface-plasmon resonances in single metallic nanoparticles. *Physical Review Letters*, 80(19):4249, 1998.

[213] Lu Wang, Morteza Hasanzadeh Kafshgari, and Michel Meunier. Optical properties and applications of plasmonic-metal nanoparticles. *Advanced Functional Materials*, 30(51):2005400, 2020.

[214] Thomas Werne, Markus Testorf, and Ursula Gibson. Local-field enhancement in metal-dielectric nanocylinders with complex cross sections. *JOSA A*, 23(9):2299–2306, 2006.

[215] Basudeb Karmakar, Tirtha Som, Shiv Prakash Singh, and Mithun Nath. Nanometal-glass hybrid nanocomposites: synthesis, properties and applications. *Transactions of the Indian Ceramic Society*, 69(3):171–186, 2010.

[216] S Toroghi and PG Kik. Design of cascaded plasmon resonances for ultrafast nonlinear optical switching. In *Enabling Photonics Technologies for Defense, Security, and Aerospace Applications VII*, volume 8054, pages 52–58. SPIE, 2011.

[217] Albert S Reyna and Cid B de Araújo. High-order nonlinearities of metal-dielectric nanocomposites. In *Metal Nanostructures for Photonics*, pages 61–86. Elsevier, 2019.

[218] Wenyun Wu, Jingying Yue, Dongqi Li, Xiaoyang Lin, Fangqiang Zhu, Xue Yin, Jun Zhu, Xingcan Dai, Peng Liu, Yang Wei, et al. Interface dipole enhancement effect and enhanced rayleigh scattering. *Nano Research*, 8:303–319, 2015.

IOP Publishing Mater. Res. Express 10 (2023) 045005 https://doi.org/10.1088/2053-1591/accb2d

Materials Research Express

PAPER

Local field enhancement factor of spheroidal core–shell nanocomposites with passive and active dielectric cores

Tolasa Tamasgen Hirpha[1,*], Garoma Dhaba Bergaga[2,3], Belayneh Mesfin Ali[2] and Sisay Shewamare Gebre[4]

[1] Department of Physics, Bonga University, Bonga PO Box: 334, Bonga, Ethiopia
[2] Department of Physics, Addis Ababa University, Addis Ababa PO Box: 1176, Addis Ababa, Ethiopia
[3] Department of Physics, Sebeta Special Needs Education Teachers College, Addis Ababa PO Box: 195, Sebeta, Addis Ababa, Ethiopia
[4] Department of Physics, Wolkite University, Wolkite PO Box: 07, Wolkite, Ethiopia
* Author to whom any correspondence should be addressed.

E-mail: tolasatamasgen2014@gmail.com

Keywords: local field enhancement factor, active dielectric, passive dielectric, depolarization factor, metal fraction, dielectric function

OPEN ACCESS

RECEIVED
27 December 2022

REVISED
17 March 2023

ACCEPTED FOR PUBLICATION
6 April 2023

PUBLISHED
14 April 2023

Abstract

We studied the effects of depolarization factor (L), metal fraction (p), and dielectric function of host matrix (ε_h) on the local field enhancement factor (LFEF) of spheroidal core–shell nanocomposites (NCs) with passive and active dielectric cores. Solving Laplace's equations in the quasi-static limit, we obtained expressions of electric potentials for spheroidal core–shell NCs. Then, by introducing L and the Drude-Sommerfeld model into these expressions, we derived the equation of LFEF in the core of spheroidal core–shell NCs. The results show that whether L, p, and/or ε_h vary or kept constant, LFEF of the spheroidal core–shell NCs possesses two sets of peaks with passive dielectric core, whereas only a set of peak is observed with active dielectric core. In NCs with passive dielectric core, an increase in any of these parameters resulted in a more pronounced LFEF peaks in the first set of resonances. With both passive and active dielectric cores, increasing L increases the peaks of LFEF of spheroidal core–shell NCs, whereas increasing p shows decreasing tendency on the peaks of LFEF of the same material with active dielectric core. Moreover, the highest peak of LFEF is obtained by increasing L than p or ε_h indicating that change in the geometry of spheroidal core–shell NCs has the highest effect on the LFEF than the metal concentration and host dielectric function. With the same increase in ε_h, intensities of LFEF of the spheroidal core–shell NCs decrease when the dielectric core is passive and increase when the dielectric core is active. Briefly, the number and intensities of peaks of LFEF of spheroidal core–shell NCs vary greatly when its core is made either passive or active dielectric. Furthermore, by changing parameters like L, p, and ε_h, adjustable LFEF could be obtained and used for applications in optical sensing, nonlinear optics, and quantum optics.

AIP Advances ARTICLE pubs.aip.org/aip/adv

Investigation of optical bistability in spheroidal core–shell nanocomposites with passive and active dielectric cores

Cite as: AIP Advances 14, 015037 (2024): doi: 10.1063/5.0180907
Submitted: 12 October 2023 • Accepted: 26 December 2023 •
Published Online: 19 January 2024

Tolasa Tamasgen Hirpha,[1,a)] Garoma Dhaba Bergaga,[2,3] Belayneh Mesfin Ali,[2] and Sisay Shewamare Gebre[4]

AFFILIATIONS

[1] Department of Physics, Bonga University, P.O. Box 334, Bonga, Ethiopia
[2] Department of Physics, Addis Ababa University, P.O. Box 1176, Addis Ababa, Ethiopia
[3] International Maarif Schools of Ethiopia, Sebeta Campus, Sheger, Sebeta, Ethiopia
[4] Department of Physics, Wolkite University, P.O. Box 07, Wolkite, Ethiopia

[a)] **Author to whom correspondence should be addressed:** tolasatamasgen2014@gmail.com

ABSTRACT

We investigated how induced optical bistability (IOB) and bistability domain (BD) of spheroidal core–shell nanocomposites (NCs) are affected by the depolarization factor (L), metal fraction (p), and host matrix (ε_h). The NCs are composed of passive and active dielectric cores coated with a metallic shell and embedded in various host matrices. By employing Laplace's equation and the Drude–Lorentz model, we calculated the electric field enhancement in various regions of the NCs and studied their IOB theoretically and numerically. The BD of the same NCs is investigated using the root analysis approach. The study reveals that when the value of L decreases, the bistable region of OB increases. However, when p increases at constant L and ε_h, the bistable region gets wider. When the value of ε_h increases, the IOB region is achieved at larger values of incident field. Moreover, the IOB produced was narrower in the passive dielectric core than in the active one, showing that the type of core material also influences the IOB of the core–shell NCs. When the value of L changes, the region of BD also changes in both types of cores. Similarly, changing the value of p in both types of cores causes the BD to vanish or emerge. Moreover, varying ε_h, BD is produced in the OB regions. Overall, the IOB and BD in each core are sensitive to changes in L, p, and ε_h. Varying these parameters leads to the possibility of tuning the bistable regions, which can be used in optical circuits, logic operations, and optical memory.

Effects of Interfacial Layer on the Enhancement Factor of Spheroidal Metal/Dielectric Nanocomposites in Passive and Active Host Matrix

Tolasa Tamasgen Hirpha[1] and Belayneh Mesfin Ali[2,*]

[1]Department of Physics, Bonga University, P.O. Box: 334, Bonga, Ethiopia

[1,2]Department of Physics, Addis Ababa University, P.O. Box: 1176, Addis Ababa, Ethiopia

*Corresponding author's e-mail address: belayneh.mesfin@aau.edu.et

Abstract

We investigated the effects of depolarization factor (L) and metal fraction (p) on the local field enhancement factor (LFEF) of spheroidal metal/dielectric nanocomposites (NCs) with passive and active host matrix. The expressions of electric potentials obtained by solving Laplace's equations in the quasi-static limit for spheroidal metal/dielectric NCs. The equation of LFEF in the host of spheroidal metal/dielectric NCs was then constructed by incorporating L and the Drude-Sommerfeld model into these formulas. The results show that, regardless of how each parameter changes or remains constant, the LFEF of the NCs has a single set of peaks in both the passive and active host matrix. The parameter L affects the LFEFs curves and the output peaks in both host media exhibit shifted symmetrical patterns. On the other hand, the media with interfacial layer (I) were significantly impacted when a field was applied to the metal/dielectric NCs medium, and the LFEF increased successively in the given frequency range with a single peak. Furthermore, in passive and active dielectric host media, the LFEF of the spheroidal shell of the NCs increased progressively with thickness. The LFEF peaks are significantly impacted by radius that was studied in both passive and active host media. We investigated that when p increases, the peak values of the LFEF in the shell structure rise. Additionally, by altering each parameter, it was possible to create an adjustable LFEF that could be utilized for optical detection, nonlinear optics, and optical sensing applications.